Mass spectrometric sampling from the atmospheric pressure ion source
by Douglas Robert Zook

A thesis submitted in partial fulfillment of the requirements for the degree of Doctor of Philosophy in Chemistry
Montana State University

Abstract:
Atmospheric Pressure Ionization Mass Spectrometry (APIMS) is an established method for ultra-trace chemical analysis. However it is infrequently applied to fundamental study of gas phase ion chemistry. This is attributable to sampling errors which preclude the accurate observation of relative ion abundances within the ion source. The objective of this thesis is characterization of sampling errors to permit application of APIMS to the fundamental study of several chemical systems. Three sampling errors are examined: 1) Perturbations encountered in sampling cluster ions, 2) mass and ion-type discrimination effects, and 3) aperture contact potentials. The former two errors are caused by dynamics occurring within a free jet expansion that accompanies non-effusive sampling of ion source contents into a mass spectrometer vacuum chamber. Both can grossly perturb relative ion currents. Contact potentials, when present, significantly diminish absolute mass spectral ion currents. The chemical systems of study include 1) two-channel dissociative electron capture reactions, 2) ion-molecule clustering reactions, and 3) cluster assisted decomposition reactions. It is demonstrated that following quantitative evaluation of APIMS sampling mass bias, observed mass spectral ion currents can be corrected to obtain accurate ion source relative ion abundances. This protocol has revealed the important influence pressure exhibits for influencing observed relative product ratios of two-channel dissociative electron capture reactions. From this study it is deduced that excited electron capture intermediates have lifetimes against dissociation which allow for internal energy modification through collisions with buffer gas, resulting in alteration of the favored channel of dissociation. Regardless of ion source sampling conditions, it is shown that useful ion molecule relative clustering propensities are available from APIMS from which qualitative fundamental information can be obtained. This is demonstrated for isomer dependent clustering between nitroaromatic molecular anions and dimethylsulfoxide. APIMS has allowed observation of previously unreported halide and dihalide hydrate cluster ions generated in the APIMS free jet expansion, for which preferred stabilities are noted. Investigations of new cluster assisted decomposition reactions for some perfluprinated molecular anions explain the occurrence of unexpected ions encountered during perfluorocarbon analysis by thermospray mass spectrometry.

MASS SPECTROMETRIC SAMPLING FROM THE ATMOSPHERIC PRESSURE ION SOURCE

by

Douglas Robert Zook

A thesis submitted in partial fulfillment
of the requirements for the degree

of

Doctor of Philosophy

in

Chemistry

MONTANA STATE UNIVERSITY
Bozeman, Montana

September 1990

APPROVAL

of a thesis submitted by

Douglas Robert Zook

This thesis has been read by each member of the thesis committee and has been found to be satisfactory regarding content, English usage, format, citations, bibliographic style, and consistency, and is ready for submission to the College of Graduate Studies.

9/28/90
Date

Eric Grimsrud
Chairperson, Graduate Committee

Approved for the Major Department

10/1/90
Date

Elwin H. Abbott
Head, Major Department

Approved for the College of Graduate Studies

10/2/90
Date

Henry J. Parsons
Graduate Dean

STATEMENT OF PERMISSION TO USE

In presenting this thesis in partial fulfillment of the requirements for a doctoral degree at Montana State University, I agree that the Library shall make it available to borrowers under the rules of the Library. I further agree that copying of this thesis is allowable only for scholarly purposes, consistent with "fair use" as prescribed in the U.S. Copyright Law. Requests for extensive copying or reproduction of this thesis should be referred to University Microfilms International, 300 North Zeeb Road, Ann Arbor, Michigan 48106, to whom I have granted "the exclusive right to reproduce and distribute copies of the dissertation in and from microfilm and the right to reproduce and distribute by abstract in any format."

Signature Douglas R. Zook

Date Sept. 26, 1990

ACKNOWLEDGEMENT

Toward completion of this dissertation I thank my advisor, Prof. Eric P. Grimsrud for the interesting and varied research experiences. Also, I would like to express gratitude to group members that have greatly assisted in my progress. Drs. W. Berk Knighton, L. Joe Sears, and R. Steve Mock always provided welcomed advice and friendship. All of the group members have made my time at M. S. U. truly memorable.

Finally to family and friends alike, who inspire and support, go equal acknowledgement and gratitude.

TABLE OF CONTENTS

TABLE OF CONTENTS-Continued

TABLE OF CONTENTS-Continued

LIST OF TABLES

LIST OF FIGURES

Figure Page

LIST OF FIGURES - Continued

LIST OF FIGURES - Continued

LIST OF FIGURES - Continued

LIST OF FIGURES - Continued

Figure Page

ABSTRACT

Atmospheric Pressure Ionization Mass Spectrometry (APIMS) is an established method for ultra-trace chemical analysis. However it is infrequently applied to fundamental study of gas phase ion chemistry. This is attributable to sampling errors which preclude the accurate observation of relative ion abundances within the ion source. The objective of this thesis is characterization of sampling errors to permit application of APIMS to the fundamental study of several chemical systems. Three sampling errors are examined: 1) Perturbations encountered in sampling cluster ions, 2) mass and ion-type discrimination effects, and 3) aperture contact potentials. The former two errors are caused by dynamics occurring within a free jet expansion that accompanies non-effusive sampling of ion source contents into a mass spectrometer vacuum chamber. Both can grossly perturb relative ion currents. Contact potentials, when present, significantly diminish absolute mass spectral ion currents. The chemical systems of study include 1) two-channel dissociative electron capture reactions, 2) ion-molecule clustering reactions, and 3) cluster assisted decomposition reactions. It is demonstrated that following quantitative evaluation of APIMS sampling mass bias, observed mass spectral ion currents can be corrected to obtain accurate ion source relative ion abundances. This protocol has revealed the important influence pressure exhibits for influencing observed relative product ratios of two-channel dissociative electron capture reactions. From this study it is deduced that excited electron capture intermediates have lifetimes against dissociation which allow for internal energy modification through collisions with buffer gas, resulting in alteration of the favored channel of dissociation. Regardless of ion source sampling conditions, it is shown that useful ion molecule relative clustering propensities are available from APIMS from which qualitative fundamental information can be obtained. This is demonstrated for isomer dependent clustering between nitroaromatic molecular anions and dimethylsulfoxide. APIMS has allowed observation of previously unreported halide and dihalide hydrate cluster ions generated in the APIMS free jet expansion, for which preferred stabilities are noted. Investigations of new cluster assisted decomposition reactions for some perfluorinated molecular anions explain the occurrence of unexpected ions encountered during perfluorocarbon analysis by thermospray mass spectrometry.

INTRODUCTION

Background

Atmospheric Pressure Ionization Mass Spectrometry (APIMS) originated from studies concerning the ion chemistry occurring within flames, electric discharges, and the electron capture detector (ECD) (1-4). APIMS has evolved over the past two decades to become an established and valuable method for ultra-trace chemical analysis. APIMS is well suited for direct real time whole air monitoring since no vacuum interlocks are needed to introduce samples to the ionization chamber (5-7). Because of high collision frequencies characteristic of ambient pressure conditions, reactant and product ions are formed with nearly thermal energies making APIMS a soft ionization technique with little mass spectral fragmentation. The chemical analytical potential of APIMS has been well characterized and detection limits at the femtogram (10^{-15} g) level have been demonstrated for analytes of environmental and biomedical interest (8-10). Several review articles have appeared over the past decade which summarize the chronological development of APIMS and detail important chemical analytical aspects which have provided the motivation for study and continual innovation (11-15).

Despite the impressive applied chemical analytical

utility of APIMS, the method has not found wide application for fundamental study of gas phase ion chemistry. Because of sampling errors, the observed APIMS mass spectral ion currents cannot be assumed to be proportional to the concentration of ions present within the API reaction chamber. This has widely been understood to be due to the non-effusive flow characteristics associated with the transfer of ions and neutral buffer gas molecules under ambient pressure conditions of the ion source through a tiny orifice into the vacuum chamber of a mass spectrometer. The gross pressure difference between the source and the expansion chamber is nearly seven orders of magnitude. These conditions violate the normally accepted criteria for perturbation-free ion sampling because the mean free path is much shorter than the dimensions of the sampling orifice (16). Such non-effusive flow dynamics result in an adiabatic free jet expansion. Cooling which accompanies the expansion may promote aggregation and net clustering between ions and polar molecules entrained within the jet. An opposing force to aggregation is collisionally induced dissociation, which may occur as ions pass through shock waves that occur at the periphery of the expansion boundaries (12). Equilibrium relative ion abundances which are known to exist within the API ion source are therefore very difficult to observe due to these sampling difficulties (16).

Gas phase conditions provide the necessary means for probing intrinsic chemical properties and reactivities of

ionic species in an isolated system free of bulk solvent effects (17,18). Broad interest in the fundamental aspects of gas phase ion chemistry has propelled much of the mass spectrometric research activity in the past quarter century or longer. The established methods for fundamental studies, such as the Pulsed e-beam High Pressure Mass Spectrometer of Kebarle (19), are all confined to pressures very low in comparison to APIMS. These relatively low pressure ionization methods presumably do not have associated significant sampling errors. However, because of the pressure limitations of the established fundamental techniques, relatively little is known of the interesting ionization conditions involving higher reagent concentrations and higher collision frequencies which occur with use of total pressures of one atmosphere.

Statement of Problem

To extend the utility and understanding of APIMS a number of significant sampling problems will be investigated. Following the characterization of sampling errors, the APIMS will be utilized for several fundamental studies. The sampling errors to be characterized fall into three broad categories :

1) Cluster ion sampling perturbations,

2) Mass and Ion type discrimination effects, and

3) Occurrences of sampling aperture contact potentials

All of these APIMS sampling errors complicate mass spectral

ion current interpretation. The former two are of particular importance because their existence precludes from direct observation the relative ion abundances which are present within the API ion source. The third category of sampling error, contact potentials, may totally inhibit ion transit through the sampling orifice.

The chemical systems to be studied for fundamental information fit into two broad categories. The first concerns two-channel dissociative electron capture reactions for which the importance of pressure will be investigated in determining the observed relative product ratios from the available dissociation channels. In order to approach this fundamental problem, the characterization of mass bias errors will be of central importance. The second category of fundamental study will involve ion-molecule clustering reactions. A range of molecular anion structural isomers that can be made to cluster with dimethylsulfoxide will be investigated to determine if qualitative clustering propensities are retained despite sampling perturbations. Then the cooling dynamics of the free jet expansion will be employed for generation of halide and dihalide hydrate cluster ions which have not been previously observed. Finally a new cluster assisted decomposition reaction recently studied by PHPMS methods will be examined by APIMS.

THEORY

Non-Effusive Flow Aperture Sampling

The accepted criteria for perturbation free cluster ion sampling, as stated in the introduction, usually dictate that the flow conditions associated with the sampling aperture be effusive. This means that the dimensions of the sampling aperture must be very small in relation to the mean free path of ions and neutrals to be sampled. The Knudson number is an established flow dynamics index for determining whether the mass transport of a gas is effusive (20), meaning that no collisions occur between the gas molecules during the transit through an orifice, and is given by equation 1,

$$K = \lambda / D \qquad (1)$$

where λ is the mean free path of a molecule or ion in the gas to be sampled, and D is the diameter of the sampling orifice. A Knudson number of less than 0.01 indicates viscous flow through the aperture. A value greater than 1.0 is indicative of effusive flow. Mean free path is a function of the gas collision rate, $\nu_{collision}$, number density, n, and average thermal velocity, v_{ave}, and may be estimated by equation 2,

$$\lambda = (\nu_{collision}\ n)^{-1}\ v_{ave} \qquad (2)$$

At atmospheric pressure, assuming $\nu_{collision}$ of 1 x 10^{-9} cm^3 $molecule^{-1}$ sec^{-1}, n of 2 x 10^{19} molecule cm^{-3}, and v_{avg} of 2 x 10^4 cm sec^{-1}, one may predict an ion or neutral collision free trajectory of approximately 10^{-2} μm. This is far below the dimensions of the typical APIMS ion sampling aperture of 20 to 50 μm. The Knudson number for sampling an atmospheric pressure gas through a 20 μm diameter orifice from equations 1 and 2 is 5 x 10^{-4}, a value four orders of magnitude below the effusive flow limit. The high collision frequency which accompanies non-effusive ion and neutral buffer gas sampling into a vacuum chamber results in an adiabatic free jet expansion.

Free Jet Expansion

The study of free jet expansions, pioneered by J.B. Fenn and others, have been the subject of many studies involving their unique physical characteristics and applications for simplification of complex molecular spectroscopy problems (21), and investigation of nucleation phenomena (22).

A free jet expansion embodies the conversion of the random motion of gas molecules in a high pressure reservoir into a directed mass flow of gas molecules expanding through a small aperture into a vacuum chamber (23). Disregarding the possibility for heat conduction in the expansion chamber, the energy required for this process is provided by the internal energy of gas molecules, thereby resulting in a self cooling effect. Molecular vibrations and rotations can be cooled to

temperatures far below the freezing point of the entrained gas molecules, and are known to decrease into the low Kelvin range (21). Aggregation processes may accordingly follow. Cooling, which is proportional to the pre-expansion pressure and orifice diameter, is the result of two body collisions which occur very early in a region called the silent zone, in which gas velocities are uniform, and with similar trajectories. The number density and local temperatures decrease with increased distance from the sampling aperture. The highest velocities are attained on axis of the direction of flow, and estimated at approximately 10^5 cm sec^{-1}. Surrounding the silent zone, are regions of shock waves, which are the boundaries between the directed flow of the jet and the random motion of the background gas in the expansion chamber. The barrel shock wave is longitudinally symmetrical, and the mach disk as a shock wave encountered normal to the direction of flow. The sampling orifice-to-mach disk separation, X_M, is estimated by the following empirical equation 3 (24),

$$X_M = 0.67\, D_o (P_o / P_1)^{1/2} \qquad (3)$$

where D_o is the sampling orifice outside diameter, P_o is the pre-expansion pressure, and P_1 is the expansion chamber pressure. These shock waves are regions of extensive scatter and collision. Figure 1 illustrates the approximate free jet expansion dimensions as predicted by equation 3 for sampling

from the atmospheric pressure ion source that is the subject of this thesis. The passage of ions and neutrals from the silent zone through a shock wave serves to raise the internal energy of the species, and may potentially result in collisionally activated dissociation.

The factors governing aggregation and nucleation phenomena in a free jet expansion are :

(1) the molecular weight of the expansion gas,

(2) the relative percentage of the aggregatable species to expansion gas,

(3) the initial upstream (pre-expansion) pressure,

(4) the initial upstream temperature, and

(5) the design of the sampling aperture.

Because of the very high ratio of neutral expansion gas (atomics or polyatomics) to entrained ions, virtually all collisions experienced by ions will be with the expansion gas. Therefore removal of ion internal energy is dependent upon collision with the expansion gas. The extent of cooling of an entrained species is dependent upon the relative velocity of the entrained ions and neutrals and the expansion gas, since similar velocities will result in higher collision frequencies (point 1). The average molecular speed of a molecule is dependent upon its mass and collisional cross section. The varying relative velocities of expansion gas and species entrained in the expansion gas forms the basis of the velocity slip effect, which accounts for the relative inefficiency of

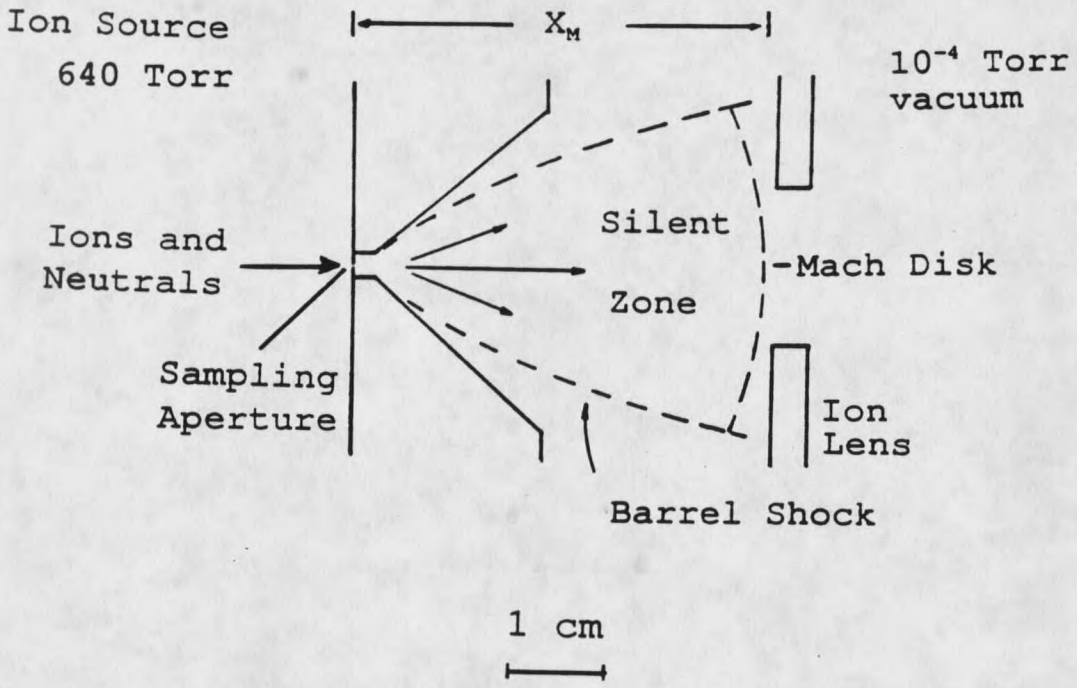

Figure 1.

Illustration of the free jet expansion associated with sampling from API ion source for study apparatus shown in Figure 2 based upon equation (3), $X_M = 0.67\ D\ (\ P_o\ /\ P_i\ )^{1/2}$, with D = 50 μm, P_o = 640 Torr, and $P_i = 5 \times 10^{-4}$ Torr. Cooling and condensation events may occur in region of Silent zone. Collisions may occur upon transit through Mach disk prior to focussing and mass analysis. Adopted from Bruins, reference 12.

lighter mass expansion gases, such as helium, to vibrationally cool entrained species (25). The lighter the mass of the expansion gas, the higher its velocity relative to the entrained species. Maximal cooling occurs with a heavier expansion gas which may more efficiently serve to increase residence times of entrained species within the Silent zone, thereby allowing for more internal energy lowering collisions and subsequent cooling. The cooling results in enhancement of aggregation and condensation events.

The extent of aggregation is also determined by the probability of an encounter between entrained species. If the number densities are very low in the expansion, few van der Waals complexes may form (point 2).

The initial pressure (point 3) will dictate the collision frequency attainable within the silent zone of the expansion. The initial internal energy of the expansion gas and entrained species are influenced by the bath gas temperature prior to the expansion (point 4). Finally, the design of the sampling aperture may strongly influence the physical characteristics of the jet, with corresponding impact on the dimensions of the effective Silent zone and location of shock waves (point 5). Reflections, or scattering from surfaces, may also influence the characteristics of the expansion.

Attainment of Gas Phase Ionic Equilibrium

A simplified rate controlled picture is presented to

illustrate that ion-molecule clustering reactions that can be made to occur within the API ion source will reach a state of chemical equilibrium. The API ion source is an ionization reaction chamber maintained at ambient pressure. To ascertain that chemical equilibrium conditions are attained within the API ion source, an examination of the steady state ionization events and rate processes for ion formation and destruction is necessary. The criteria for attainment of gas phase ionic chemical equilibrium, as put forth by Kebarle (17) follow :

1) the reactants and products must be in thermal equilibrium with their surroundings (carrier gas and reaction vessel walls),

2) The path(s) that reactively couple the ions engaged in the equilibrium must be appreciably faster than all other processes effecting the concentration of ions, and

3) sufficient time allowed for chemical reactions of interest to reach steady state equilibrium.

Thermalization is known to occur under conditions of sufficiently high pressures, and are considered to be attained within ion sources maintained in the low Torr range. Accordingly, thermalization is certainly attained in an ambient pressure gas by comparison. These latter two criteria require a clear understanding of the ion formation and destruction mechanisms, which will be considered below.

API Rate-Controlled Picture

The API ion source that is the focus of this study has a

^{63}Ni β^- activity of 15 mCi for 5.6 x 10^8 β^- ejections per second. The average nickel-63 β^- particle energy of 19 keV is sufficient to produce approximately 650 thermal energy electron-positive ion pairs for a steady state ion density of nearly 2 x 10^8 ions cm^{-3}. The primary ionization and electron thermalization period is estimated to occur in approximately one nanosecond (15). Following these primary ionization events, a multitude of ion formation and destruction processes rapidly occur as the ion chemistry evolves in time. The predominant destruction mechanisms include positive ion-electron recombination, ion diffusion to the source walls, and bulk ventilation of the ionized gas out from the source interior. Ion-molecule reactions continue to proceed until the ions are destroyed by one of the above three loss mechanisms. The ionization ultimately resides with the chemical entity, or entities, which possess the greatest propensity to retain the charge. It is this terminal ion population which is sampled by bulk ventilation into the mass spectrometer. Kebarle has estimated the time required to reach gas phase ionic equilibrium within the Pulsed e-beam High Pressure Mass Spectrometer (PHPMS) ion source to be on the order of 100 microseconds (26). Because of the much higher pressures and higher reagent concentrations possible within the API ion source, an even shorter period of time would be expected for attainment of equilibrium within the APIMS.

Cluster Ion Formation. Reactions 4 through 7 represent a generalized ion-molecule clustering system in which initially an ion of either polarity, $A^{+/-}$, formed by interaction with a reagent ion $R^{+/-}$ (reaction 4), is clustered with a solvating agent, S, (reaction 5) in the presence of a third body for the collisional stabilization of the clustering reaction product,

$$R^{+/-} + A \rightleftharpoons A^{+/-} \qquad (4)$$

$$A^{+/-} + S + B \rightleftharpoons A^{+/-}S + B \qquad (5)$$

$$A^{+/-}S + S + B \rightleftharpoons A^{+/-}(S)_2 + B \qquad (6)$$

$$\vdots$$

$$A^{+/-}(S)_n + S + B \rightleftharpoons A^{+/-}(S)_{n+1} + B \qquad (7)$$

after which many fast successive clustering steps are possible (reaction 6), proceeding rapidly to a state of dynamic chemical equilibrium for the particular conditions of ion source temperature and solvating agent source partial pressure. $R^{+/-}$ may be, for example, a stronger gas phase acid or base, or a thermalized electron, which ionizes A. S is any suitable solvating agent such as a molecule of water or dimethylsulfoxide. Reaction 7 constitutes the general forward clustering reaction in which an existing cluster ion successfully associates with a neutral solvating agent to form the next largest cluster ion. Therefore reaction 7 is the only clustering reaction necessary for the steady state model.

Cluster Ion Destruction. Reactions 8 through 11 are the mechanisms for cluster ion destruction within the API ion source,

$$A^{+/-}(S)_n + B \longrightarrow A^{+/-}(S)_{n-1} + S + B \quad (8)$$

$$A^{+/-}(S)_{0\ to\ n} + I^{-/+} \longrightarrow Neutral(s) \quad (9)$$

$$A^{+/-}(S)_{0\ to\ n} \longrightarrow Wall\ Neutralization \quad (10)$$

$$A^{+/-}(S)_{0\ to\ n} \longrightarrow Bulk\ Ventilation\ Out \quad (11)$$

where reaction 8 is the collisionally induced dissociation of any cluster ion, (the reverse of reaction 7), reaction 9 is the destruction of any ion by means of ion-ion recombination with an ion of opposite polarity, reaction 10 is ion loss due to contact and neutralization with the grounded surface of the ion source walls, and reaction 11 is convective ion loss due to bulk ventilation of ionized gas out of the ion source volume.

Steady State Model. An overall steady state equation is obtained from solving conservation equations involving ion formation and destruction reactions 7 through 11 to yield equation 12,

$$\frac{A^{+/-}(S)_{n+1}}{A^{+/-}(S)_n} = \frac{k_{clust}\ [\ S\ ]\ [\ B\ ]}{k_{declust}\ [\ B\ ] + k_{ion\text{-}ion}\ [\ I^{+/-}\ ] + k_{diff} + k_{vent}} \quad (12)$$

In order to attain a state of clustering equilibrium, it is

necessary that the relative rate processes allow the forward and reverse clustering reactions of interest to be faster than all other ion destruction mechanisms. Therefore the magnitude of these ion concentration controlling rate coefficients must adhere to

$$k_{clust}\ [\ B\ ] = k_{declust}\ [\ B\ ] >> (k_{ion\text{-}ion}\ [\ I^{+/-}\ ] + k_{diff} + k_{vent})$$

Under API conditions, the magnitude of $k_{clust}\ [\ B\ ]$ and $k_{declust}\ [\ B\ ]$ are approximately 500 fold greater than for PHPMS conditions due to pressure differences. It is well-known from diffusional loss temporal profiles that ion-molecule clustering equilibrium is readily established within the PHPMS ion source maintained at 1 Torr. Because of their minuscule mass, the diffusion rate coefficient for electrons is approximately 10^3 fold greater than that for positive ions of 100 dalton mass. However, due to the high charge density within the API ion source, the diffusion of electrons and positive charge carriers are linked, due to attractive coulombic forces. As a consequence, the free diffusional rate coefficients are replaced by the ambipolar diffusional rate coefficient, D_a. At atmospheric pressure, the first order wall diffusional loss rate coefficient , k_{diff}, is calculated from

$$k_{diff} = D_a / \Lambda^2 \qquad (13)$$

where Λ is the ion source characteristic diffusion length, given by $\Lambda = r\ \pi^{-1}$, r being the diffusion volume radius, and D_a is the ambipolar diffusion coefficient mentioned above (27). For the APIMS ion source in this study, r is 0.8 cm, for a characteristic diffusion length of 0.25 cm. A representative positive ion mass-electron ambipolar diffusion coefficient is given by equation 14,

$$D_a = 0.11(T/273)^2(760/P) \qquad (14)$$

where T is the absolute ion source temperature, and P is the pressure in Torr (28). At 150° C and 640 Torr pressure a typical ambipolar diffusion coefficient of 0.314 cm^2sec^{-1} is calculated. The corresponding k_{diff} obtained from equations 13 and 14 is approximately 4.8 sec^{-1}, a diffusional loss rate coefficient nearly 500 fold smaller relative to the PHPMS conditions, because of the inverse dependence of diffusion on pressure.

The first order ventilation rate coefficient, k_{vent}, is given by

$$k_{vent} = F / V \qquad (15)$$

where F is the buffer gas flow rate, and V is the ion source volume. The total maximum API ion source flow operating flow is kept at or below 1 ml sec^{-1}, and the total ion source volume

is 1.5 cm^3, for a k_{vent} loss rate coefficient of 0.7 sec^{-1} from equation 15. The total steady state cluster ion density, $[A^{+/-}(S)_{0\ to\ n}]$, within the API source is calculated from production rate per unit volume, and was estimated above to be approximately 2 x 10^8 ions cm^{-3}. The ion-ion recombination rate for loss of cluster ions is given by equation 16,

$$rate_{ion-ion} = k_{ion-ion}\ [\ I^{-/+}\ ]\ [\ A^{+/-}(S)_{0\ to\ n}\ ] \qquad (16)$$

Using a pseudo-first order ion-ion loss rate coefficient, $k_{ion-ion}\ [\ I^{-/+}\ ]$, of 1 x 10^{-6} cm^3 sec^{-1} one calculates a loss rate due to ion-ion recombination of 200 sec^{-1} (29), close to the experimentally determined value from Grimsrud and coworkers on the order of 500 sec^{-1} for an ion source of this design (30). At atmospheric pressure the pseudo first order ion-ion recombination loss rate coefficient, $k_{ion-ion}\ [\ I^{+/-}\ ]$, is therefore seen to be far greater than either k_{diff} or k_{vent}.

The ion-molecule clustering reactions are often nearly collisionally limited. For an atmospheric pressure gas, the second order collision rate coefficient is approximately 10^{-9} cm^3 $molecule^{-1}$ sec^{-1}, and the number density is about 2 x 10^{19} molecules cm^{-3}, leading to $k_{clust}\ [\ B\ ]$ of about 2 x 10^{10} sec^{-1}, a pseudo first order clustering rate coefficient far exceeding the ion destruction rates due to ion-ion recombination, wall diffusion, or bulk ventilation out of the source volume. Therefore equation 12 can be reduced to equation 17,

$$\frac{A^{+/-}(S)_{n+1}}{A^{+/-}(S)_n} = \frac{k_{clust}\ [\ S\ ]}{k_{declust}} = K_f\ [\ S\ ] \qquad (17)$$

since successive ion molecule clustering and declustering reactions are much faster than all possible ion destruction mechanisms.

One may take a representative third order ion-molecule clustering rate expression

$$rate = k_{clust}\ [\ B\ ]\ [\ S\ ]\ [\ A^{+/-}(S)_n\ ] \qquad (18)$$

to verify that the ion-molecule association reactions are indeed much faster than other ion loss routes. Using a typical ternary k_{clust} of 10^{-28} cm^6 $molecule^{-2}$ sec^{-1} (31), [B] of 2×10^{19} buffer gas molecules per mL, and [S] of 2×10^{17} for 10 ppt solvating agent, one obtains an enormous pseudo-first order clustering rate coefficient. Hence the established criteria necessary for ion chemistry thermodynamic equilibrium are shown to be safely met within the API reaction chamber.

Estimation of Ion-Molecule Clustering Equilibrium

The Pulsed High Pressure Mass Spectrometry (PHPMS) techniques of Kebarle and others have provided a wealth of knowledge regarding the energetics of a wide range of ion-molecule reactions (19). For example, successive clustering equilibrium reactions made to occur within the PHPMS ion source are monitored in order to determine free energies,

enthalpies, and entropies of solvation. Such measurements constitute an enormous volume of thermodynamic parameters, from which equilibrium constants may be obtained and used in turn to determine the relative abundances of the ions present for a given set of thermodynamic equilibrium conditions. Negligible temperature dependencies for the parameters are assumed. A procedure described by Kebarle (32), has been adapted by which individual equilibrium cluster ion abundances within a given ion-molecule clustering system are calculated from established thermodynamic parameters.

EXPERIMENTAL

The component parts of the API mass spectrometer that is the subject of this thesis are described below.

API Ion Source

The API ionization source seen in Figure 2 follows the first generation ^{63}Ni design of Carroll and coworkers (3). There are no restrictions to flow for gas through the source, such that the pressure is ambient, which is typically 640 Torr for the 5,000 ft. elevation of Bozeman, Montana. The ion source is machined from stainless steel, and fitted with a platinum foil impregnated with 15 mCi of ^{63}Ni (New England Nuclear) which lines the walls of a 1.5 cm^3 cylindrical volume. A compressed gold o-ring seals the connection between the ion source and vacuum envelope flange, to which it is securely bolted. The contents within the source volume are continually irradiated by the spontaneous β^- particle decay of nickel-63.

An axially positioned pin within the center of the ion source has two possible functions. During normal mass spectrometric measurements this pin is positioned at least 6 mm away from the sampling aperture, and is electronically connected to ground. The position of the grounded pin is of no importance whatsoever to mass spectral sampling.

APIMS Ion source and Expansion chamber

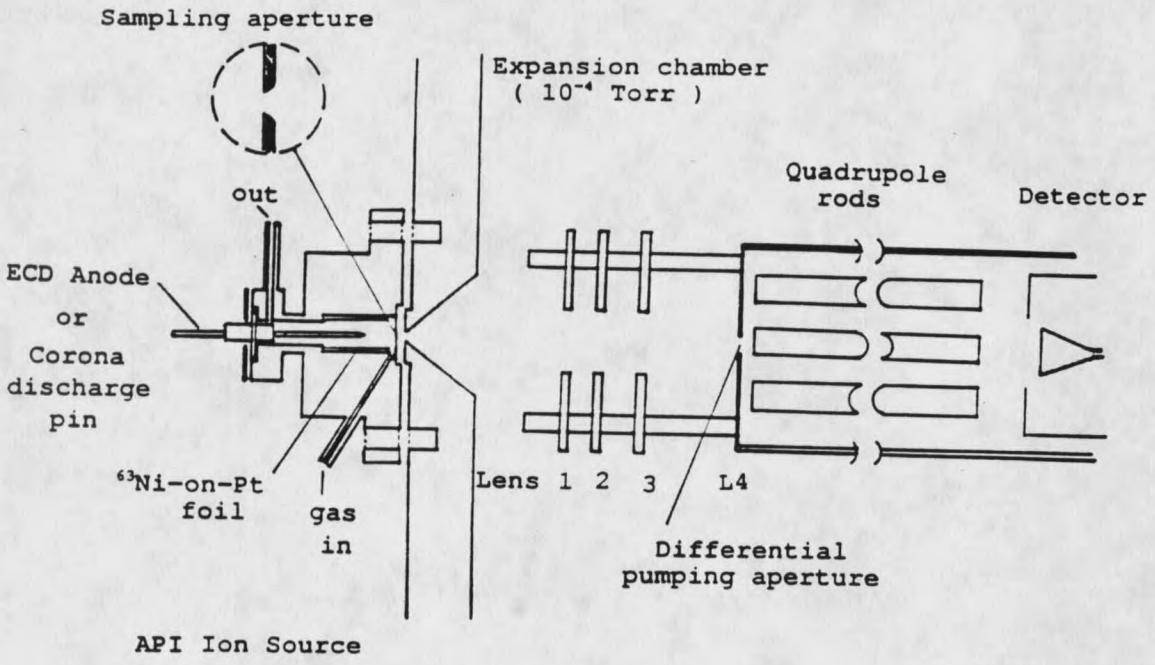

Figure 2.

Atmospheric Pressure Ionization (API) ion source, expansion chamber, mass analysis and ion detection apparatus. Axially positioned pin may be utilized to obtain a normal ECD function, or for corona discharge ionization superimposed over the continuous nickel-63 irradiation. The free jet expansion occurs on vacuum side (right) of aperture (See Figure 1). Ion optics (L1, L2, L3) shown which culminate ion beam through differential pumping aperture for mass analysis and detection. L1 is the ion extraction lens. L4 is the quadrupole ion transmission energy. Resistive heater cartridges (not shown) embedded in flange make contact with the ion source block.

When desired, a standard electron capture detector ECD function may be obtained by connection of this pin to a fixed frequency pulsing circuit (33). The pin serves as a pulsed anode (5 μsec width x 300 μm period, + 50 V) to which electrons are periodically collected, for a normal ECD time averaged standing current. The ECD response is of value for obtaining a measure of the degree of consumption of the thermalized electrons initially available within the ion source by a given sample size.

A corona ionization function (superimposed over the nickel-63 ionization) may be obtained by appropriately positioning and biasing this pin. The corona discharge is typically very stable, both for initiation and maintenance of discharge, a feature which may be attributed to the continual background of beta ionization from the nickel-63. The corona discharge mode of ionization was only employed for the first study to be described in Results and Discussion, because of the higher attainable ion densities which afforded higher ion currents with the smaller (22 μm) diameter apertures. The pin tip is positioned several millimeters away from the sampling orifice for two reasons. The first is to assure sufficient ion residence times so that the mass spectral ion signals reflect thermodynamic and not kinetic control. The second is to avoid capacitive aperture charging effects that are known to perturb ion sampling. This general topic of aperture charging effects is also taken up in Results and Discussion.

The total carrier gas flow rate through the ion source is typically maintained at 60 mL min^{-1}. Prepurification of the compressed buffer/ expansion gas is effected by oxygen removing traps (Oxy-traps, Alltech) and water and contaminant removing traps ($CaSO_4$ desiccant / molecular sieve traps, Alltech). The presence of small leaks in the system gas lines, and about the ion source, result in a total background water pressure estimated at about 100 ppm, or roughly 0.1 Torr water partial pressure within the 640 Torr source pressure.

The ion source is heated by two resistive heating cartridges of a Watlow temperature controller. These heater cartridges are embedded in the vacuum envelope flange and are in direct contact with the ion source block, the exterior of which is insulated with a blanket of fiberglass. It was necessary to calibrate this temperature controller because of the discrepancy found to exist between its lower temperature settings and the true resulting ion source block temperature. This was effected by means of insertion of a reliably calibrated mercury thermometer into a hole adjacent to the ion source volume (34). Heat paste was used to ensure optimal heat conduction to the thermometer bulb, and stem corrected temperature readings where thereby taken to calibrate the Watlow. Good agreement was later obtained by this calibration method and use of an iron-constantan thermocouple thermometer inserted into the ion source block (Omega,Inc). The reliability of the ion source temperature is conservatively

estimated to be within ± 2° C.

Analyte and Solvating Agent Introduction

All chemicals were obtained from commercial suppliers, (Aldrich, PCR, Matheson) and are purified by chromatographic methods. A nitrogen pressurized 4.1 L glass carboy is utilized for preparation of ambient temperature gaseous samples. Successive nitrogen dilutions of carboy samples are performed within a glass 50 cc syringe fitted with a teflon valve (B D Yale Syringe, Hamilton valve). Analyte samples are introduced into the ion source following separation by gas chromatography (GC). Gaseous analytes are placed onto an ambient temperature 10 ft by 1/8 inch chromatographic column packed with 10 % SF-96 oil that is adsorbed onto Chromosorb-W, by means of a 1.0 ml sample loop (Karle valve). Liquid analytes are prepared in toluene and placed onto a 3 m by 340 µm I.D. methyl silicone macrobore capillary column (Hewlard-Packard) by means of a heated splitless injection port associated with an isothermal gas chromatograph (Gow-Mac, Bridgewater, NJ). A 1.0 µl syringe is used for delivery of liquid samples into the GC injection port (Hamilton). In one study gaseous samples of bromotrichloromethane were introduced onto the capillary column by means of a 10 µl gas-tight syringe (Hamilton), a method inferior to the sample loop. The gas chromatographic eluent passes through heated transfer lines and is mixed with the gas stream flowing through heated

make-up lines prior to introduction into the API ion source.

For all ion-molecule clustering experiments, it was necessary to introduce a known partial pressure of the desired solvating agent into the source. This was effected by means of a gas saturation device containing a 6-8 inch high column of the desired solvating agent in liquid form. This saturator is plumbed into the make-up line. Figure 3 shows this device in conjunction with the gas chromatograph for the total analyte and solvating agent introduction system. Make-up line buffer gas is slowly bubbled upward through a column of the liquid after passage through a fine fritted glass inlet located at the bottom of the saturator. The entire solvating agent saturation device is immersed in a temperature controlled water bath. Thoroughly heated transfer lines connect the saturator effluent to the heated gas chromatograph for mixing upstream from the ion source. By measuring the relative flow rates of the saturator and GC, it is possible to determine the saturator flow dilution factor upon mixing so that the final partial pressure of solvating agent entering the ion source may be known.

The reliability of the saturator was tested by varying the flow rate from 10 to 100 mL min^{-1}, as a check for a possible shift from the liquid-vapor phase equilibrium. No detectable change could be observed in the cluster ion distribution, and therefore solvating agent partial pressure.

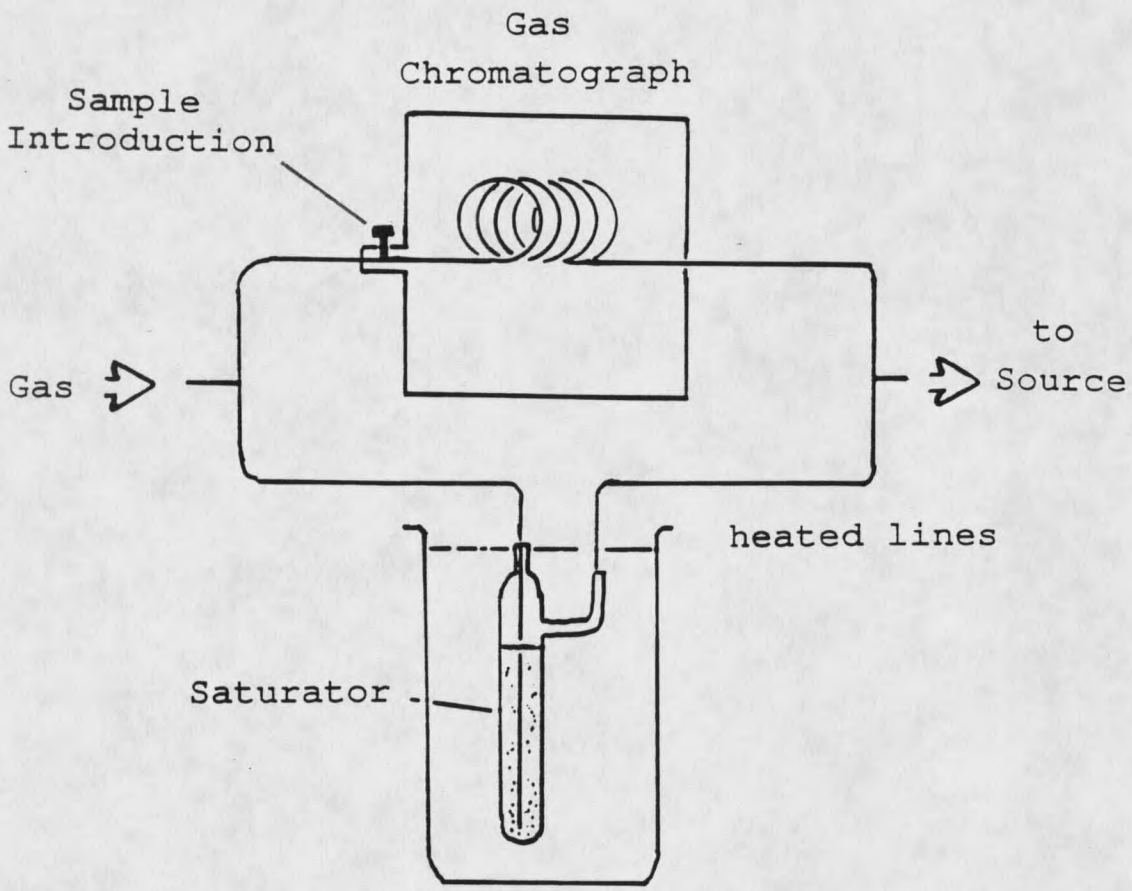

Figure 3.

Sample and Solvating Agent Introduction.
Gas chromatography eluent mixes in heated transfer lines with saturator solvent vapor stream prior to introduction into ion source. Saturator is fully immersed in temperature controlled bath. Solvating agent partial pressure is determined by relative flows, from which appropriate dilution factor is obtained.

Sampling Aperture

The mass spectral ion current results from leakage of a portion of the total ionized gas ventilated through a small aperture into an evacuated expansion chamber held at a typical stagnation pressure of 5×10^{-4} Torr (nitrogen calibrated ion gauges, KHF, Willmington, DE). Unless noted, an electroformed nickel sampling aperture with an inside diameter of 50 μm and 20 μm thickness located in the center of a 5/8 inch disk, is used for ventilative ion sampling (Stark-Veco Int'l, Brookline, MA). The leak corresponds to approximately 18 mL min^{-1} for nitrogen, corrected for temperature difference between aperture and bubble flow meter (x 423/298) for a flow of 25 mL min^{-1}. In practice the viscous flow through an aperture may be estimated (35) from

$$\text{Flow (l/sec)} = 15\ D^2 \qquad (19)$$

where D is the aperture diameter in cm. For a 50 μm aperture one calculates 23.5 ml min^{-1}.

An extensive set of measurements concerning cluster ion sampling perturbations includes work carried out with a stainless steel, 22 ± 2 μm diameter and 10 μm thick, laser drilled aperture (Optimation, Inc, Windham, NH). The flow with this aperture is predicted from equation 19 to be approximately 4 mL min^{-1}.

Expansion Chamber and Free Jet Expansion

The ions entrained in the ambient pressure gas leaking through the sampling orifice shown in Figure 2 enter directly into the expansion chamber which is the first stage of a differentially pumped vacuum envelope. The expansion chamber stagnation pressure, as mentioned above, is typically maintainable at approximately 5 x 10^{-4} Torr for nitrogen carrier gas, evacuated by an 6" Edwards diffusion pump operated with Santovac-5 oil (Monsanto). Ions entrained in the free jet expansion pass through a mach disk shock wave 3.4 cm from the aperture for a 20 μm sampling aperture, and 3.8 cm from a 50 μm aperture (from equation 3). This ion beam is then directed by a set of ion optics through a 2 mm differential pumping aperture into the second stage of the vacuum envelope. The pressure in the analyzer is typically held at a stagnation pressure of 8 x 10^{-6} Torr, evacuated by a 3" Edwards diffusion pump. Both of the diffusion pumps are backed with a single Edwards M18 two stage rotary pump, operated with Invoil 20 oil.

Ion Optics

The ion optics within the expansion chamber are comprised of three circular ion lenses shown in Figure 2, and follows a design which was guided by a combination of ion trajectory calculations by Simion (36), and trial and error for optimal ion currents. The forth lens dictates the ion transmission

energy through the mass filter described below.

Mass Analysis and Detection

The second stage of the vacuum envelope houses a quadrupole mass filter with 0-500 dalton mass range (Extranuclear,Inc, Model 162-8), and channeltron detector (Galileo Electro-Optics,Inc, Model 4039). The quadrupole filter mass resolves the ion beam, either by means of a sweep generator for linearly mass scanning the ion beam, a peak switching unit for simultaneously monitoring two ions of interest during a chromatographic run, or simply by selected ion monitoring by means of manual tuning. The mass filter is routinely operated at very low resolution in order to minimize possible quadrupole mass discrimination effects.

The channeltron detector is positioned on axis to the ion beam, and utilized for ion counting detection by means of a counting pre-amplifier which is capacitively coupled to the channeltron. The detector high voltage DC power supply (Fluke,Inc) is operated at a sufficiently high bias for a plateaued ratemeter response, which coincides with elimination of a bias favoring lower mass ions. The counting preamplifier signal is sent to a 100,000 counts sec^{-1} full-scale ratemeter (EG & G Ortec). The linear dynamic range for ion detection is from 0 to 50,000 counts sec^{-1}. Because of the slow response times associated with ion counting, mass scan rates far slower than those attainable with the quadrupole are required. This

constraint in scan rate necessitates careful adjustment of chromatographic parameters for wide chromatographic peaks in order to obtain mass spectra, when desired, which reflected a constant ion source sample concentration over the mass range of interest. Typically a scan rate of 10 to 15 amu sec^{-1} was suitable for obtaining a mass spectrum free of chromatographic artifactual effects for chromatographic peaks with 30 sec widths at half maximum. Selected ion monitoring or peak switching is performed in repetitive trials in every case to obtain reliable relative ion current measurements.

Finally the mass spectral ion signal is sent from the ratemeter in analog form to the pen of a strip chart recorder (Houston Inst.,Inc), from which all mass spectral measurements are obtained. A minimum of three trial repetitions are always secured to ensure reliability of the ion signal measurements obtained in a given study, reported as the sum average.

RESULTS AND DISCUSSION

This chapter is divided into two broad sections which follow the duel objectives of this thesis. The first half of Results and Discussion concerns the characterization of ion sampling perturbations uniquely associated with an the APIMS ion source. The remainder of the chapter will conclude with use of APIMS for study of fundamental gas phase ion chemistry.

Preliminary to characterization of ion sampling errors, it was first necessary to ensure that other components of the mass spectrometer are not causing measurement artifacts. An examination of these parameters which include the ion optics, quadrupole mass analyzer, and ion detector, is the first consideration for Results and Discussion.

Operating Parameters Characterization

The ion optics, quadrupole mass analyzer, and ion detection system have each been characterized for potential mass discrimination effects. From these investigations it was possible to establish a reliable set of operating parameters for which instrumental mass discrimination effects were minimal, so that the sampling perturbations caused by the ion source, alone, could be characterized.

Ion Optics

The focusing effect of each ion lens has been examined for potential mass discrimination effects. Figure 4a shows the absolute focusing characteristics for each ion lens. Figure 4b illuminates potential mass discrimination effects that may be associated with the ion extraction potential (lens 1), or the quadrupole mass filter ion transmission energy (lens 4), as seen by the relative ratio of two ions separated by 231 daltons. The observed variation in the ratio of these ions indicates that the first ion lens inefficiently collects ions of lower mass, and this effect is exacerbated as the lens 1 potential is decreased. This ion extraction focussing behavior is generally observed to some degree for both positive and negative ions. The issue of non-uniform ion collection is important if the API mass spectrometer is to be useful for deriving fundamental measurements. This is a subject taken up in a later section addressing mass and ion type bias effects. The quadrupole bias against higher mass ions is seen to be minimized for ion transmission energies in excess of 20 eV. Despite their absolute focusing effects in Figure 4, neither variations in lens 2 nor lens 3 potentials significantly alter the relative abundance of ions widely separated on the mass scale, and therefore do not appear to introduce focusing ascribed mass discrimination effects. High ion extraction potentials result in different focusing characteristics for maximum ion current.

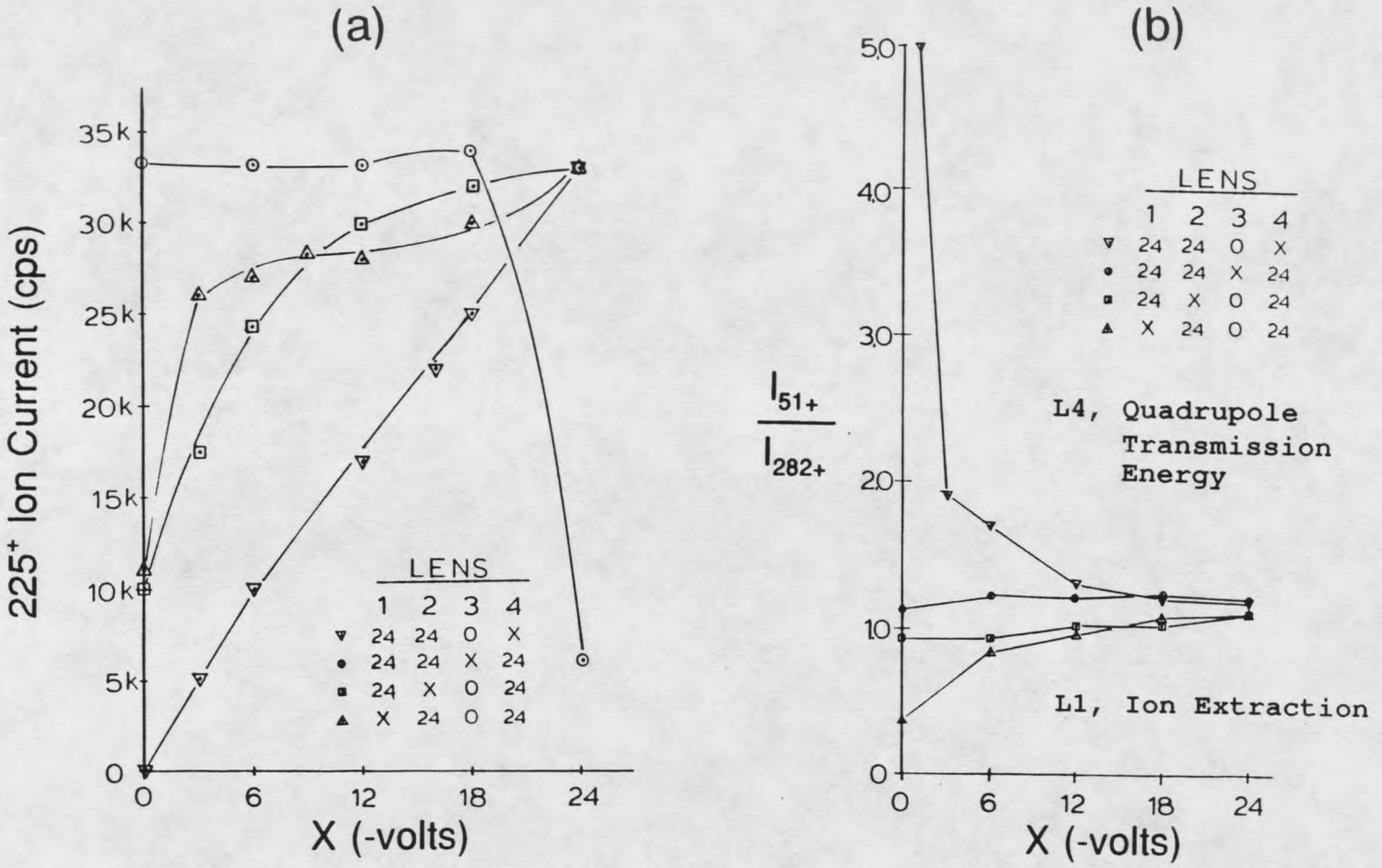

Figure 4.

a) Effect of varying individual lenses on absolute ion current.

b) Demonstration of mass discrimination effects associated with ion lenses L1 and L4. Bias against lighter mass ions occurs at inappropriately low ion extraction (L1) potentials. Bias against higher mass ions is observed at inappropriately low quadrupole ion transmission energy (L4).

Quadrupole Mass Filter

Unless indicated, the quadrupole operating parameters are adjusted for low resolution transmission of ions in order to eliminate the inherent mass discrimination effects associated with quadrupole operation at high resolution. Figure 5 shows the effects of varying resolution on the absolute intensities for several ion signals. At higher resolution the allowed ion trajectories through the quadrupole is more constrained, and ion currents are accordingly reduced. Despite the observed effect on the absolute ion currents, the relative ion abundances are shown to be essentially invariant at low resolution settings. Other quadrupole tuning effects were examined and found to be of no importance at low resolution.

Detector

Detection efficiencies are known to be more sensitive to changes in ion mass and velocity, than to variations in chemical structure (37). The importance of acceleration voltage for ion detection is shown in Figure 6. A detection mass discrimination effect which favors lower mass ions is observed at low detector voltage settings. This effect is virtually eliminated by selection of an appropriately high channeltron voltage setting. Minimization in this mass bias effect corresponds to reaching a ratemeter response plateau, which is obtained at appropriately high detector voltages.

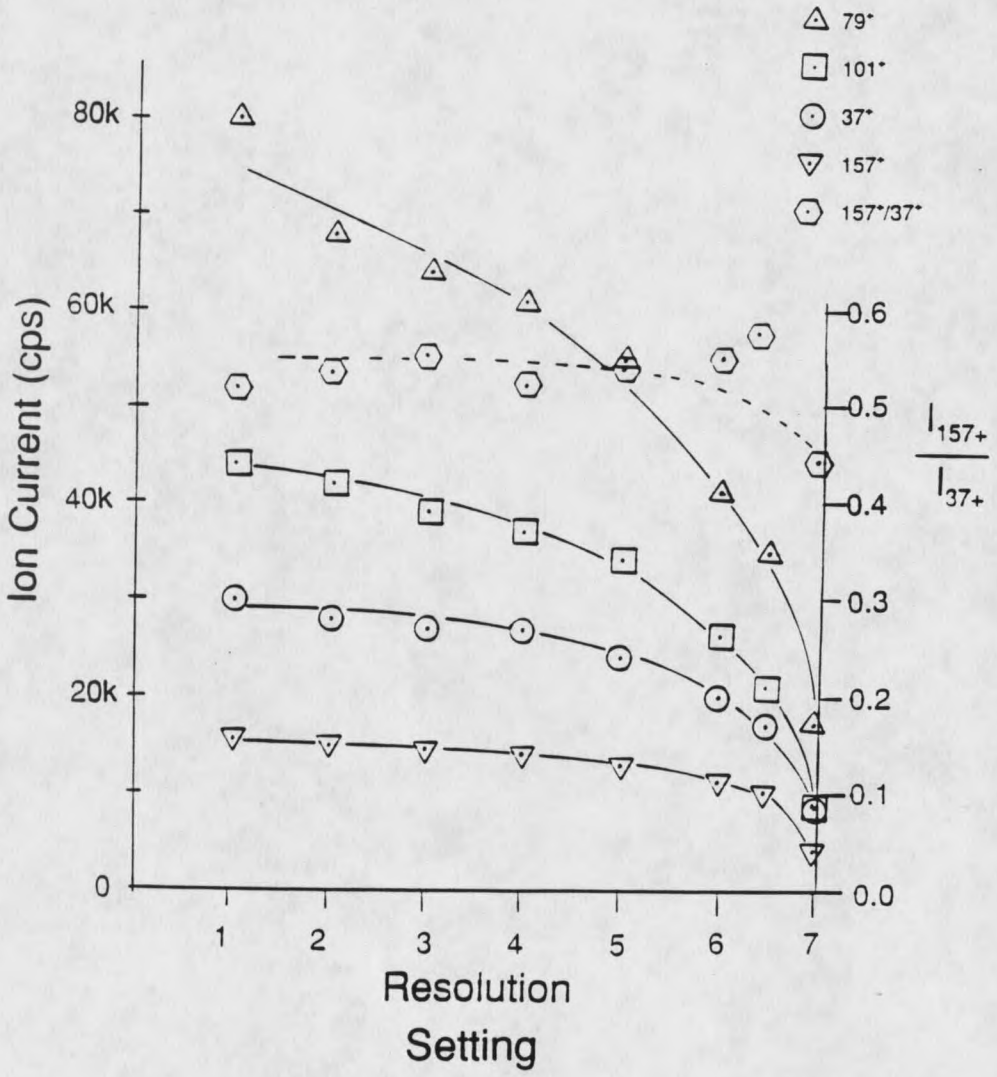

Figure 5.

Demonstration of quadrupole mass filter ion transmission resolution on observed absolute and relative ion intensities. Open symbols are absolute ion currents. Dashed line is ratio of 157^+ / 37^+ to show invariance of relative ion currents at low ($R \leq 6$) resolution.

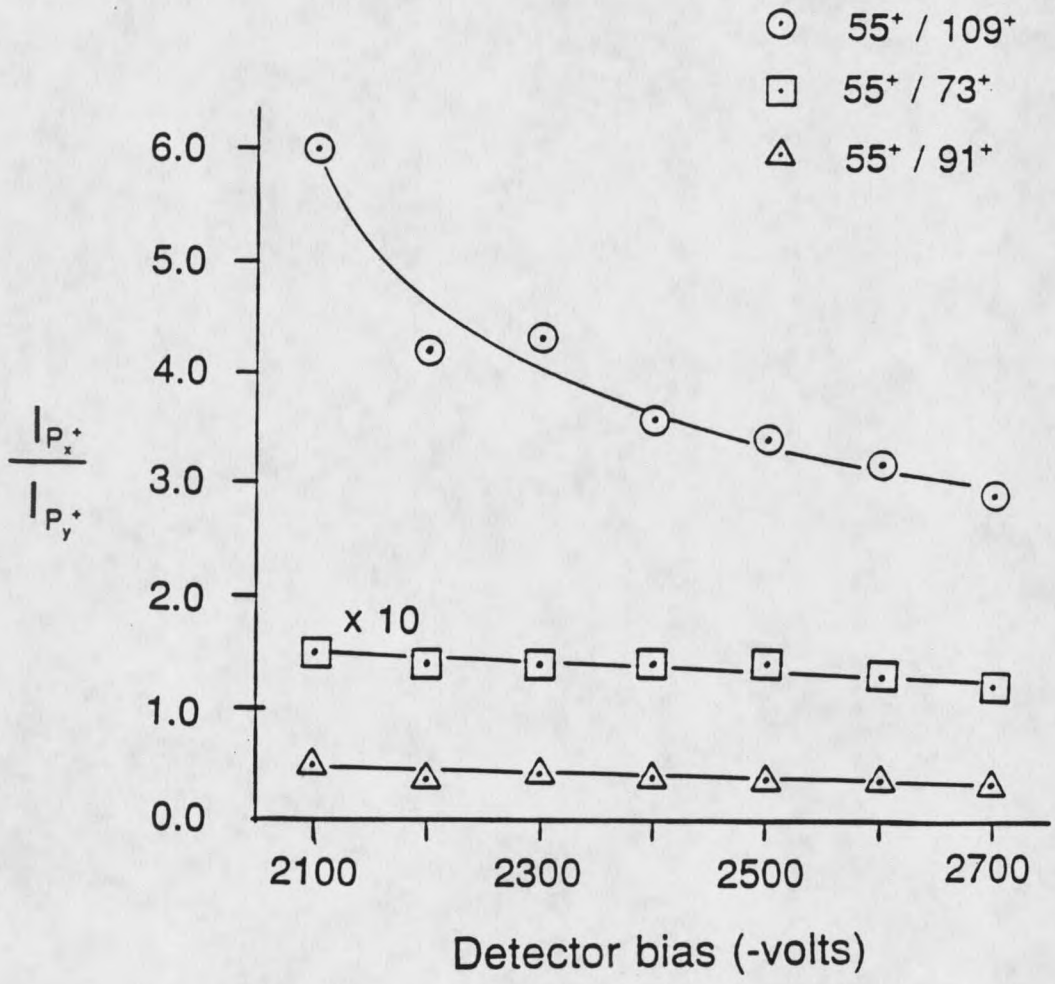

Figure 6.

Effect of channeltron detector DC high voltage setting on the observed relative abundances of various ions. It is seen that mass discrimination is negligible above a minimum detector bias. The APIMS is operated with detector bias in response plateau region to minimize detector mass discrimination effects.

Errors Encountered for Sampling Cluster Ions

Because diffusional losses are slow at atmospheric pressure, ion-molecule clustering reactions that can be readily made to occur within the API ion source are known to attain a state of chemical equilibrium, as outlined in Theory. The very high total ion source pressure also allows for high reagent concentrations not permissible in low pressure mass spectrometric techniques from which most fundamental measurements are obtained. Accordingly, equilibrium reactions which would not be favored under lower reagent concentrations are therefore possible with APIMS. Unfortunately the measurement of the equilibrium conditions within the API ion source, as sampled by an orifice or slit, is known to be problematic due to aperture non-effusive flow dynamics.

The following section will examine errors that may be encountered for sampling an equilibrium distribution of cluster ions formed by APIMS.

Hydrated Hydronium Ions as Sampling Diagnostic

The ion-molecule clustering reactions to be used for characterization of APIMS sampling errors will be the well studied proton-hydrate system. This system was first studied by Kebarle and coworkers (38) in 1965 by examining the successive clustering of water molecules to a hydronium ion, generally shown by reaction 20,

$$H^+(H_2O)_n + H_2O \rightleftharpoons H^+(H_2O)_{n+1} \qquad (20)$$

Because of the fundamental importance in the proton hydrate water clusters, numerous subsequent investigations have characterized the energetic and kinetic aspects of clustering for this system. For these reasons, the hydrated hydronium cluster ions were chosen as a well studied ion molecule clustering system with which to characterize APIMS ion sampling perturbations.

Corona Discharge Operating Parameters

In order to characterize the nature of the ion sampling perturbations caused by the ion sampling aperture of the APIMS, it was first necessary to assure that the ionizing conditions within the source truly produced a condition of chemical equilibrium. For this reason, the effects of various corona discharge ionizing parameters on APIMS signals were first systematically examined. For a given buffer gas, the corona ionization parameters include

1) the position of the corona needle tip relative to ion sampling aperture, and

2) the corona discharge current, which follows the applied voltage in a manner characteristic for each buffer gas.

By varying the corona pin tip-to-aperture distance it is clear

that ionization can be made to occur under thermodynamic, rather than under kinetic control. This feature is demonstrated in Figure 7, in which the position of the corona pin tip is varied from 1 mm to 8 mm away from the sampling aperture. It is seen that when the tip of the corona pin is kept a minimum of 4 mm away from the sampling aperture, the relative intensities of the cluster ions are unchanged, and exactly match the ion distribution observed when ionization is by nickel-63. For any chemically reacting system the observed product composition may be controlled by either thermodynamic or kinetic factors, dependent upon the allowed reaction time. The effects of kinetic control are ascribed at very short pin-to-aperture separations, because it is seen that the relative cluster ion intensities have shifted to favor the smaller cluster ions. This result appears to reveal successive ion-molecule clustering steps that are being interrupted prior to attainment of equilibrium in the ion source. It appears that the high positive polarity electrostatic fields originating at the corona pin tip are strongly accelerating all positive ions toward the sampling aperture, and thereby reducing cluster ion residence times within the source (39). Because of this effect, the corona pin tip is always positioned 6 mm away from the sampling aperture, the nearest position which mirrored the field-free nickel-63 result, so that maximal ion currents are obtained and thermodynamic equilibrium ionization

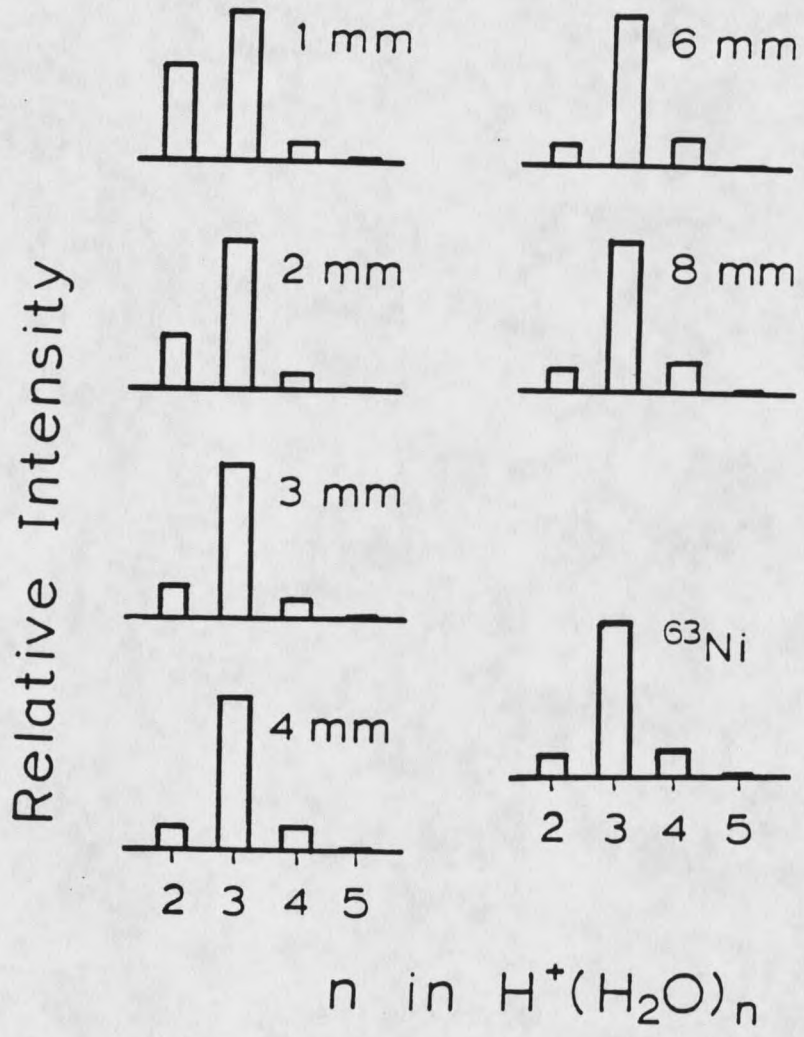

Figure 7.

Importance of corona discharge needle tip position relative to ion sampling aperture, as shown for hydrated hydronium ion clusters. Ion source temperature is 243° C, with 4.6 Torr water partial pressure. Nickel-63 ionization result is obtained when the pin-to-aperture separation is in excess of 4 mm.

conditions are assured. As described in Theory, nickel-63 β^- emission is a uniform and describable mode of ionization, and is definitely expected to lead to a condition of chemical equilibrium. The strong similarity between the results obtained in Figure 7 by means of the nickel-63 ionization mode and the corona discharge ionization result, when pin-to-aperture distance is greater than or equal to 6 mm, strongly suggests that chemical equilibrium is established within the API ion source in either of these ionizing conditions. The use of corona discharge ionization is favored in this study due to the higher total ion currents which accompany it, typically showing ion current enhancement over nickel-63 by over one order of magnitude. The stability of the corona discharge ionization is demonstrated in Figure 8 for three consecutive mass scans.

The corona discharge voltage was selected in each case so as to provide a uniform discharge current of approximately 1.5 microamperes. It was clear that mass spectral ion currents always showed gradual increases with increased corona discharge currents, finally reaching a plateau beyond 10 microamperes, but with no changes in relative ion ratios. The magnitude of the discharge current was therefore determined to be of no importance. It is perhaps noteworthy that the identity of the buffer gas significantly effected the total ion currents attainable. For example, among the study buffer

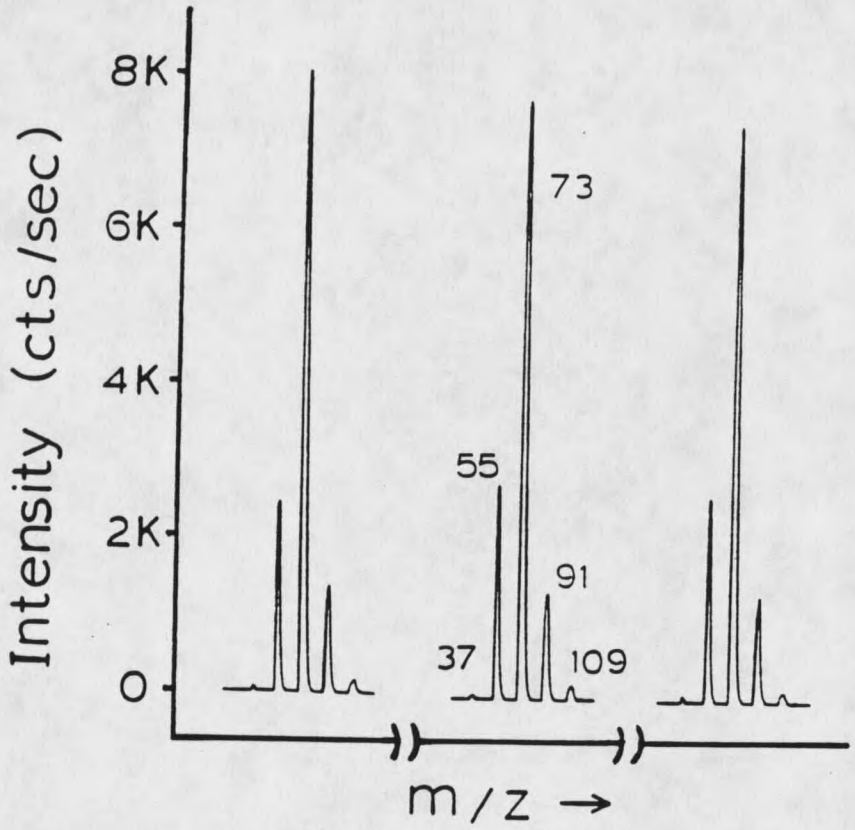

Figure 8.

Demonstration of corona discharge stability. Representative successive APIMS measurements of hydrated hydronium ion clusters formed by a 1 μA corona discharge in ambient pressure helium. The corona pin tip is positioned 6 mm from the ion sampling aperture. Ion source temperature is 200° C, with 15.5 Torr water partial pressure.

gases, methane, helium, and hydrogen provided the highest mass spectral ion currents, a characteristic that follows their relatively high conductances through the sampling aperture.

Variation in Expansion Gas, Temperature, and Aperture Diameter

It is known from the free jet expansion literature that the dynamics occurring within an expansion are also very dependent upon the properties of the expansion gas. Figures 9 and 10 demonstrate the effect of buffer gas for selected conditions of ion source temperature and partial pressure of water on the observed distribution of proton hydrates, sampled with a 22 μm diameter by 10 μm thick stainless steel aperture. Three temperature conditions are shown for two water partial pressures studied with a variety of atomic and polyatomic buffer gases which also act as the free jet expansion gases upon sampling. The uppermost cluster ion distribution shown in each figure corresponds to calculated equilibrium distributions for the indicated temperature and partial pressure of water, using the thermodynamic parameters of Kebarle (42). Since the relative rate processes occurring within the atmospheric pressure ionized gas favor fast chemistry over other ion loss mechanisms, as shown in Theory, one may expect that these equilibrium predictions represent the cluster ion distributions as they exist prior to sampling perturbations associated with the free jet expansion. A

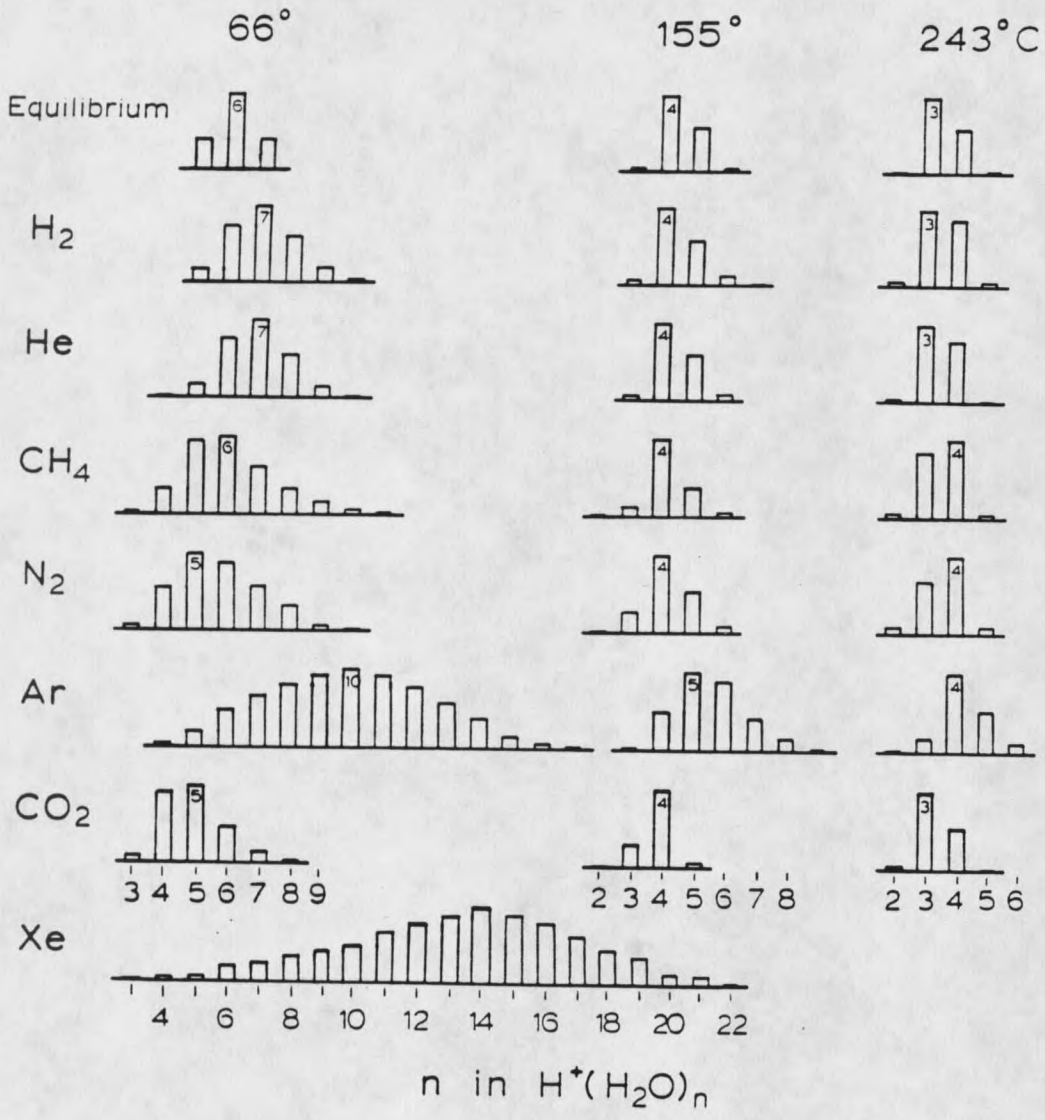

Figure 9.

Comparison between the expected equilibrium distribution of hydrated hydronium cluster ions at 18.7 Torr water and ion source temperatures of 66, 155, and 243° C, to API mass spectral measurements obtained with a 22 μm aperture for a variety of buffer/expansion gases. Corona discharge ionization with a pin-to-aperture separation of 6 mm is used for all measurements shown. Equilibrium distributions are calculated from the thermodynamic parameters of Kebarle and coworkers, reference 42.

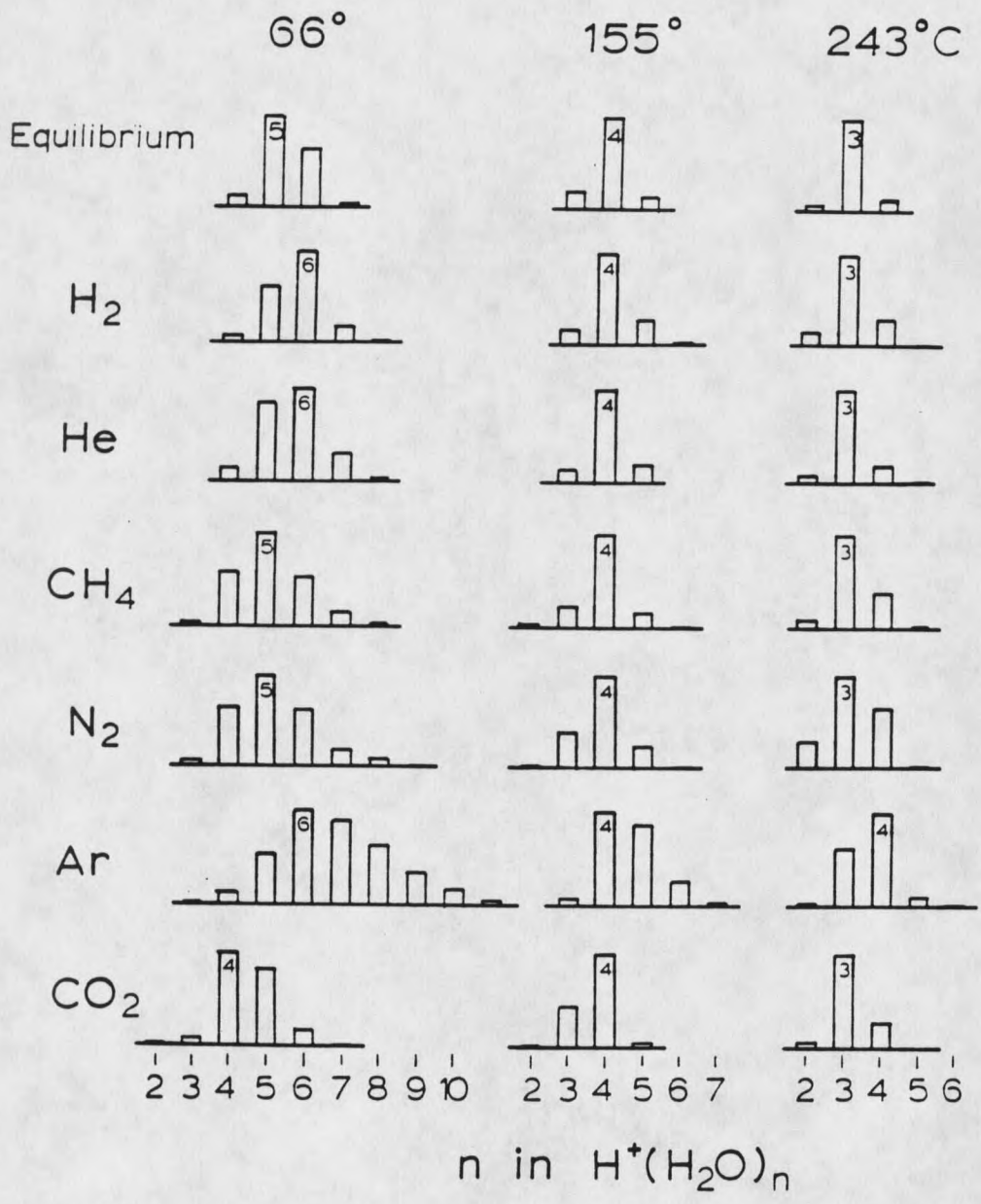

Figure 10.

Comparison between the expected equilibrium distribution of hydrated hydronium cluster ions at 4.6 Torr water and ion source temperatures of 66, 155, and 243° C, to API mass spectral measurements obtained with a 22 μm aperture for a variety of buffer/expansion gases. Corona discharge ionization with a pin-to-aperture separation of 6 mm is used for all measurements shown. Equilibrium distributions are calculated from the thermodynamic parameters of Kebarle and coworkers, reference 42.

computer algorithm allowed for convenient calculation of the equilibrium ion abundances for a given study temperature and water partial pressure.

Sampling with Noble Gases and 22μm aperture. Searcy and Fenn have also studied the hydrated proton hydrate water cluster system in a free jet expansion (40). The focus of their study was aimed toward an understanding of nucleation phenomena, and the experimental emphasis was for creating conditions which favored free jet expansion clustering events, rather than minimization of them. A later report followed from Searcy (41) providing a kinetic model for the hydrated hydronium ion clustering dynamics occurring within the jet. The proposed model with which to describe the net aggregation events ascribed to the free jet expansion cooling effects involved a cross-section for cluster and neutral association, a cross-section for collision stabilization of newly formed clusters, and a rate constant for unimolecular dissociation of excited clusters. In the model to be presented here, the growth of cluster ions is thought to occur by perturbations in the relative rates of the reactions of reactions 21 and 22 shown below,

$$H^+(H_2O)_n + H_2O \rightleftharpoons H^+(H_2O)_{n+1}^* \qquad (21)$$

$$H^+(H_2O)_{n+1}^* + B \rightleftharpoons H^+(H_2O)_{n+1} + B^* \qquad (22)$$

which both occur during the initial stages of the free jet expansion where the number density and corresponding collision frequencies are highest. Reaction 21 represents association of a neutral water with an existing cluster resulting in a vibrationally excited cluster with internal energy in excess of the current heat of hydration. The kinetics for collisional stabilization are essentially three body for smaller clusters which do not have the sufficient complexity with which to dissipate the increased internal energy provided by the enthalpy of hydration evolved upon association. For this reason the moderating influence of a third body is required for removal of this excess energy if the clustering reaction is to occur successfully. Larger cluster ions with sufficient heat capacity may not necessarily require a third body. Hence the dynamics in the earliest stages of the jet tend to progress from predominantly three body to predominantly two body kinetics. The excited (fresh) cluster ion, $H^+(H_2O)_{n+1}^*$, formed in reaction 21 can therefore be unstable against the reverse declustering reaction. The reverse of reaction 21 will occur in accordance with some time constant that will depend strongly upon the total internal energy of $H^+(H_2O)_{n+1}^*$. In competition with this declustering reaction, the excited species, $H^+(H_2O)_{n+1}^*$, may be stabilized against declustering by collision with a buffer gas molecule, B, as shown in reaction 22. In the region of the ion sampling aperture, the expansion of the gas tends to lower the effective translational

temperatures of the buffer gas and ions which are carried within its bulk flow. The metastable $H^+(H_2O)_{n+1}^*$ will have lower internal energy if formed by reaction 21 in the expanding gas. This, in turn, will increase the lifetime of $H^+(H_2O)_{n+1}^*$ against the declustering (reverse reaction 21) in the expanding gas and will increase the probability of its stabilization by reaction 22. The lower temperature of the expanding gas will also greatly decrease the population of excited buffer gas, B^* , which have sufficient energy to cause the reverse of reaction 22. These temperature related factors can therefore result in net cluster growth of the proton hydrates during transit from the ionization chamber through the aperture into the expansion chamber, primarily by decreasing the rates of the reverse reactions 21 and 22.

Amirov and coworkers have described the relative cooling efficiencies for noble gas free jet expansions (25). The efficiency of cooling within a given free jet expansion is dependent upon a number of factors, mentioned in Theory, including the initial pressure of the gas prior to expansion, the initial temperature of the gas, aperture design, molecular weight of the carrier gas, collisional cross-sections, efficiency of energy transfer, and residence time in the jet. The lowest expansion temperatures are achieved with noble gases because they have no vibrational or rotational modes. For the noble gases investigated, the efficiency of vibrational cooling follows Xe > Ar > He. Vibrational

cooling with helium is less favored due to its low collisional cross section for vibronic depopulation, resulting in less ion-molecule clustering within the expansion. The relative ordering of cluster growth observed in Figure 10 for helium, argon, and xenon is qualitatively consistent with this relative ordering for cooling efficiency. Searcy and Fenn have also observed a greater tendency for cluster growth in the proton hydrate series for expansions of argon verses helium (40).

The pronounced differences in the degree of clustering observed at 66° C for the three noble gases shown in Figure 9 can also be ascribed to at least one other factor in addition to the translational temperature in the expanding gas. The residence time in the jet influences the degree of aggregation. Longer residence times allow for more collisions therby affording increased opportunity for reactions 21 and 22 to occur. Because of velocity slip, described in Theory, it is understood that the cluster ions will experience higher collision frequencies in an expansion of a larger, heavier gas, because of the lower beam velocities and correspondently longer residence times. The residence time of ions and neutrals entrained in a free jet expansion is less for helium than for argon, and for argon less than xenon, due to their significant differences in collision cross-sections, mass and velocity. If the residence time of material in the jet is very short, the magnitude of any perturbations expected due to

very low temperature conditions will be reduced. This variation in cooling has been shown by Amirov to be important for expansions of helium.

The inefficiency of energy transfer by helium has been demonstrated by Dunbar (43). Because the efficiency of energy transfer between the helium atoms and the ions and neutral molecules is particularly inefficient, the rate at which internal energy is removed from the entrained ions and molecules will lag significantly behind the decreasing translational temperature of the expanding gas. In an expansion of helium or hydrogen there are expected to be significantly fewer collisions with the entrained proton hydrates in comparison to an expansion with argon or xenon, so that less internal energy is removed from cluster ions with less subsequent cooling and correspondingly less cluster aggregation.

With use of higher ion source temperatures in Figures 9 both the expected and observed distributions of cluster ions are shifted downward in the degree of ion-molecule cluster aggregation. In argon buffer gas, the degree of cluster growth relative to the known equilibrium distribution is much less pronounced at either 155° or 243° C, than at 66° C. At both of the higher temperatures shown in Figure 9, the ion of greatest abundance possesses only one water molecule more than the most abundant proton hydrate under the equilibrium conditions within the source. At the higher source

temperatures (155 and 243° C) with helium as the expansion gas, the degree of aggregation is seen to be in accordance with the above discussion concerning relative condensation efficiencies when compared to argon. However, with helium, observed relative ion intensities at the higher ion source temperatures are sufficiently close to the known equilibrium abundances that it appears that a reasonably accurate mass spectral measurement of the ion contents is demonstrated. This point will be returned to following discussion of the results obtained from the polyatomic expansion gases.

Sampling with Noble Gases and 50 μm aperture. Because cooling and aggregation effects are known to be proportional to the product of upstream pressure and aperture diameter (23), this parameter is also examined. It is expected that use of a larger diameter orifice will result in more pronounced condensation perturbations. To demonstrate this effect, Figure 11 shows the sampling results obtained with an 50 μm aperture. The experimental conditions employed are identical to those described for the 22 μm aperture that are presented in Figure 9. It is seen that the increase in aperture diameter indeed results in more extensive net clustering at all temperatures examined. However, the unusual bimodal contour of the cluster ion distribution observed with both argon and xenon at 66° C is indicative of increased collisionally induced dissociation, resulting in an accumulation of lower mass proton hydrate cluster ion debris.

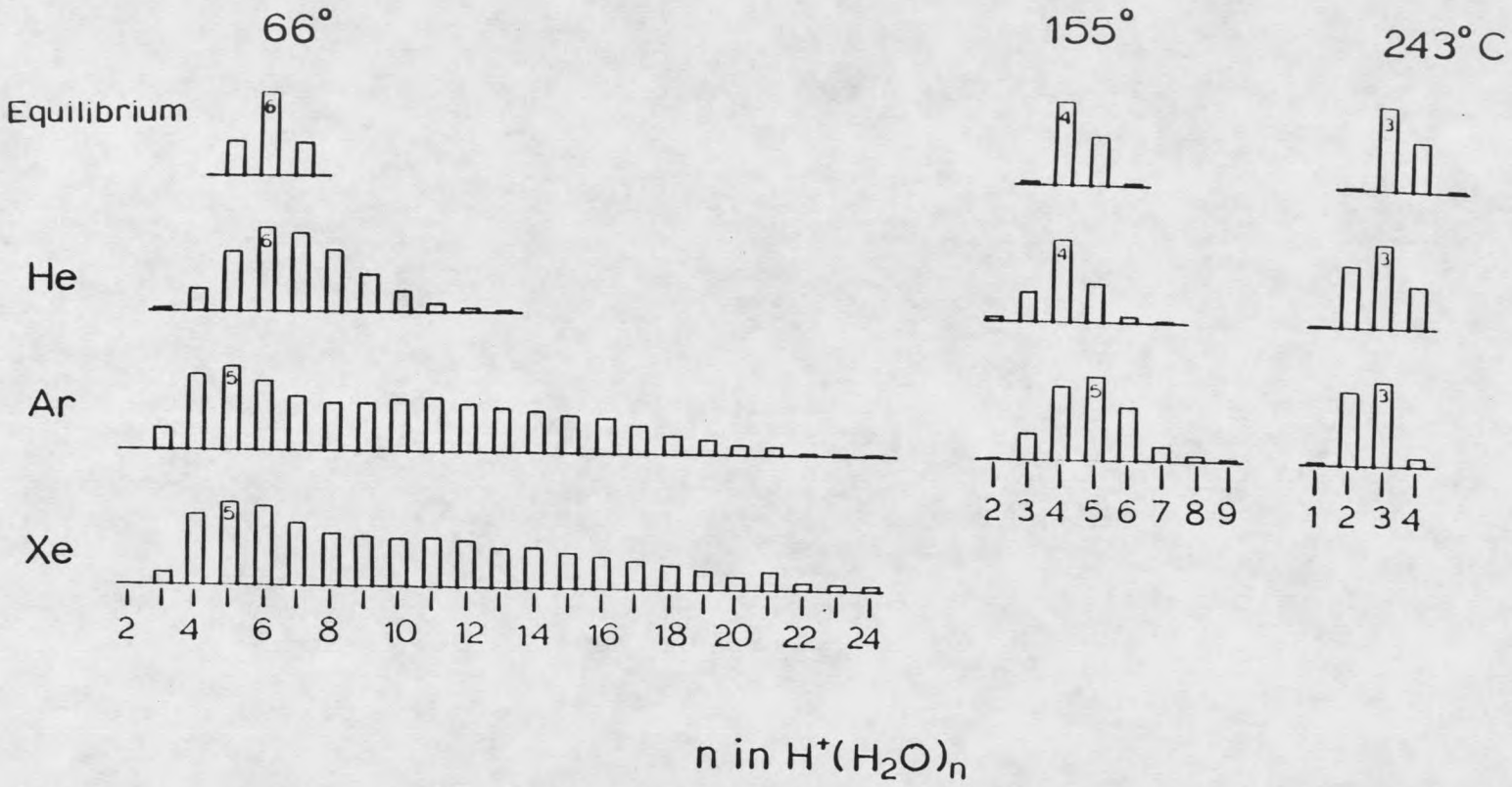

Figure 11.

Comparison between the expected equilibrium distribution of hydrated hydronium cluster ions at 18.7 Torr water and ion source temperatures of 66, 155, and 243° C, to API mass spectral measurements obtained with a 50 μm aperture for helium, argon, and xenon buffer/expansion gas. Nickel-63 ionization is used. Equilibrium distributions are calculated from the thermodynamic parameters of Kebarle and coworkers, reference 42.

This effect is consistent with an increased expansion chamber pressure observed to accompany use of a 50 μm aperture relative to that for a 22 μm aperture. This is due to the significantly enhanced mass flow for the 50 μm aperture, which increases the pumping load on the vacuum system fourfold.

Increased ion source temperature using the 50 μm aperture has a similar effect as the 22 μm aperture, seen by lowering the extent of net clustering beyond the pre-sampling equilibrium distributions. The use of helium buffer gas at the higher source temperatures again provides the least perturbation, which is consistent with the results obtained with the 22 μm aperture, despite the observed significant accumulation of cluster collision debris.

Sampling with Polyatomic Gases and 22 μm Aperture. A number of polyatomics were chosen for inclusion in this study because of their wide use as buffer gases in high-pressure mass spectrometry. The use of a polyatomic as a free jet expansion gas, as seen from the literature (21-25), is atypical for a number of reasons. The effective temperatures attainable with polyatomics are not as low as those that can be reached with atomics. This may be attributed to the higher heat capacities associated with the polyatomic internal modes of vibrational and rotational motion.

The influence of hydrogen buffer/ expansion gas is seen in Figures 9 and 10 to very closely resemble the observations obtained with helium. At the lowest temperature of 66° C,

only a modest condensation effect is noted. At the higher ion source temperatures (155 and 243° C) the observed ion signals closely reflect the known equilibrium ion distribution existing within the ion source. The same arguments for explaining the effects seen with helium are expected to hold for hydrogen, owing to their very comparable masses, and also very similar mass flow characteristics.

Cancellation of Opposing Forces. The effects of collisionally induced dissociation, which oppose those of aggregation processes will next be considered. As seen in Figure 9 and 10, two of the polyatomics, methane and nitrogen have produced sampling perturbations from the equilibrium distributions that are very similar to one another, but very different from those caused by any of the noble gases. Inspection of spectra shown in Figure 9 for an ion source temperature of 66° C and 18.7 Torr water, suggests that with either of these two buffer/expansion gases there appear to be two opposing processes operative within their respective free jet expansions. One of these processes results in net cluster aggregation beyond the equilibrium distribution, as seen by prominent cluster ions containing eight water molecules. The opposing process is leading to smaller than expected proton hydrates, as evidenced by clusters containing three and four water molecules. The general model presented above by reactions 21 and 22 may still be applied in the same manner for net cluster growth, but with additional emphasis on the

events which result in smaller than expected cluster ions. As mentioned above, the effective expansion temperatures reached in methane or nitrogen free jet expansions are known to above those possible within expansions of argon. This may partially explain why the observed clustering is more extensive with argon, in comparison to that attained with methane or nitrogen. The model proposed by Searcy includes a unimolecular decomposition path for declustering of newly formed clusters (reverse reaction 21) which may perhaps be more efficient at higher temperatures. As described in the introduction, collisionally induced dissociation can be problematic when sampling high-pressure gases (16). The static expansion chamber pressure for the apparatus employed in this study is typically in the low 10^{-4} range with the 22 μm aperture, and is comparable among the buffer gas. Collisionally induced dissociation, represented by reaction 23,

$$H^+(H_2O)_n + B \text{ ---> } H^+(H_2O)_{n-1} + H_2O \qquad (23)$$

is expected to be most probable in the mach disk shock wave regions of the jet, but may potentially occur anywhere within the expansion chamber. The energy required for collisionally induced decomposition is primarily supplied by the translational energy of $H^+(H_2O)_n$. This process has been clearly demonstrated for argon and xenon at low temperatures with a 50 μm aperture. However, it may not be apparent with

the 22 μm aperture results due to the lower expansion chamber pressures, resulting in lower probability of collisionally induced dissociation. With use of the 22 μm aperture and either hydrogen or helium as the buffer/ expansion gas, reaction 23 would be expected to be less important due to their smaller cross sections for collisional activation. To further investigate this point the expansion chamber pressure was varied to examine collisional activation effects on the proton hydrate cluster ion distribution. It was found that a tripling in the expansion chamber pressure from 1.5×10^{-4} to 5×10^{-4} Torr helium resulted in negligible increase in collision debris. In contrast, a noticeable increase in the smaller cluster ions debris is observed when the expansion pressure is doubled using nitrogen. If reaction 23 had been operative and served to cancel a tendency for cluster aggregation in the free jet expansion of the 22 μm aperture, one might have expected this increase in the helium expansion chamber pressure to result in a noticeable shift in the observed cluster ion distribution toward the smaller cluster ions. The effect is in fact evident for helium sampled through the 50 μm aperture, where the expansion chamber pressure reaches 1.1×10^{-3} Torr.

An additional test of the importance of collisionally activated dissociation is made by increasing the ion extraction energy. It is seen from Figure 12 that the proton hydrate cluster ions are progressively declustered upon

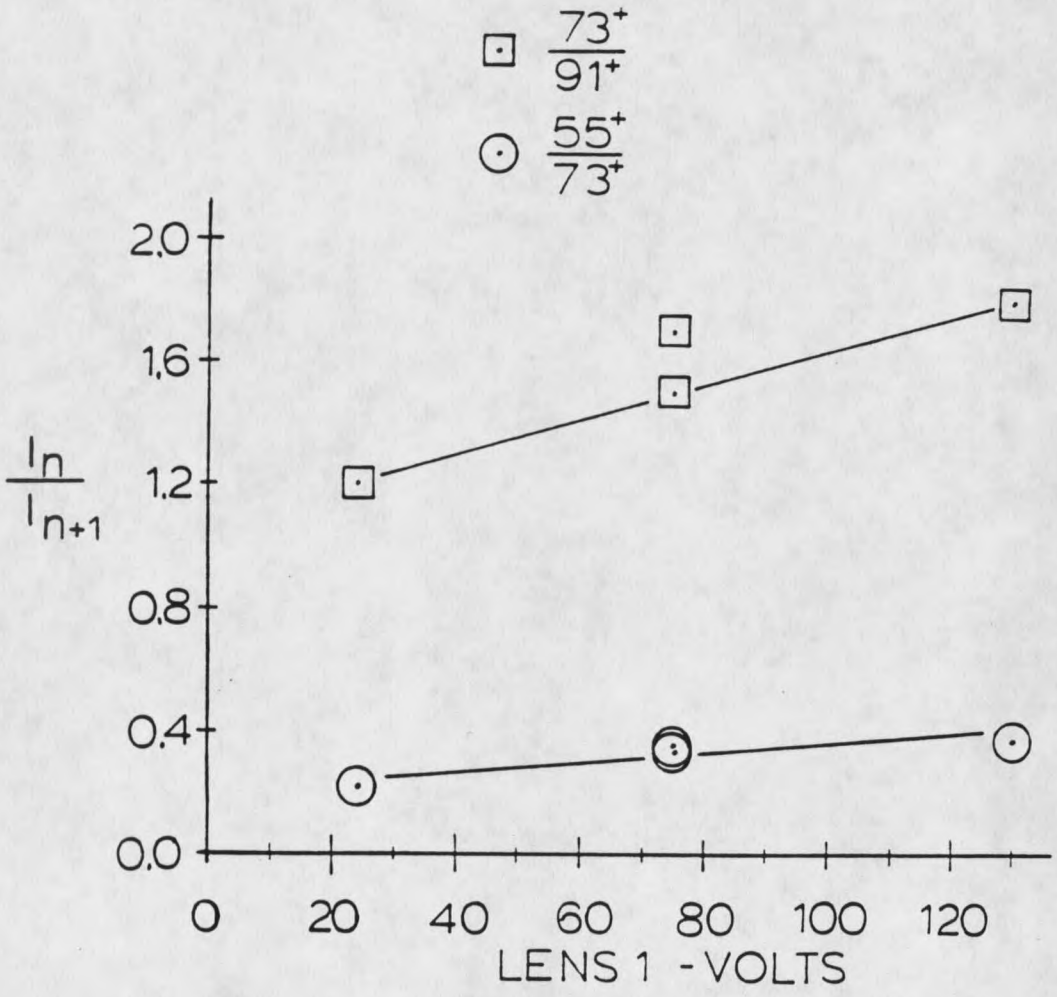

Figure 12.

Effect of ion acceleration by ion extraction potential on subsequent collisionally induced dissociation (CID) of hydrated hydronium cluster ions. Higher extraction ion energies are seen to alter relative cluster ion abundances due to CID effects with nitrogen buffer/ expansion gas.

increases in the ion extraction kinetic energy.

It is interesting to consider the results shown in Figure 9 and 10 with use of methane or nitrogen at the two higher source temperatures (155 and 243° C). It is seen that at 155° C, the ion currents observed in these gases are in close agreement with the ion abundances known to be present within the ion source under these conditions of temperature and water partial pressure. At 243° C, however, the observed ion abundances differ significantly from the known equilibrium cluster ion distribution. It appears therefore that accurate ion sampling is not occurring with use of methane or nitrogen at the source temperature of 155° C, but rather the results from methane or nitrogen at this temperature is attributable to a cancellation of the opposing perturbations that have been discussed above.

The results shown in Figures 9 and 10, in which carbon dioxide is used as the buffer gas, are similar to those just described for methane and nitrogen, but with one noticeable difference. For carbon dioxide it is the ion intensities measured at 243° C, rather than 155° C, which appear to be in close agreement with the known ion abundances. This again would appear not to be a circumstance of accurate ion sampling but as with carbon dioxide at 155° C, a result accounted for by the cancellation of opposing perturbations occurring during the sampling process.

Appearance of Accurate Ion Sampling

Following the above consideration of the variability in sampling perturbations that can be encountered for systems comprised of cluster ions involving successive clustering steps, perhaps the most interesting result is the appearance of accurate ion sampling which consistently accompanied use of helium or hydrogen with the 22 μm aperture at the two higher ion source temperatures. This point is further investigated by a careful temperature study performed employing helium as the buffer/expansion gas. Figure 13 shows the result of a temperature study from 50 to 250° C using a water partial pressure of 4.6 Torr. The smooth curves are the ion abundances present within the equilibrium conditions of the ion source, which were again calculated from the thermodynamic parameters for the proton hydrate cluster ions as measured in Kebarles laboratory (42). The plotted points show the actual ion abundances sampled through a 22 μm aperture with helium as the buffer/ expansion gas. At the higher ion source temperatures, very good agreement exists between the observed ion abundances and the known pre-sampling ion abundances. It appears that accurate cluster ion sampling is made possible when the source is maintained above 150° C, using a 22 μm aperture and helium as the buffer/expansion gas. A similar temperature study was repeated but using a much higher (18.7 Torr) partial pressure of water. The results are presented in Figure 14, which reveal the same temperature dependence for apparently accurate ion

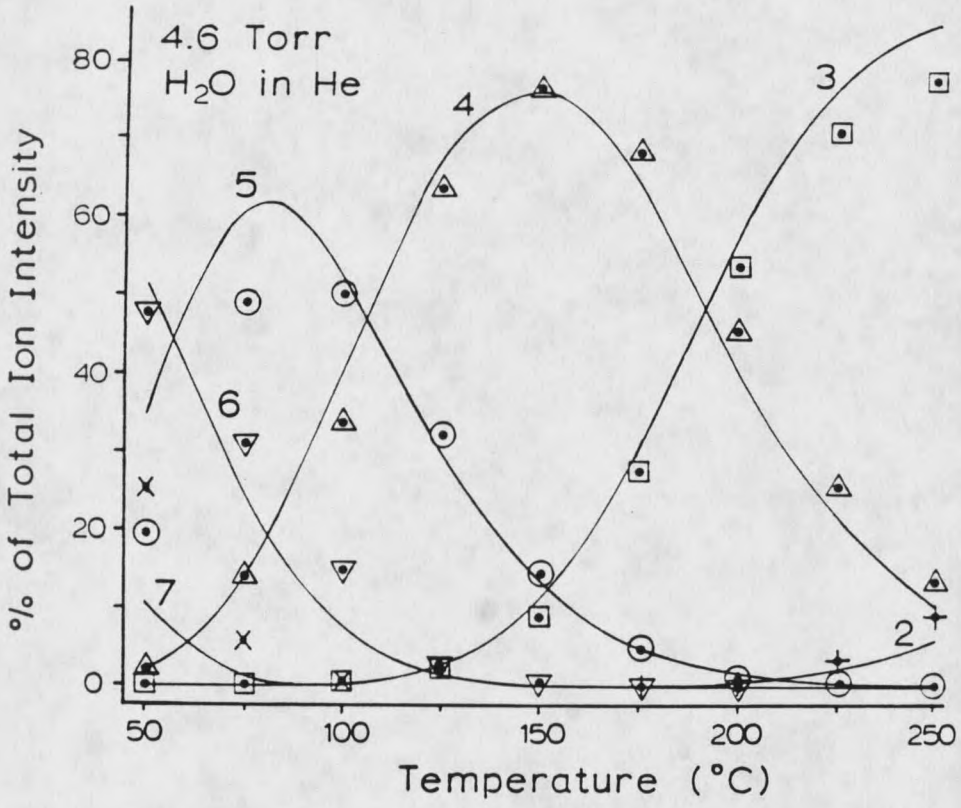

Figure 13.

Hydrated hydronium ion clusters, $H^+(H_2O)_n$, plotted as percentage of the total sampled ion current using 4.6 Torr water partial pressure as a function of ion source temperature. The data points corresponding to n = 2 (+), n = 3 (⊡), n = 4 (△), n = 5 (⊙), and n = 6 (▽), are the APIMS observations using helium as the buffer/expansion gas with a 22 μm aperture. The solid curve is the expected equilibrium ion abundance calculated from thermodynamic parameters of Kebarle and coworkers, reference 42.

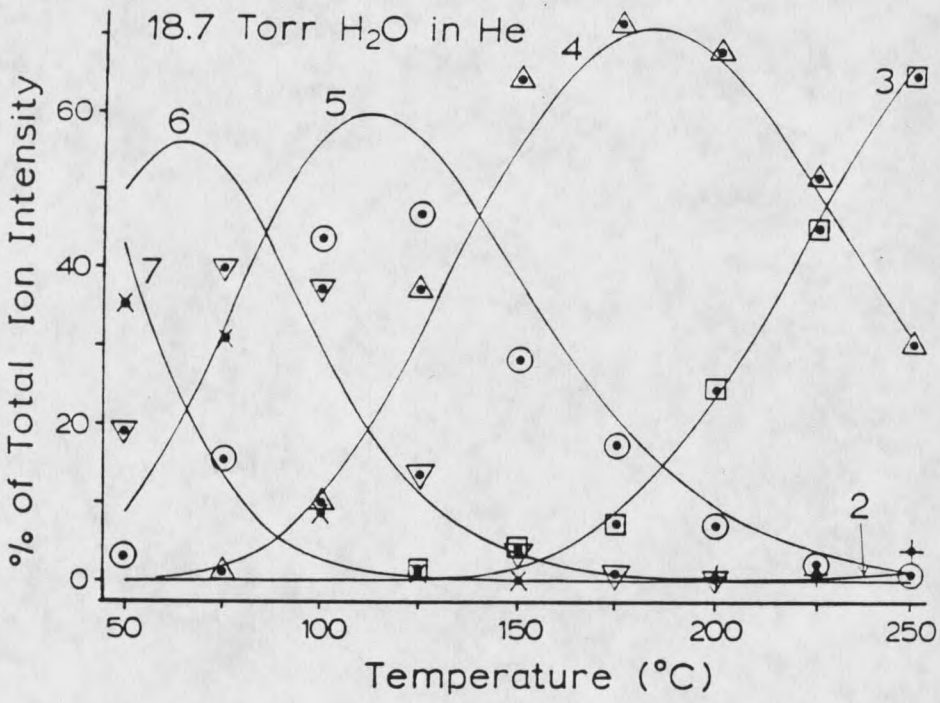

Figure 14.

Hydrated hydronium ion clusters, $H^+(H_2O)_n$, plotted as percentage of the total sampled ion current using 18.7 Torr water partial pressure as a function of ion source temperature. The data points corresponding to n = 2 (✛), n = 3 (⊡), n = 4 (△), n = 5 (⊙), n = 6 (▽), and n = 7 (✕), are the APIMS observations using helium as the buffer/expansion gas with a 22 μm aperture. The solid curve is the expected equilibrium ion abundance calculated from thermodynamic parameters of Kebarle and coworkers, reference 42.

sampling, that is, above a source temperature of 150° C, using a 22 μm aperture and helium as the buffer/expansion gas, the observations reflect the known equilibrium ion abundances. Paulson and coworkers (44) have shown that the rate coefficient for energy transfer, k_q, is inversely related to the bath gas temperature as

$$k_q \propto (T^{-1})^X \qquad (24)$$

The magnitude of the exponent, X, as well as the proportionality constant, are empirically derived. To the extent that the initial ion source temperature influences clustering events downstream in the free jet expansion, such temperature dependent energy transfer may have significance toward an explanation of the results shown in Figures 13 and 14. Other investigators have examined the merits of higher ion source temperatures toward reduction in condensation effects (45,46). The effect of increased temperature is related to an increased internal energy of the buffer gas and entrained ions which presumably provides a resistance to free jet aggregation processes.

Test of Accurate Ion Sampling. An important test of the appearance of accurate ion sampling by means of a 22 μm aperture with helium as the buffer/expansion gas at ion source temperatures in excess of 150° C, is presented in Figure 15. The ion source temperature is maintained at 200° C while the water partial pressure is varied from 2 to 16 Torr. Apparent equilibrium constants are calculated for two of the successive

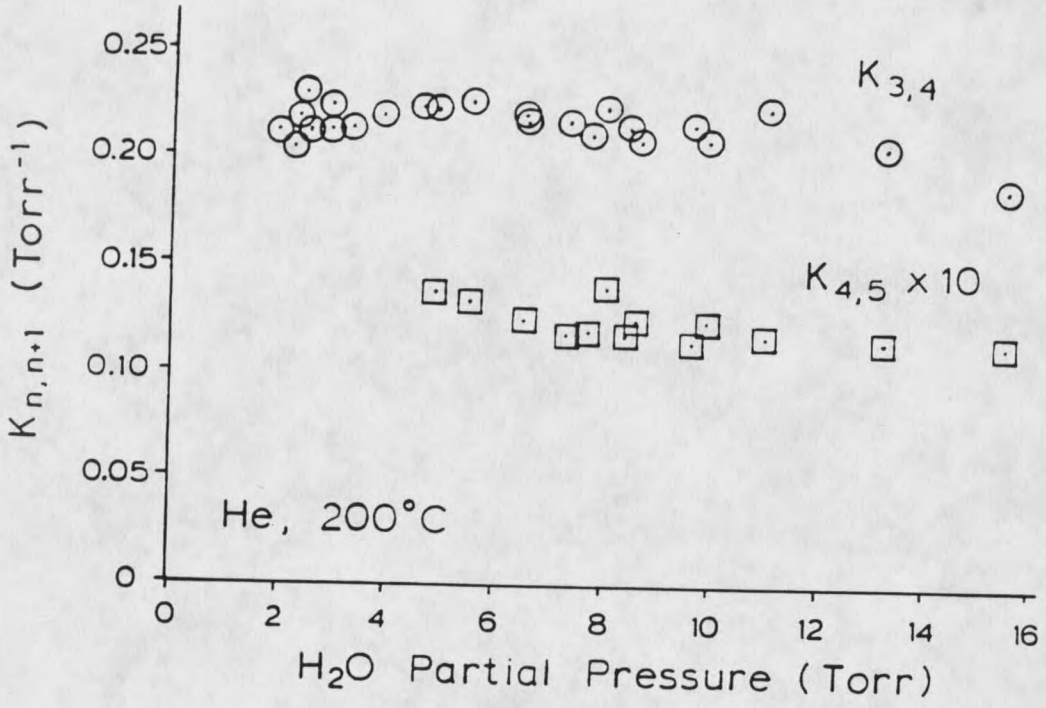

Figure 15.

Hydrated hydronium cluster ion apparent equilibrium constants obtained by application of equation (25) to APIMS measurements as a function of the ion source water partial pressure. The ion source is maintained at 200° C, and helium buffer/ expansion gas is sampled with a 22 μm aperture.

clustering reactions from the observed ion signals by means of equation 25, which is general for any clustering reaction,

$$K_{n,n+1} = I_{n+1} / (I_n P_{H2O}) \qquad (25)$$

where $K_{n,n+1}$ is the apparent equilibrium constant for addition of one water to a proton hydrate water cluster containing n water molecules, I_n and I_{n+1} are the experimentally observed ion abundances for the n^{th} and $(n^{th} + 1)$ clusters of interest, and P_{H2O} is the ion source partial pressure of water. The apparent equilibrium constants shown are calculated from equation 25 from measurements for which the ions involved in the clustering reaction constituted at least 3 % of the total ion current. A variation of water partial pressure of nearly one order of magnitude was possible for measurements of $K_{3,4}$, and a factor of 3 variation in partial pressure was possible for the measurements involving $K_{4,5}$. The redundancy of measurements at a given partial pressure of water shown in Figure 16 results from the mixing of different combinations of dry and humidified flow rates possible that result in the same water partial pressure. The measured equilibrium constants for the clustering reactions shown are seen to be independent of water partial pressure, a fundamental requirement for measured equilibrium constants. The magnitude of each measured constant is essentially equivalent to those reported by Kebarle and co-workers at this temperature, $K_{3,4}$ = 0.15

$Torr^{-1}$ and $K_{4,5} = 7.4 \times 10^{-3}$ $Torr^{-1}$ (42). The discrepancies between the apparent equilibrium measurements obtained from these APIMS sampling conditions and those from PHPMS are not unreasonable considering measurement uncertainties associated with each method. The API result for $K_{3,4}$ is approximately 0.22 $Torr^{-1}$ verses the PHPMS result of 0.15 $Torr^{-1}$. The API result for $K_{4,5}$ is approximately 14×10^{-3} verses the PHPMS result of 7.4×10^{-3}.

The evidence provided above suggests a system for investigation of ion molecule clustering equilibria that occur within the conditions of an atmospheric pressure ion source. The absence of sampling perturbations is apparent when helium or hydrogen are used as the buffer/expansion gas at higher ion source temperatures while employing a 22 μm sampling aperture. The possibility that the appearance of accurate ion sampling under these conditions is due to an accidental cancellation of opposing perturbation forces for cluster aggregation (reactions 21 and 22) and collisionally induced dissociation (reaction 23) is refuted by the experiments in which the expansion chamber pressure was tripled. Helium was observed to have minimal collisionally induced dissociation effects compared to nitrogen over upon pressure doubling. However, very high helium expansion chamber pressures can result in enhancement of cluster ion collision debris, as shown above in Figure 11.

Minimization of Sampling Perturbations

Although the physical conditions used for ion sampling in APIMS are in gross violation of the criteria normally considered necessary for the accurate ion sampling of a high pressure ion source, the results discussed above suggest that cluster ion sampling errors can be substantially minimized. This has been effected by means of smaller sampling apertures, inefficient expansion gases, and higher initial ion source temperatures. Several physical properties unique to helium are consistent with this conclusion.

1) Helium is relatively inefficient at promoting free jet expansion aggregation dynamics owing to a low heat capacity and low collisional cross-section.

2) It is known that the helium is notably inefficient at energy transfer and that this inefficiency is exacerbated at increased temperatures.

3) Because of its high self-diffusion coefficient and high aperture flow throughput, the residence times for expansion entrained cluster ions may be reduced with helium.

4) Additionally, the significant mass differences between entrained cluster ions and helium lower the Silent zone collision frequency due to velocity slip.

Capacitive-like Charging Events and Contact Potentials as Sampling Perturbations

The following section will demonstrate mass spectral ion current sampling problems that have been encountered when moderate to high electric fields are in the vicinity of the ion sampling aperture. Negative ions are notoriously difficult to sample, much more so than positive ions. Sigmond has explored the effect of aperture diameter and material on ion sampling (47). The observations to be related here are potentially important for furthering the appreciation of very high-pressure mass spectrometric sampling whenever the sampling orifice may be exposed to moderate or high electrostatic fields. These ion current limiting fields may be applied upstream from the sampling aperture (within the ionization chamber) or from the expansion chamber (vacuum side of sampling aperture).

Three general experimental conditions have been encountered which result in aperture charging events:

1) ECD anode pulsing
   (perturbation from inside source)

2) Corona discharge ionization mode
   (perturbation from inside source)

3) High Ion Extraction potentials
   (perturbation from outside source)

Internally Applied Electrostatic Fields

Figure 16 demonstrates an ion sampling effect ascribed to aperture discharging following application of periodic +50

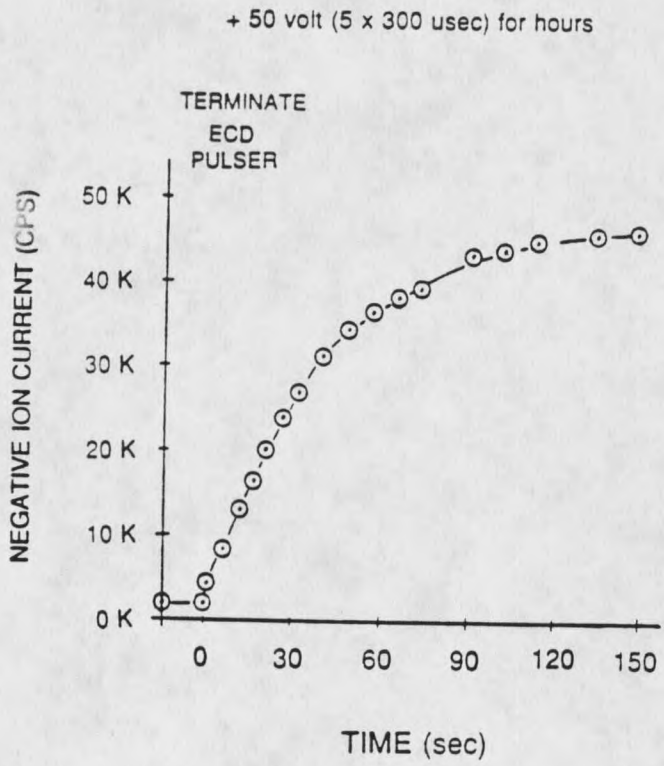

Figure 16.

Demonstration of aperture discharging period required in order to sample negative ions. ECD function (+ 50 volt pulsing) responsible for aperture charging effect is terminated at time zero. It is seen that a period of two minutes must elapse for full recovery of negative total ion current.
Ionization by nickel-63.

volt pulses (5 μsec width x 300 μsec period) to the ECD anode shown in Figure 2. It is seen from Figure 16 that during and immediately following the termination of fast ECD anode pulsing, ions cannot be sampled, presumably evidence that a discharging period must elapse prior to recovery of full ion sampling ability. The effect is seen to effectively inhibit negative ion sampling for a period of 1 to 2 minutes to reach maximal negative ion current mass spectral response after termination of ECD anode pulsing. This particular effect has been observed for APIMS sampling previously (48), and is generally ascribed to the existence of contact potentials or space charge effects. A plasma in contact with a grounded surface will develop a thin interface region within which strong electric fields may exist (49). The sampling aperture is located at the wall-plasma boundary-interface and is therefore potentially vulnerable to fields which may build in this region, and cause aperture contact potentials.

Figure 17 shows an analogous effect to that shown in Figure 16, but the aperture charging is by application of a negative corona discharge with nitrogen buffer gas while monitoring several mass resolved positive ions. The effect of a negatively biased corona discharge is qualitatively identical to the effect of termination of the ECD pin +50 volt pulsing upon sampling of negative ions described above. It is seen that a charge dissipation period must necessarily elapse prior to full recovery of ion sampling ability accompanied by

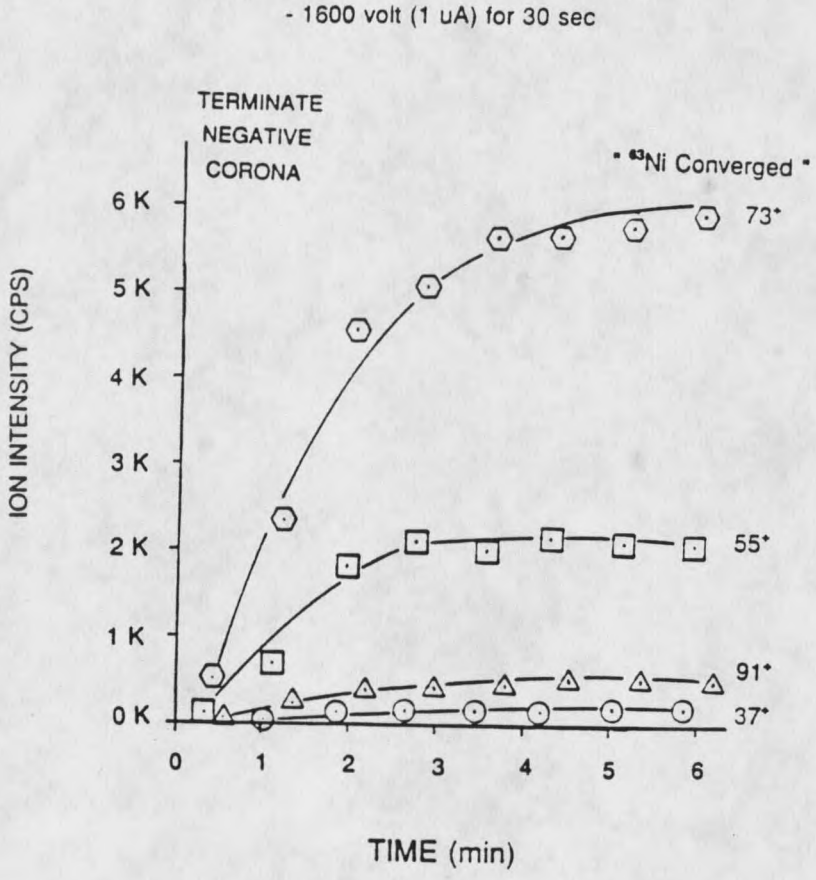

Figure 17.

Demonstration of aperture discharging period required in order to sample positive ions. Corona discharge (biased at -1600 volts for 30 sec) responsible for this aperture charging effect is terminated at time zero. It is seen that a period of six minutes must elapse for full recovery of total positive ion current, analogous to the experiment shown above in Figure 16. "^{63}Ni Converged" means the mass spectral responses have resumed to the pre-charging nickel-63 ionization results.

nickel-63 ionization. The relative ion abundances are not seen to change over the charge dissipation period. In contrast, Figure 18 shows the effect of charging due to a positive corona. The same set of proton hydrates are being sampled, and in this experiment a dynamical mass discrimination effect is observed. The shift from the nickel-63 result develops in accordance to the period of charging, i.e., application of the corona discharge. Again, a presumed charge dissipation occurs over a time period dependent upon the charging period, roughly analogous to a capacitor, prior to convergence back to the nickel-63 ionization result.

Externally Applied Electrostatic Fields

Figure 19 shows the focusing effects observed by varying the ion extraction potential between 0 and 400 volts on the absolute ion intensities of bromide and dibromide ions generated upon electron capture from 1,2-dibromohexafluoro-propane. Also shown are measurements obtained three minutes after initial adjustment of the ion extraction potential to the indicated voltage. A modest increase is observed at the a potential setting after 3 minutes, and conversely, at high ion extraction potentials, a marked decrease in ion current is observed after 3 minutes.

Figure 20 demonstrates this charge building effect in a more systematic manner. Plotted are the absolute ion intensities for bromide and dibromide which are observed to be initially enhanced upon adjusting the ion extraction potential

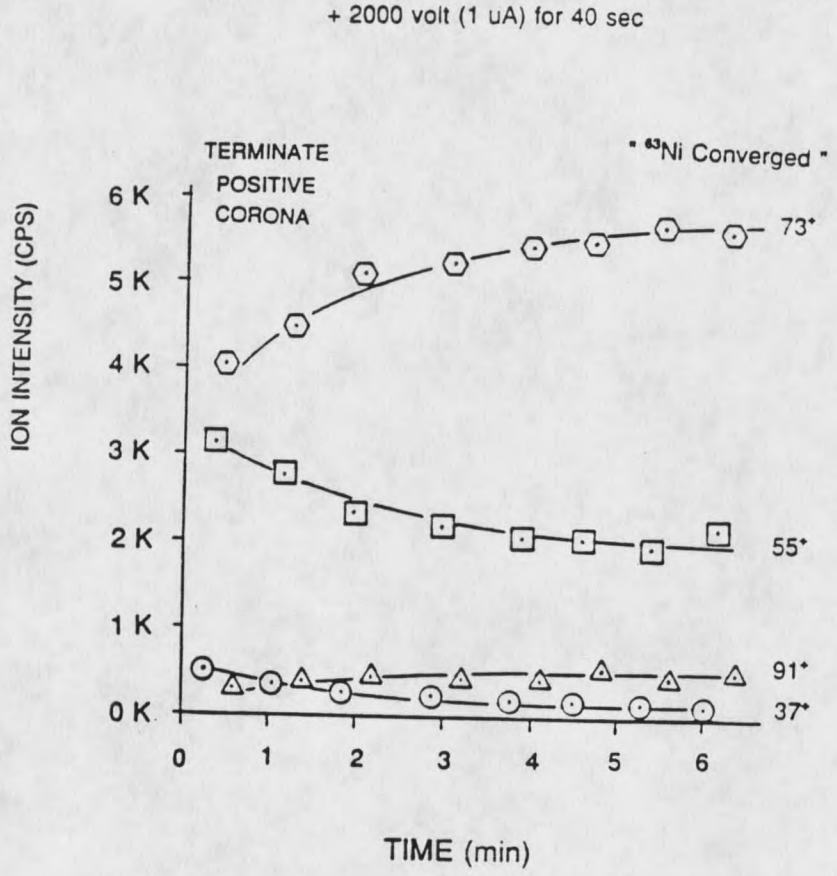

Figure 18.

Demonstration of aperture discharging period required in order to sample positive ions. Corona discharge (biased at +2000 volts for 40 sec) responsible for this aperture charging effect is terminated at time zero. It is seen that a dynamical mass discrimination effect, for which no explanation has presently been found, is operative over a period of six minutes. "^{63}Ni Converged" means the mass spectral responses have resumed to the pre-charging nickel-63 ionization results.

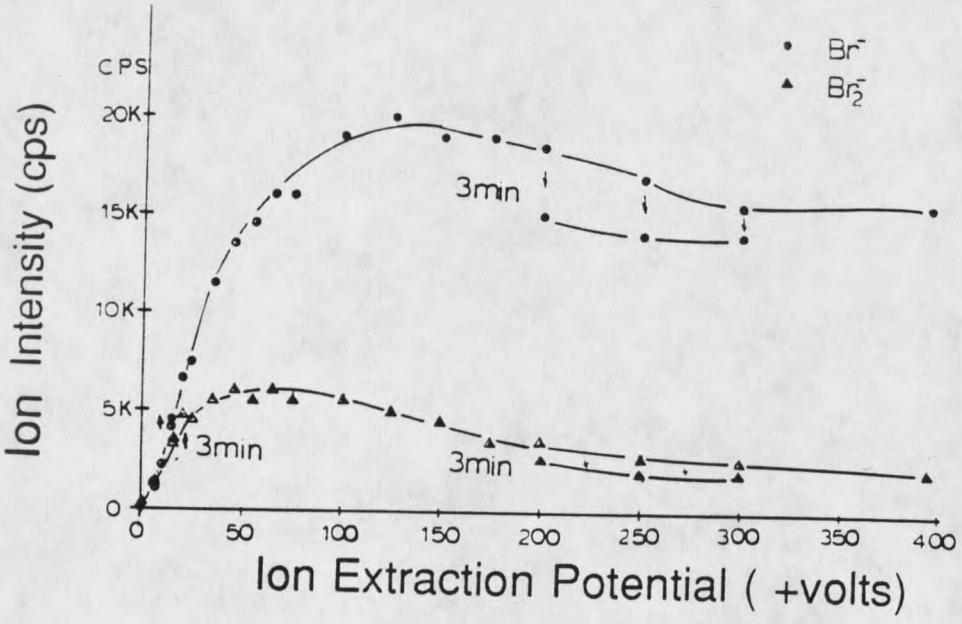

Figure 19.

Effect of increased ion extraction (lens 1) potential on ion currents of bromide and dibromide generated from 1,2-dibromohexafluoropropane. Superimposed over lens 1 focussing effects, it is seen that an aperture charging effect that inhibits ion sampling at high potentials, is building rapidly over time, as shown by the measurements taken 3 min following adjustment of lens 1 to the indicated potential.

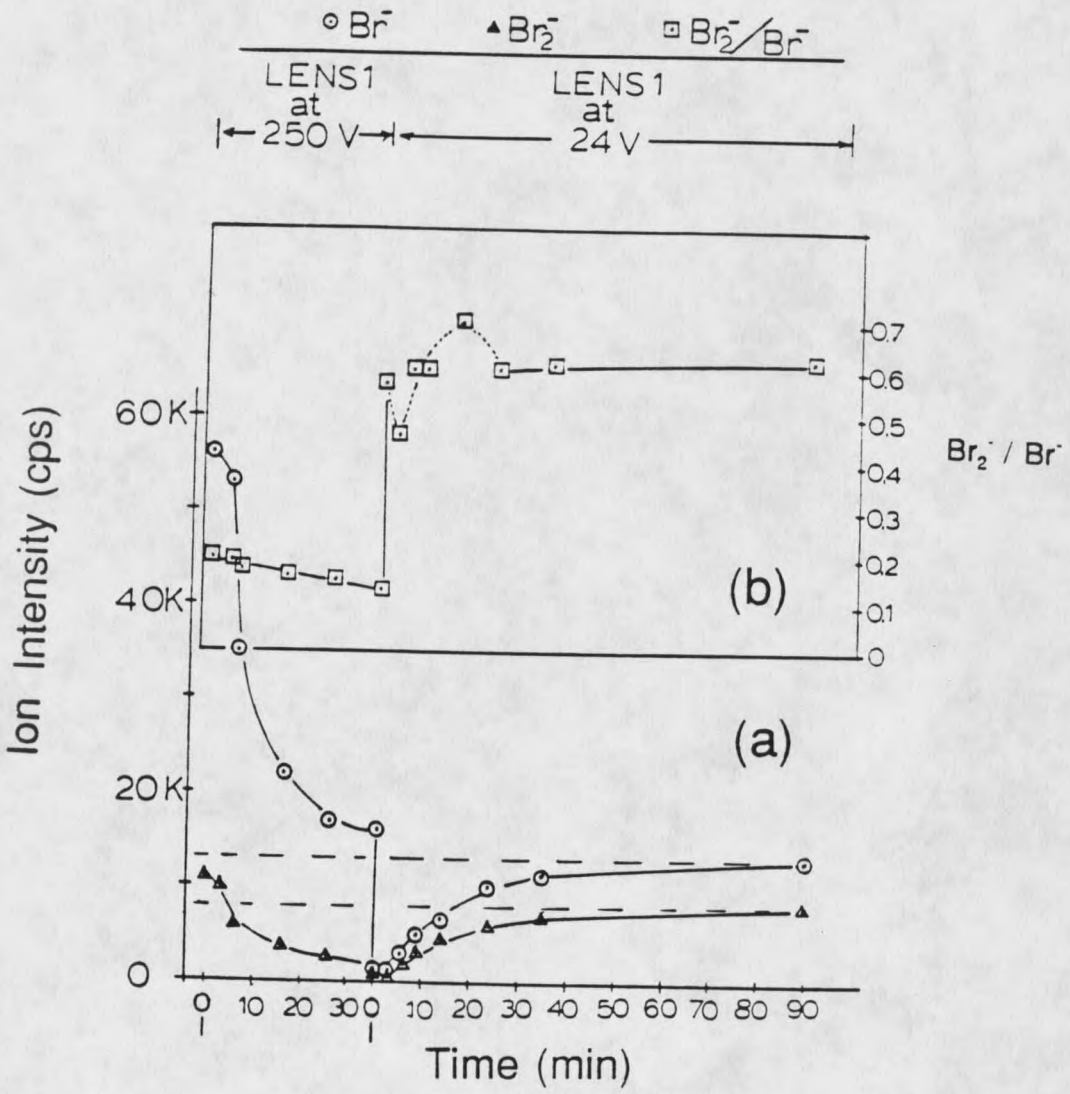

Figure 20.

(a) Demonstration of aperture charging effects caused by high ion extraction (lens 1) potential of +250 volts, applied at time zero from an initial ion extraction potential of +24 volts. Upon returning to the +24 volt lens 1 setting 35 min later, the ion currents are virtually non-existent due to sampling inhibition. Recovery to normal ion sampling occurs during an apparent aperture discharge period of approximately 40 minutes. The bromide and dibromide ions are generated from the dissociative electron capture branching reaction of 1,2-dibromohexafluoropropane.

(b) Relative ratio of the two ions (Br_2^- / Br^-) over the course of the experiment described in (a). It is seen that charging phenomena may influence the observed relative ion currents of interest.

(lens 1) from +24 to +250 volts. This significant change due to the increase in the lens 1 potential is immediately followed by a decay in the absolute intensity for each of the two ions shown. After 35 minutes the ion extraction potential is readjusted from +250 to + 24 volts. This is concomitant with loss in the ion currents until a period of approximately 40 minutes have elapsed, for recovery of ion currents to the normal +24 volt lens 1 levels (dashed line in figure). Also shown in Figure 20 are the relative intensities of dibromide to bromide, illustrating an ion extraction potential dependent mass discrimination effect. This effect is due to a non-uniform efficiency in ion extraction from the free jet expansion, a subject that will be closely examined in the next section of Results and Discussion.

The aperture charging and charge dissipation effects are presented for three halide ions in Figure 21. The chloride, bromide, and iodide ions are generated from very large samples of carbon tetrachloride, dibromomethane, and methyl iodide, respectively, so that nearly all of the available ion source ionization is transferred to the single ion of interest as these compounds individually elute through the ion source. The dashed lines show the non uniform absolute ion currents obtained for the halides, indicating a mass discrimination effect ascribed to imperfect ion sampling. If ideal or perturbation-free ion sampling were occurring, then the

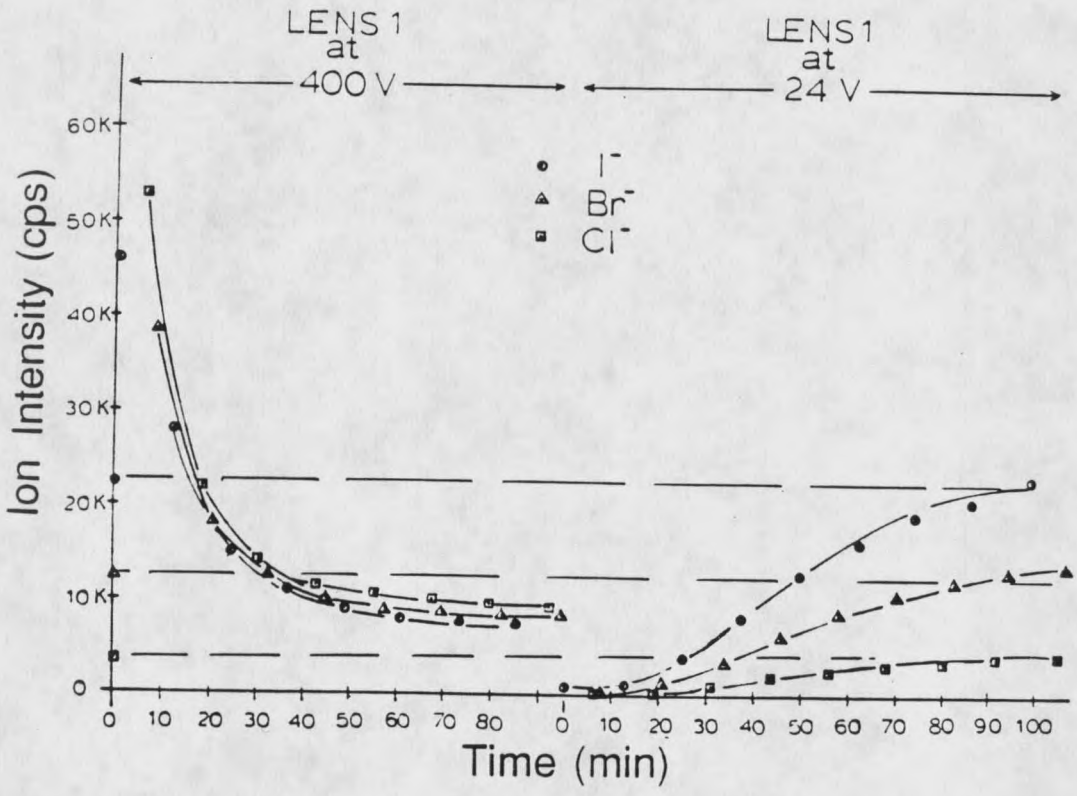

Figure 21.

(A) Demonstration of aperture charging effect which inhibits ion sampling caused by high ion extraction (lens 1) potential of +400 volts, applied at time zero from an initial ion extraction potential of +24 V. Upon returning to the +24 volt lens 1 setting 95 min later, the ion currents are virtually non-existant due to sampling inhibition. Recovery to normal ion sampling occurs during an apparant aperture discharging period of 95 minutes. The chloride, bromide, and iodide ions are generated by dissociative electron capture of nearly ion source saturation samples of CCl_4, CBr_2H_2, and CH_3I, respectively.

absolute intensities of these different mass ions would be identical. Instead, lower mass ions can be seen to be less efficiently extracted from the free jet expansion than higher mass ions. Again it is seen that initial increases in the ion extraction potential (+24 to +400 volts) are accompanied by enhanced ion currents for the halide ions. But immediately following this marked enhancement in ion currents, a gradual decay ascribed to aperture charging is manifested, after 60 minutes bringing the ions into a region of convergence whereby the relative ion intensities are very near unity. This would indicate a sampling condition has been attained for which a uniform relative efficiency in ion extraction is achieved, but at some expense of the absolute ion currents for bromide and iodide.

It seems apparent that this observed capacitive-like aperture charging behavior coincides with a reduction in the effective aperture ion sampling diameter, resulting in diminished, but more uniform, ion currents for bromide and iodide. It seems reasonable that the effective sampling diameter for chloride is also reduced, but a relative gain in the extraction efficiency for chloride from the jet results in the overall enhanced chloride ion current. Following the readjustment of the lens 1 potential from +400 volts back to the initial setting of +24 volts, the ion currents are all lost, but again they slowly recover to the normal +24 volt levels as the aperture dissipates charge acquired from the ion

extraction electrostatic fields.

The question of uniformity in ion extraction in the region of ion current convergence after application of +400 volts (Figure 21) is examined more closely in Figure 22. This plot shows the mass spectral ion currents for the three halide ions as a function of ion mass-to-charge ratio, m/e. Perfectly uniform ion sampling, free of mass discrimination effects, would provide equivalent ion currents for identical sample sizes, regardless of the mass of the ion. Figure 22 shows data obtained from Figure 21, 60 and 85 minutes following application of the high (+400 V) ion extraction potential of lens 1. The plot indicates an improved ion sampling uniformity compared to the relative ion abundances from low ion extraction potentials, but mass discrimination has not been eliminated as seen by the non-zero slope. Furthermore, the dynamical effects of aperture charging on the absolute ion currents is still observable 85 minutes after application of the increased ion extraction voltage.

Avoidance of Sampling Perturbations due to Aperture Charging Effects

It has been demonstrated by the above examples that dynamical capacitive-like charging and discharging events may be operative in influencing the absolute, and in some cases relative, ion currents obtained by aperture sampling whenever moderate to high electrostatic fields are present. Electrostatic fields applied from either side of the sampling

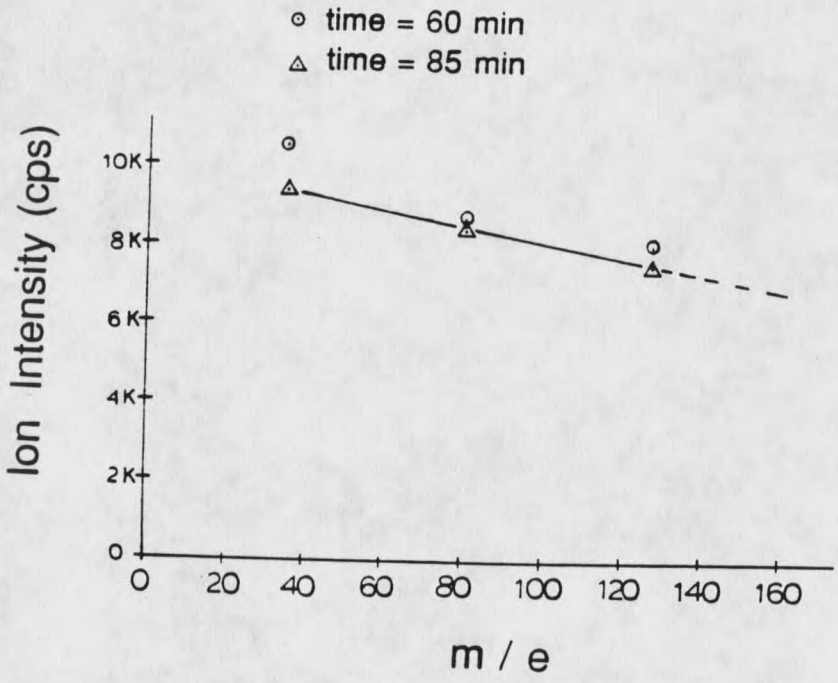

Figure 22.

Mass Discrimination Curve for charged aperture.
The chloride, bromide, and iodide near saturation ion currents, (from Figure 21) following application of +400 volts to lens 1 after 60 (⊙) and 85 (△) minutes, are plotted as a function of ion m / e. It is apparent that mass discrimination is minimized under this high ion extraction potential sampling condition, despite the overall reduction in ion currents relative to those using +24 volts shown in Figure 21.

aperture may be implicated in sampling perturbations which are manifested by reduction or loss of mass spectral ion currents. Therefore caution must be taken in use of ionizing discharges, repellers, or other electric field producing elements within the API source that may be positioned very near the sampling orifice. Also the use of very high ion extraction potentials outside the sampling region may be accompanied by aperture charging events that can reduce or eliminate mass spectral ion currents.

Mass and Ion Type Sampling Errors

A very significant and problematic feature associated with sampling from the API ion source, briefly considered in the above section, concerns the system mass discrimination against lighter mass ions. This form of sampling error is of particular importance if relative ion abundances, as they exist within the ion source, are of interest. An earlier report by Kim and Grimsrud recognized a source of mass bias observed to exist between chloride and bromide mass spectral responses (50). Sampling errors against lower mass ions have been noticed to exist within other free jet expansions and is often attributed to a tendency for higher momenta ions to retain on-axis trajectories during sampling, whereas the lighter mass (lower momenta) ions are less prone to remain so, and are assumed to be more effectively sprayed or scattered off-axis (12). The result is a preferential enrichment of

larger mass ions into a sampling acceptance cone dictated by the ion optic electric field contours within the expansion chamber. The concept regarding a preferential radial movement of lighter mass neutral species outside a free jet expansion, with subsequent enrichment in heavier mass neutral species, has previously been challenged. Fenn concluded that the cause of the relative inefficiency to sample lighter mass species in a free jet expansion is attributable to imperfect free jet expansion sampling, and that particular enrichment effects are dependent upon the associated method of sampling (51).

Figure 23 provides an example of the severity of this sampling error for APIMS. The electron capture API mass spectrum of 1,2-dibromohexafluoropropane is shown for low and high ion source sample concentrations. For sufficiently large sample concentrations, bromide ion formed by dissociative electron capture of this compound may attach to a neutral parent molecule to form an adduct ion, $(M + Br)^-$. From inspection of Figure 23 it is apparent that ion sampling is grossly non-uniform for ions on extremes of the mass scale. This is seen from the loss of bromide signal due to adduct formation which is not proportional to the increase in adduct ion between the two sample concentrations shown. The increase in the bromide adduct ion current is seen to be exaggerated by approximately a factor of seven beyond that which might be

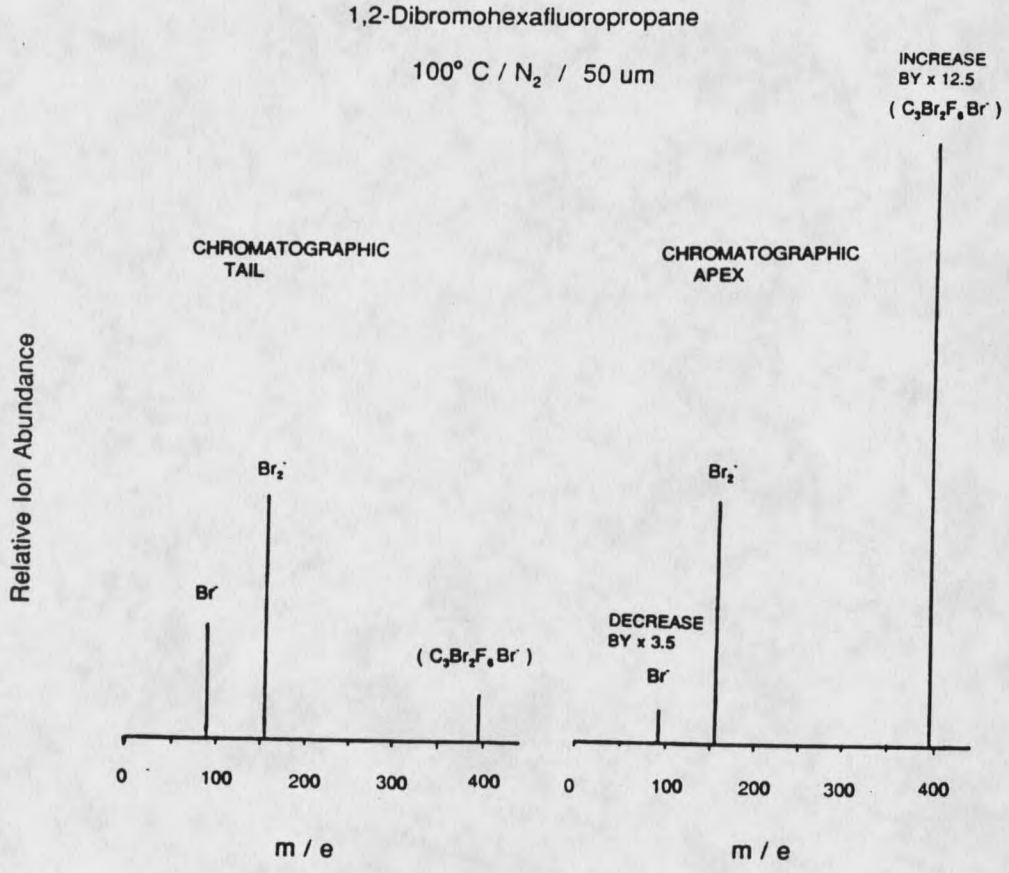

Figure 23.

Demonstration of non-uniform sampling efficiency for ions of widely differing mass. The two API mass spectra shown are for low and high ion source concentrations of 1,2-dibromohexafluoropropane at 100° C with nitrogen buffer/expansion gas. Sampling is by means of a 50 μm aperture. A mass discrimination effect is seen from the disparity between bromide and bromide adduct ion currents for the two sample concentrations.

expected based upon the decrease observed in the bromide ion current.

The method for examining sampling related mass discrimination effects to be described below is based upon conversion of the total negative ion current available within the ion source to one ionic species of interest. This is possible with a nickel-63 type ion source because in the limit of large ion source analyte concentrations, only a finite amount of analyte ionization is possible, regardless of the ionizable species identity. This is effected by means of introduction of a saturation quantities of material, that are in excess of the total negative reagent ion population, which within the APIMS source is comprised of superoxide hydrates, $O_2^-(H_2O)_n$, and thermalized electrons. The relative sampling efficiency for a given mass ion can then be observed. Figure 24 demonstrates the approach to ion source saturation as seen from the mass spectral ion currents for a range of ions with different mass-to-charge ratios, m/e. The Cl^-, Br^-, I^-, SF_6^-, and $C_7F_{14}^-$ ions shown were generated by the electron capture of carbon tetrachloride, dibromomethane, methyl iodide, sulfurhexafluoride, and perfluoromethylcyclohexane, respectively. The minor $(M-F)^-$ ions formed from sulfurhexafluoride and perfluoromethylcyclohexane are disregarded, since they comprise less than 5% of the ion current for these two compounds. The relative mass spectral responses are plotted as a function of effective ion source concentration,

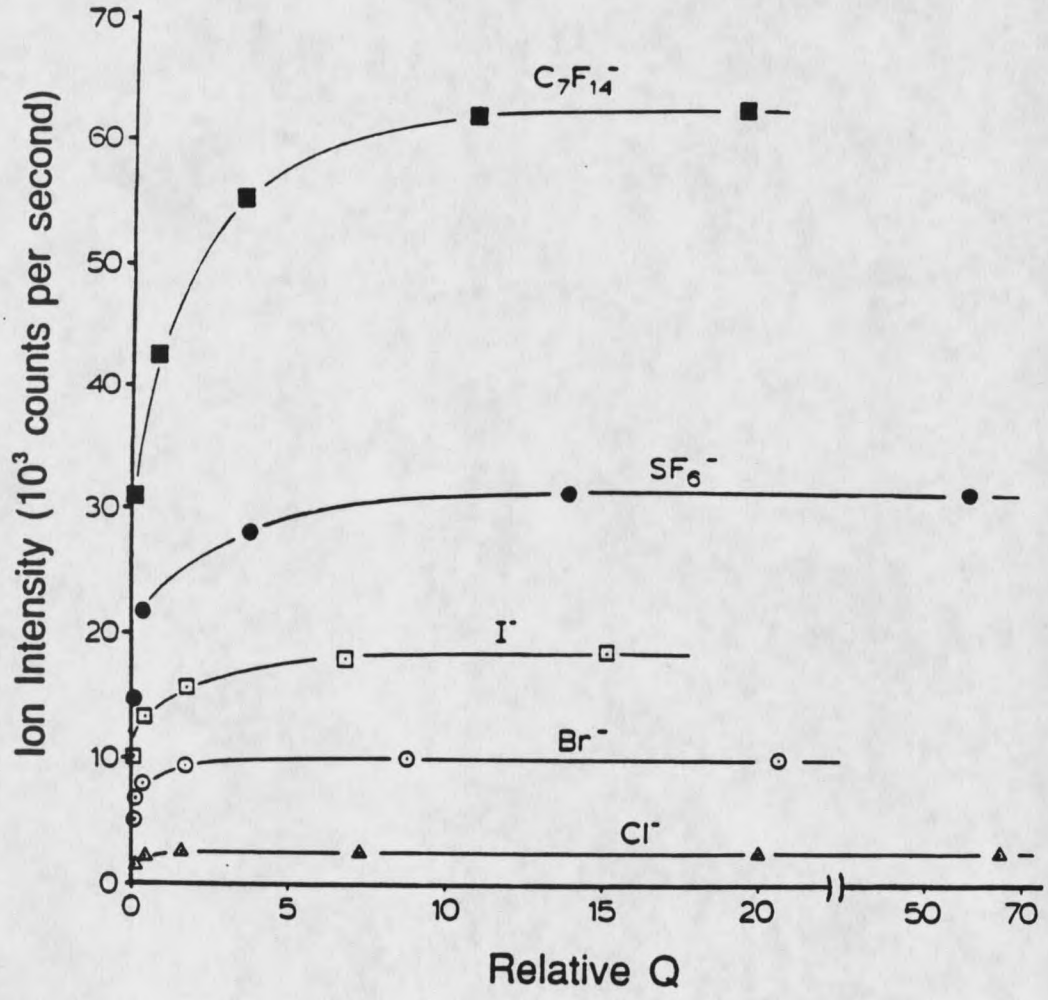

Figure 24.

Approach to ion source saturation. The plateau regions correspond to sufficiently large sample sizes which effectively consume the total available ionization which is thereby transferred to one desired ion. Relative Q (equation 26) represents the total effective concentration of a particular electron capturing species by taking into account sample size, electron attachment rate coefficient, and eluent chromatographic spreading. A significant mass discrimination effect is demonstrated by the varying magnitudes for the plateau APIMS saturation responses. The buffer gas is nitrogen, the ion source temperature is 150° C, and sampling is by means of a 50 μm aperture.

or relative Q. This is a term that accounts for the molar quantity of ionizable material introduced, its electron attachment rate coefficient, and for the eluent chromatographic spreading, as shown by equation 26,

$$\text{Relative Q} = (g \times k_e) / (MW \times PW) \qquad (26)$$

where g is the quantity of compound introduced in grams, k_e is the rate coefficient for electron capture, MW is the compound molecular weight, and PW is the eluent chromatographic peak width at half maximum. The electron attachment rate coefficients in units of $cm^3\ sec^{-1}$ used in equation 26 are CCl_4 (3.7×10^{-7}) (52), CBr_2H_2 (1.6×10^{-7}) (53), CH_3I (1.8×10^{-7}) (53), SF_6 (4.5×10^{-7}) (52), C_7F_{14} (1.3×10^{-7}) (53). The calculated relative Q values shown in Figure 24 are normalized to chloride, for which a relative Q of 5, sufficient for total ion source saturation, corresponds to approximately 80 nanograms of material introduced into the ion source.

All subsequent experiments in this section regarding mass and ion type bias will involve API mass spectral saturation responses in which all of the available ionization is transferred to one ion, whereby the non-uniformity in ion extraction from the free jet expansion may be examined. For assurance that ion source saturation is indeed attained, samples with relative Q values in excess of 15 were utilized by introduction of 3 ppt gaseous samples in 1 mL aliquots,

corresponding to low microgram quantities of material.

Figure 25 is a mass discrimination curve obtained in nitrogen at 150° C for sampling with a 50 μm aperture showing relative mass spectral responses from ion source saturation samples of the various ion producing analytes. All ion currents have again been normalized to the chloride response. The X's correspond to the saturation responses from 1,2-dibromohexafluoropropane, which dissociatively captures an electron by either formation of bromide or dibromide ion. The estimated dibromide point arises from comparison between the bromide response from this compound (X) and that of dibromomethane, which has only one predominant dissociative electron capture channel. Since the bromide response from 1,2-dibromohexafluoropropane is approximately half that from dibromomethane, the observed dibromide point (X) is half what it would be if it were the sole electron capture product. Therefore, doubling the dibromide saturation response from this compound (X) provides an additional point that can be included on the mass discrimination curve (circle). It is seen from Figure 25 that a fairly linear relationship exists for the simple atomic and diatomic halide ions, but the complex polyatomic molecular anions appear to form a line of differing slope and intercept. This may potentially indicate differences in the channeltron detector response characteristics for ion structural details. Alternatively, the polyatomic curve may indicate that molecular anions are

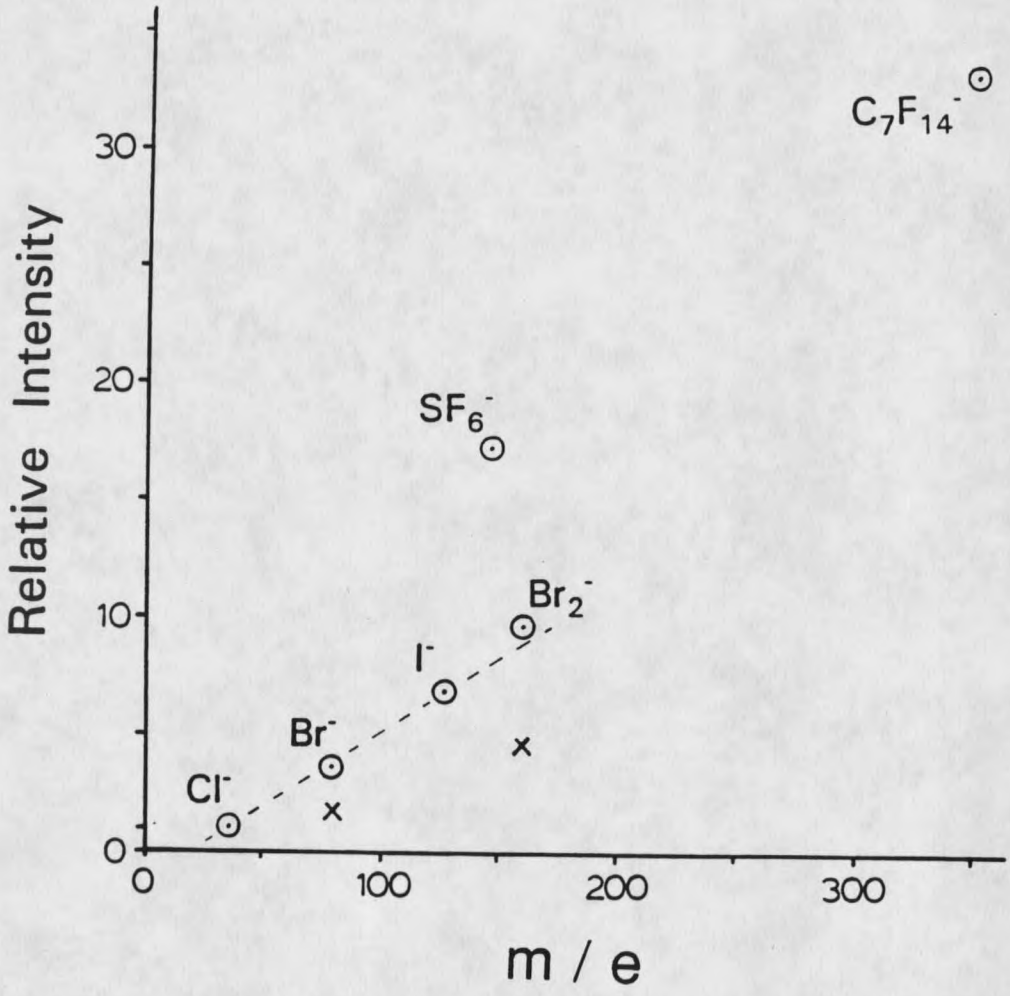

Figure 25.

Data presented in Figure 24 from API saturation responses, normalized to chloride and plotted as a function of ion mass-to-charge ratio, m/e. The buffer gas is nitrogen, and the ion source temperature is 150° C. The X's correspond to the saturation responses from 1,2-dibromohexafluoropropane, which dissociatively captures an electron by either formation of bromide or dibromide. The estimated dibromide point (circle) arises from comparison between the bromide response from this compound and that of dibromomethane, which has only one dissociative electron capture channel. Note how polyatomic sampling appears to be preferred.

sampled more efficiently, perhaps due to their larger cross-sectional area for collisions that allows them to be more effectively entrained within the free jet expansion, relative to the simpler ions. Support for this later explanation has been seen from experiments designed to test the degree of scatter for all of these mass discrimination study ions. It has been observed that the polyatomic anions SF_6^- and $C_7F_{14}^-$ are more prone to signal attenuation attributed to collisional scattering upon increases in the expansion chamber pressure. It is interesting to observe that polyatomics appear to be more efficiently sampled from the free jet expansion. This effect may perhaps be explained by larger collisional cross sections that allow for preferential entrainment on-axis within the free jet expansion.

Effect of Ion Extraction Potential

Figure 26 shows the importance of ion extraction potential on the slope of the mass discrimination curve for nitrogen buffer/expansion gas at an ion source temperature of 150° C. It is seen that a low lens 1 voltage sharply accentuates the non-uniformity in the relative mass spectral responses to API saturation responses, against the lighter mass ions. It should be noted that electrostatic lenses do not focus on the basis mass-to-charge ratio, but rather on ion kinetic energy. The location in space one ion has relative to that of another is also an important factor. The experiments demonstrate that absolute ion currents of heavier mass ions

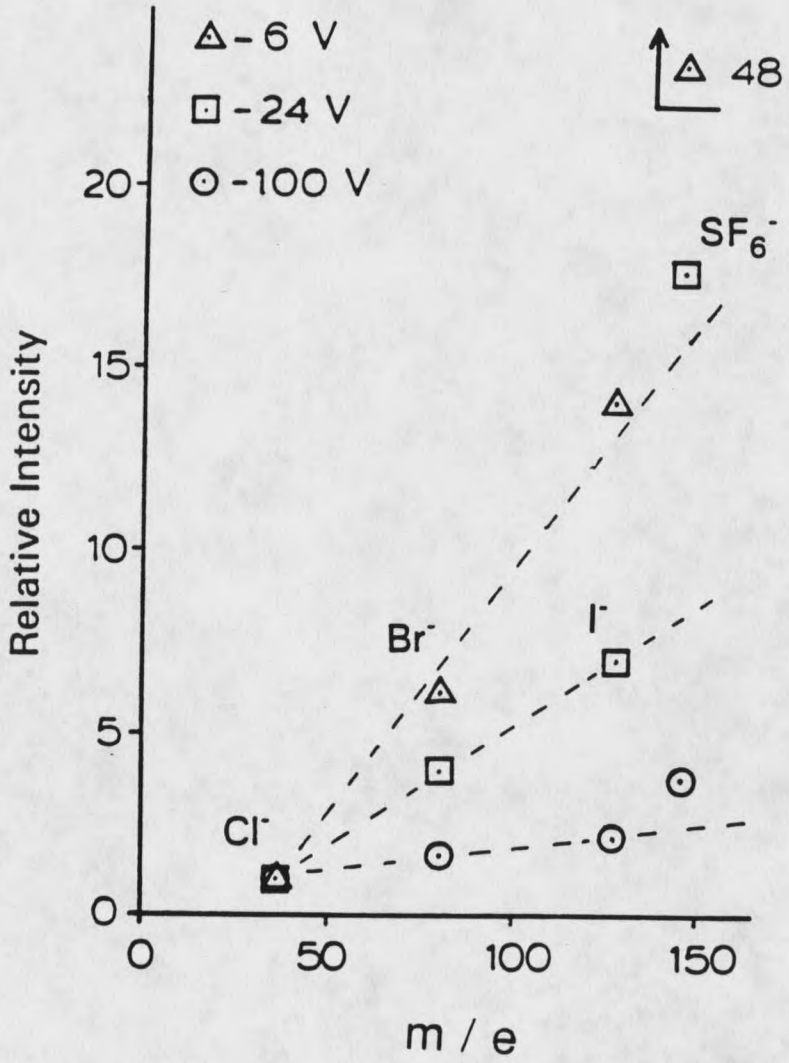

Figure 26.

API saturation responses at varying lens 1 ion extraction potentials, normalized to chloride, and plotted as a function of ion mass-to-charge ratio, m/e. The buffer/expansion gas is nitrogen, the ion source temperature is 150° C, and sampling is by means of a 50 μm aperture. The increasing slope shows that the relative inefficiency for extraction of lighter mass ions is greatly exacerbated at progressively lowered lens 1 settings.

are, by comparison to the lighter mass ions, quite insensitive to the ion extraction potential. Figure 26 also shows that the higher lens 1 potentials greatly improve the uniformity in relative efficiency for ion extraction, as is seen by the slope of the +100 volt mass discrimination curve. The indications are therefore that larger mass ions have preferred on-axis trajectories over lighter mass ions which tend to be scattered off-axis much more extensively.

Effect of Ion Source Temperature

The effect of ion source temperature was empirically found to be of importance in determining the relative efficiency of ion extraction from the jet. Figure 27 shows mass discrimination curves obtained in nitrogen at 100, 150, and 200° C. As seen by the decreasing slopes of the mass discrimination curves , the non-uniformity in sampling is slightly minimized by use of a lower source temperature. A correlation between aperture flow and ion source temperature is of potential significance toward an explanation of this effect. Figure 28 shows aperture flow measurements obtained by monitoring the vacuum system backing pump effluent with a bubble flow meter. The reliability of this method for monitoring aperture flow is supported by two independent means. The first is by measuring the rotary backing pump effluent. When the diffusion pumps are isolated from the vacuum envelope there is essentially no detectable flow (0.5 to 1 ml min^{-1}, maximum, due to foreline leaks). Upon exposing

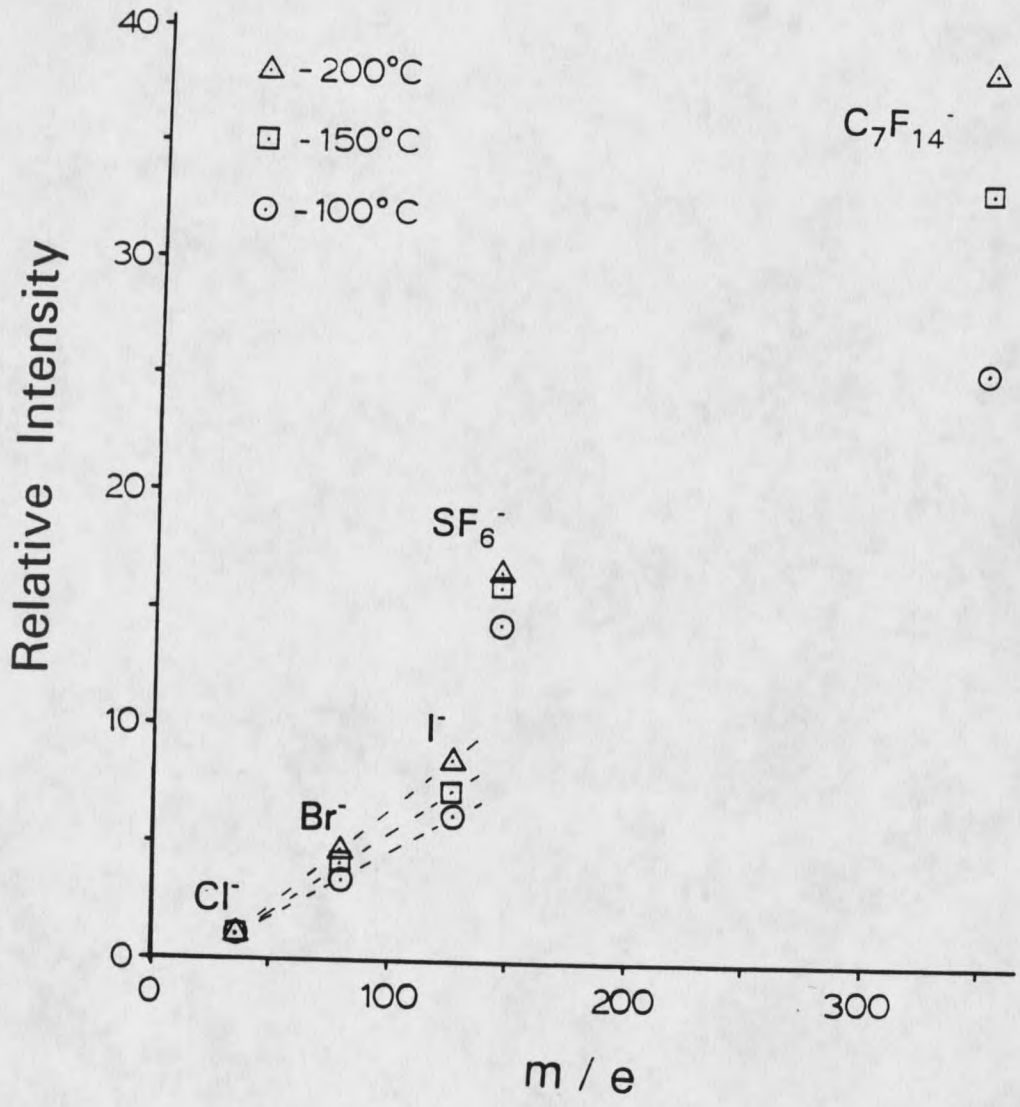

Figure 27.

API saturation responses at three ion source temperatures, normalized to chloride, and plotted as a function of ion mass-to-charge ratio, m/e. The buffer/expansion gas is nitrogen, and sampling is by means of a 50 μm aperture.

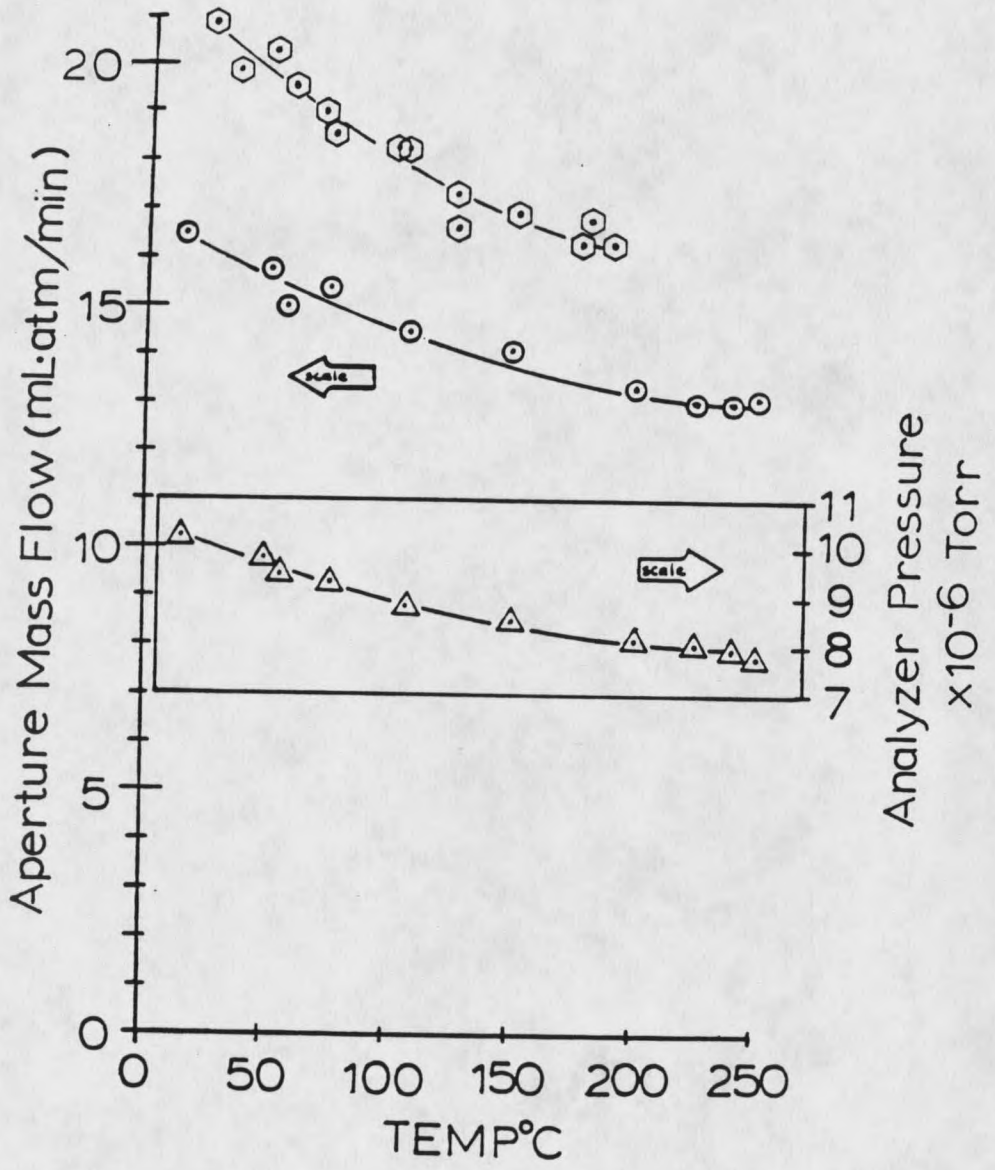

Figure 28.

Aperture flow measurements and analyzer vacuum pressure plotted as a function of ion source temperature with argon buffer/ expansion gas for sampling with a 50 µm aperture. The argon flow (circles) and analyzer pressure (triangles) measurements were collected over a period of hours. Nitrogen flow data (hexagons) collected over a period of months is also shown.

the diffusion pumps to the vacuum envelope, and hence aperture leak, the pump effluent is measured. The vacuum envelope has been leak tested, and the pump effluent is considered to be a direct measure of the aperture mass flow. A second check on the aperture mass flow is obtained by comparing the ion source effluent line flow when the vacuum envelope is vented verses being evacuated. When vented there is no pressure differential across the aperture and all of the ion source gas will flow out through its effluent, or gas out line, shown in Figure 2. However, when the vacuum envelope is under vacuum, the decrease in flow through the source effluent is taken as a measure of the flow lost through the aperture into the expansion chamber. Both of these measures of aperture flow are identical.

Since the location of flow (heated ion source) differs in temperature from the location of flow measurement (ambient temperature of backing pump effluent), it is expected that the flow measurements shown in Figure 28 should be corrected for temperature difference. However upon doing so, by multiplication of flow by a (T_{source}/T_{room}) factor, the flow appears to increase with increased temperature. This result would be reasonable, however the conflict with the observed lower vacuum pressures at higher temperature is compelling evidence that aperture flow indeed decreases with increased source temperature. Additionally a routinely observed attenuation in mass spectral ion currents at increased source

temperature is indicative of aperture diameter constriction at higher temperatures. It appears therefore that flow through the aperture is indeed moderately obstructed at higher temperature.

From the above discussion it seems reasonable to assume that temperature is influencing some physical aspect of ion sampling. Perhaps a minor change in the actual shape of the free jet expansion follows a minor but real constriction in the aperture, which effectively exacerbates the bias against the lighter mass ions.

Effect of Buffer/Expansion Gas

The slope of the mass discrimination curve also shows a sensitivity to the identity of the buffer/expansion gas. Figure 29a shows the mass spectral relative responses to saturation samples at 150° C for three different sampling gases. The relative responses appear to be most uniform with use of methane. A recent effort to model the beam speeds and temperature profiles within a free jet expansion has been reported by Randeniya and Smith (54). It was shown that beam velocity is dependent upon expansion gas. This was demonstrated for the three gases (Ar, N_2, and CH_4) examined in Figure 29, whereby the highest attainable velocity in the region nearest to the sampling aperture follows Ar > N_2 > CH_4. This trend is consistent with the observed relative ordering of mass discrimination curves, where Ar exhibits the steepest slope, followed by N_2, then CH_4. Since argon expansions attain

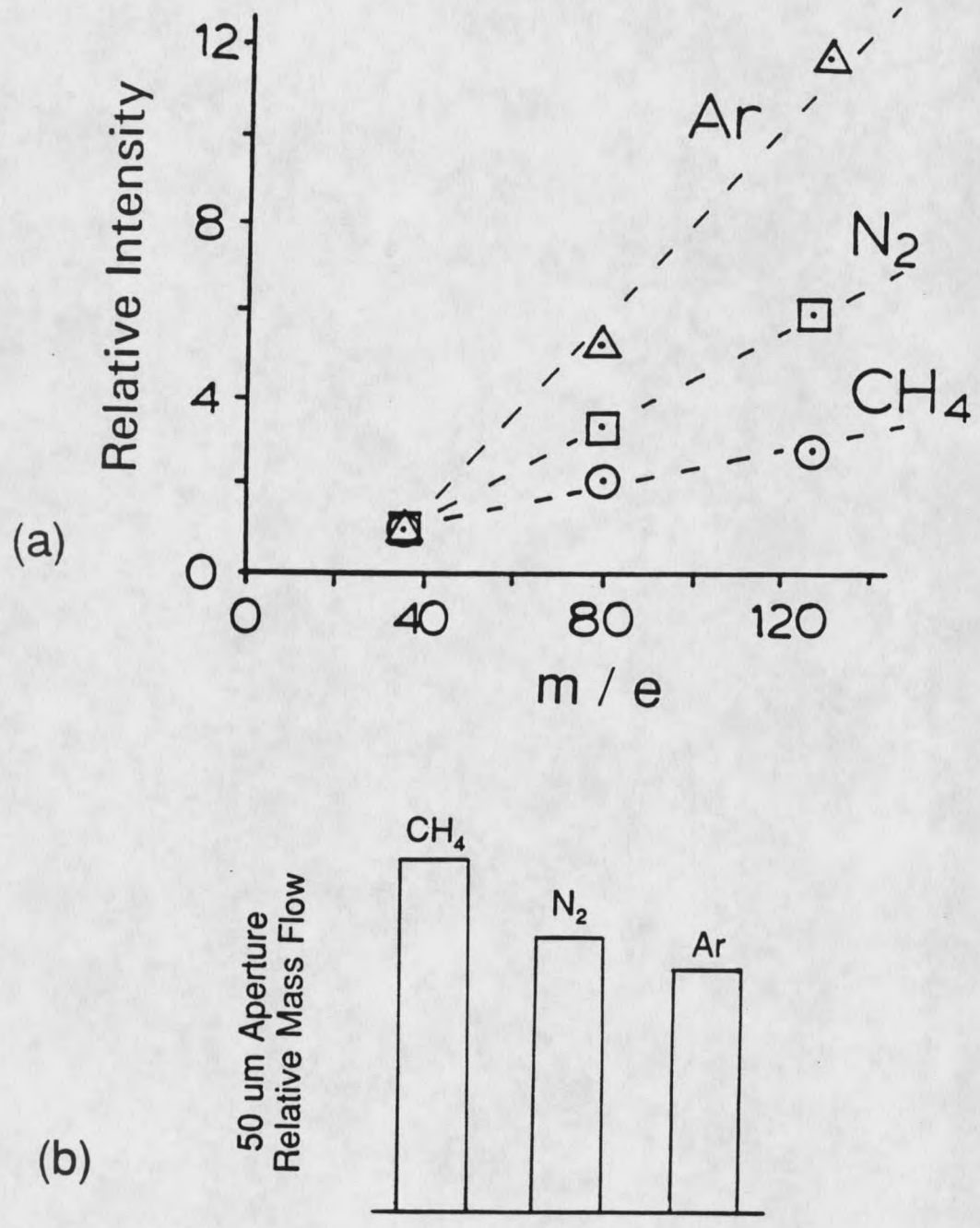

Figure 29.

(a) API saturation responses with variation in the buffer/ expansion gas. Argon, nitrogen, and methane results are normalized to chloride and plotted as a function of ion mass-to-charge ratio, m/e. The ion source temperature is 150° C, and sampling is by means of a 50 μm aperture.

(b) Relative aperture flows for argon, nitrogen, and methane. Note the correlation between flow and the slope of mass discrimination curves shown in (a).

the highest beam speed (in the range of 10^5 cm sec^{-1}) it seems reasonable to conclude that the sampling mass discrimination against lighter mass ions is related to beam velocity characteristics, where a lower beam velocity coincides with lessened mass bias against lower mass ions.

It is also interesting to compare the observed trends seen among the buffer gases for their respective mass discrimination curves and their relative measured aperture mass flows, shown in Figure 29b. The relative ordering observed for the slopes of the mass discrimination curves are seen to follow the ordering of relative aperture conductances for the three gases studied. It would appear therefore that more uniform sampling may also coincide with a higher aperture conductance. Despite the highest mass flow with methane, the beam velocities attained are lowest, as shown from the work by Randeniya and Smith,. It is also interesting to note that absolute ion currents are strongest in methane, and weakest for argon, a feature not indicated in Figure 31a due to normalization of all responses to that of chloride.

Minimization of Sampling Perturbations

The aforementioned experiments were designed to examine the possible importance of ion extraction potential, ion source temperature, and buffer/expansion gas identity on the uniformity in mass spectral ion sampling. It was shown that the relative responses among different mass ions appeared to be improved by use of certain experimental parameters. The

improvements in sampling were manifested by conditions which resulted in decreases in the slope of the mass discrimination curves. Of the parameters examined which improved the ion sampling characteristics included use of higher lens 1 ion extraction potential, lower ion source temperatures, and methane as the buffer/expansion gas. It was of interest to investigate the combined effects of these experimental parameters on the observed relative responses for ions over the mass range of the API mass spectrometer that was shown in Figure 27. This collective sampling effect is demonstrated in Figure 30, for which an ion extraction potential of +100 volts, ion source temperature of 100° C, and methane sampling gas are used to measure the relative responses for the study ions. Clear improvement in the uniformity of ion sampling is attained across the mass range. This is seen from the responses relative to chloride which do not exceed a factor of two over the mass range, in contrast to the mass sampling efficiency differences seen in Figure 27, where efficiency of sampling $C_7F_{14}^-$ was a factor of 30 greater than for Cl^-. It is noteworthy that aperture diameter is also of importance in determining the degree of APIMS mass bias sampling errors. Grimsrud and Kim found that the relative mass bias between chloride and bromide with a 20 μm aperture is a factor of ~2 preference for bromide over chloride ion. The results from above for otherwise similar sampling conditions but a 50 μm

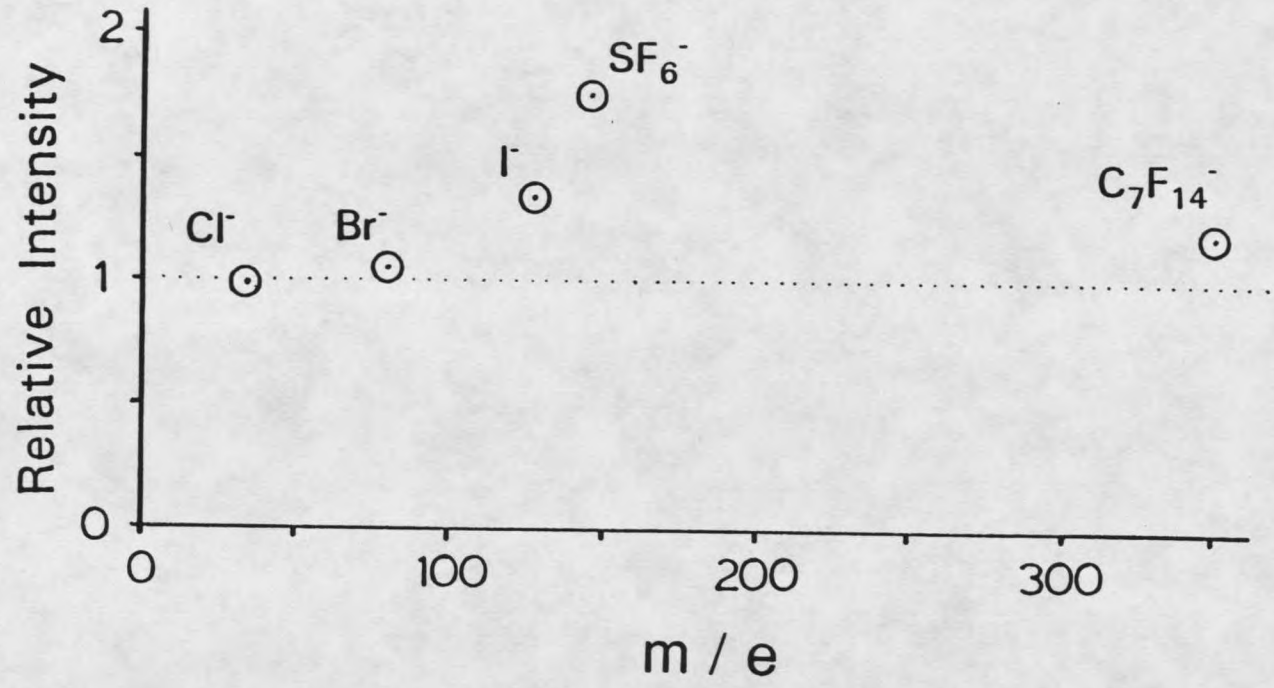

Figure 30.

Sampling conditions which minimize non-uniform ion sampling efficiency. API saturation responses, using methane buffer gas, lens 1 ion extraction potential of +100 volts, and ion source temperature of 100° C. Ion currents are normalized to chloride and plotted as a function of ion mass-to-charge ratio, m/e. The sampling conditions shown have significantly improved relative response uniformity in comparison to those shown in Figure 25.

aperture show a factor of ~4 preference for bromide to chloride ion. Hence a larger diameter aperture exacerbates the preferential aperture sampling for larger mass ions.

Correction for Mass Discrimination

The above sections have empirically demonstrated that an inherent mass discrimination against low mass ions is operative during ion sampling from the API free jet expansion. Numerical correction for this effect is made possible by application of a factor obtained by the slope of the mass discrimination curve between the two ions for which a relative ratio of ion currents is to be determined. Through quantitative knowledge of the sampling bias that exists between two ions of interest, it is possible to correct the observed relative ion abundances so that interpretation of signals in terms of ion source conditions may be made. Since the slope of the mass discrimination curve is dependent upon the ion extraction potential, ion source temperature, and buffer/ expansion gas identity, it is necessary to derive correction factors for the specific experimental conditions of interest. This procedure for mass discrimination correction is carried out in the following section in which dissociative electron capture branching reactions will be examined by APIMS for comparison to low pressure ionization studies conducted by other workers. The relative errors associated with the corrected branching ratios are typically on the order of ± 15 % of the reported ratio upon final propogation of error.

Fundamental Information from APIMS

The difficulties associated with the mass spectrometric sampling of ions from the API ion source have generally precluded its use for studies which address fundamental questions. The previous three sections of Results and Discussion were concerned with characterization of ion sampling effects associated with APIMS aiming toward avoidance or minimization of, or correction for, ion sampling errors encountered during mass spectrometric sampling of the API ion source. Three sampling errors have been examined. Ion sampling perturbations associated with APIMS free jet expansion dynamics have been shown to significantly perturb the sampling of cluster ions, but conditions may be found which serve to minimize their effects for the sampling of equilibrium cluster ions. Mass and ion-type discrimination effects shown to favor larger mass and more structurally complex ions were later examined. Capacitive-like aperture charging events which inhibit or impede mass spectral ion currents were shown to be encountered when moderate to high electrostatic fields are in proximity to the aperture.
It is only following a thorough characterization of these important effects related to ion sampling that fundamental problems can be approached by means of APIMS.

The following section will entail application of the knowledge of mass discrimination effects, and correction thereof, in order to obtain fundamental insight into the

pressure dependence of several two-channel dissociative electron capture branching reactions. This is information that would have been totally unavailable prior to identification and characterization of the significant ion sampling errors. The pressure dependence for the electron capture chemistry of bromotrichloromethane will first be considered. This compound forms either chloride or bromide ion upon attachment of a thermalized electron. The bromotrichloromethane branching reaction results from mass discrimination corrected APIMS will be compared to measurements obtained by another atmospheric pressure experiment, and then to measurements obtained by a very low pressure ionization experiment. Following that discussion, the electron capture chemistry of several dibrominated fluorocarbons and hydrocarbons will be investigated. Many of these compounds also have two available dissociative electron capture channels, one leading to bromide ion, and the second to dibromide ion. Again mass discrimination corrected APIMS measurements will be compared to low pressure ionization experiments from other workers.

Pressure Dependence of EC Branching Reactions of $CBrCl_3$

The attachment of thermalized electrons to a halocarbon most commonly proceeds by means of a single channel dissociative electron capture mechanism shown by reaction 27, in which a single halide ion is generated as the product ion,

$$MX + e(th) \longrightarrow M + X^- \qquad (27)$$

The presence of a low level unoccupied molecular orbital makes electron capture feasible. Dissociative electron capture is ascribed to electron capture which places electron density into an antibonding molecular orbital, resulting in the rupture of a bond, with charge retention by the most electronegative moiety.

The capture of a thermal electron by bromotrichloromethane ($CBrCl_3$), however, may proceed through one of two possible unimolecular dissociative electron capture reaction channels, by generation of either a bromide or chloride ion as shown by reactions 28a and 28b,

$$CBrCl_3 + e(th) \begin{cases} \dashrightarrow Br^- + CCl_3 & (28a) \\ \dashrightarrow Cl^- + CBrCl_2 & (28b) \end{cases}$$

Previous Measurements. The atmospheric pressure electron capture chemistry of $CBrCl_3$ has been previously investigated using APIMS by Kim and Grimsrud. It was shown that reaction 28 proceeds with a relative branching ratio, 28a / 28b, of 4 to 1, i.e., 80% of the $CBrCl_3$ molecules follow reaction channel 28a to produce bromide ion, and 20% proceed by reaction 28b to produce a chloride ion (50). This relative branching ratio

was found to be invariant over a study temperature range of 150 to 300° C, and also showed no dependence upon either ion source $CBrCl_3$ concentration, or variation in ion source residence time. The results collectively indicated a stoichiometric electron to $CBrCl_3$ molecule relationship of 1 to 1, as no evidence was obtained for displacement reactions, or electron capture side reactions by the neutral radical species, CCl_3 or $CBrCl_2$, formed in reactions 28a or 28b, respectively.

A more recent study of $CBrCl_3$ by Adams and coworkers, using a flowing afterglow/ Langmier probe (FALP) apparatus, indicated a substantially different dissociative electron capture branching ratio , 28a / 28b , of nearly 1 to 1 , whereby 45% of the $CBrCl_3$ molecules follow reaction channel 28a to produce bromide, and 55% follow reaction 28b forming chloride (55). However, the FALP experimental conditions differ significantly from those of the APIMS. The FALP apparatus employs a pressure that is two orders of magnitude lower than that maintained within the API ion source. Furthermore the FALP experiments were performed at a much lower temperature. Specifically, the FALP experiments used 1 Torr total helium pressure that was maintained at 27 ° C. As stated above, the APIMS bath gas comprised 1 atm total argon/10% methane pressure and was maintained between 150 and 300° C.

Additionally, Adams and coworkers established that the

neutral radical products CCl_3 and $CBrCl_2$, formed from reactions 28a and 28b, respectively, exhibit fast electron attachment rate coefficients for their study conditions, as shown below in reactions 29, 30a, and 30b,

$$CCl_3 + e(th) \longrightarrow Cl^- + CCl_2 \qquad (29)$$

$$CBrCl_2 + e(th) \begin{cases} \longrightarrow Br^- + CCl_2 & (30a) \\ \longrightarrow Cl^- + CBrCl & (30b) \end{cases}$$

This observation by Adams and coworkers is particularly significant, being the first report of electron capture reactions by neutral radical species, for which no evidence had previously been obtained by Grimsrud and Kim.

Due to these very inconsistent descriptions of the electron capture chemistry of $CBrCl_3$, it was of interest to address the above apparent discrepancies by means of additional API experimentation. The original experiments performed by Kim and Grimsrud, with correction for mass discrimination effects, are reinvestigated by APIMS. Also, an investigation of the electron capture chemistry of CBrCl by means of the recently developed photo-detachment modulated-electron capture detector (PDM-ECD) developed by Mock and Grimsrud (56) will be summarized.

APIMS Measurements : $CBrCl_3$ in excess of electrons. The APIMS observations from the current study are compared to the previous results of Kim and Grimsrud (squares), as shown in Figure 31. The most recent APIMS measurements, (circles and triangles), were obtained by monitoring the ion currents of $^{35}Cl^-$ and $^{79}Br^-$ while using $CBrCl_3$ ion source concentrations in great excess of the available thermalized electrons, for a condition of ion source saturation. This was effected by introduction of >100 nanogram gaseous samples. Consequently there are no electrons available for any secondary electron capture side reactions involving the neutral radicals $CBrCl_2$ and CCl_3, and the observed branching ratio is therefore representative of only the initial electron capture reaction by $CBrCl_3$. Over the range of ion source $CBrCl_3$ concentrations that could be studied, the electron capture branching ratio remained constant. This indicated that the electron capture chemistry by the neutral radicals was never possible due to the unavailability of free electrons. This also indicated that nucleophilic displacement mechanisms are inoperative which might otherwise alter the observed relative bromide and chloride ion abundances. In relation to the earlier APIMS study of $CBrCl_3$ by Kim and Grimsrud, squares, it is also seen in Figure 31 that the mass discrimination corrected branching ratio under atmospheric pressure conditions is indeed confirmed to result in 80% bromide ion and 20% chloride ion,

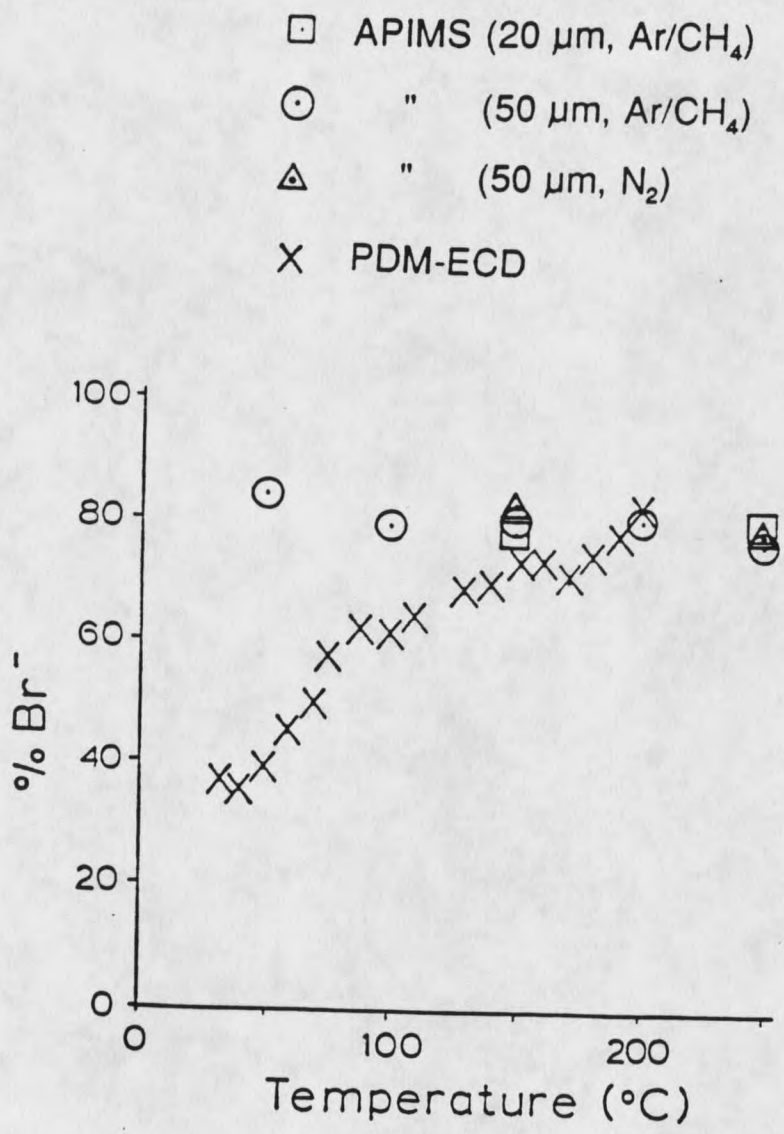

Figure 31.

Bromotrichloromethane dissociative electron capture (EC) relative branching ratio represented as % Br^-, at atmospheric pressure determined by APIMS and PDM-ECD over a wide temperature range. As shown by the PDM-ECD results, with an excess of electrons available following the initial EC event (Reaction 28a/b), the radical species $CBrCl_2$ and CCl_3 may capture electrons dissociatively to produce additional chloride ion, thereby altering the observed relative branching ratio. However, at higher temperatures these radical species are apparently unable to react by electron capture, perhaps due to a wall destruction mechanism. The PDM-ECD measurements were obtained from Mock and coworkers, reference 56.

and no temperature dependence is observed over the extended study temperature range of 50 to 250° C.

PDM-ECD Measurements: Electrons in excess of $CBrCl_3$. All of the PDM-ECD measurements to be related here were provided by R. S. Mock. In addition to the APIMS results, Figure 31 also shows the relative electron capture branching ratio of $CBrCl_3$ over the temperature range from 30 to 200° C as determined from the PDM-ECD experiments. The electron density within the PDM-ECD atmospheric pressure plasma was always maintained in excess of the introduced $CBrCl_3$ concentration, so that the observed relative branching ratio will represent the initial electron capture reaction by $CBrCl_3$ and any potential secondary electron capture side reactions which may occur by the neutral radical species $CBrCl_2$ and CCl_3. In contrast to the APIMS results, for which $CBrCl_3$ is always kept in excess of the available thermal electron population, the PDM-ECD demonstrates that additional chloride ion is produced by electron capture of the radicals at low temperatures. This is seen to alter the observed relative branching ratio well below the initial electron capture reaction by $CBrCl_3$ to form 80 % bromide / 20% chloride.

It is also seen in Figure 31 that an important temperature effect is observed for the PDM-ECD results, indicating that only the initial electron capture branching reaction occurs at the higher temperatures. The electron attachment rate coefficients of $CBrCl_2$ and CCl_3 is not expected

to have a negative temperature dependence. Hence it is assumed that these neutral radicals are precluded from electron capture at the higher ion source temperatures. Further PDM-ECD experiments were undertaken in which the electron density was reduced. It was shown that by limiting the number of electrons available for electron capture, even at low temperatures, the electron capture reactions by the neutral radicals $CBrCl_2$ and CCl_3 could be effectively inhibited.

Pressure Considerations. Since the APIMS measurements reflect the initial dissociative electron capture branching ratio, and since this ratio was shown to be invariant with temperature, it becomes apparent that the discrepancy between the APIMS results and those of FALP, are due to ionization pressure differences, and not to differences in temperature. Therefore, it is necessary to consider the influence that collision frequency may have upon the particular dissociative electron capture reaction channel taken by the initially formed electron capture intermediate. If the lifetime of the intermediate species, $CBrCl_3^{-*}$, shown in reaction 31,

$$CBrCl_3 + e(th) \longrightarrow CBrCl_3^{-*} \begin{cases} \longrightarrow CCl_3 + Br^- & (31a) \\ \longrightarrow CBrCl_2 + Cl^- & (31b) \end{cases}$$

is on the order of a molecular vibration, or 10^{-13} sec, the branching reaction would not be expected to depend upon the buffer gas pressure.

A report by Walter and coworkers (57) has shown, by kinetic energy release experiments, that the dissociative electron capture reactions of CH_3I, CF_3I, and CF_3Br all proceed very rapidly through an intermediate of extremely short lifetime, on the order of a molecular vibration. By the same method Walter and coworkers (58) have also demonstrated that dissociative electron capture by CCl_4 and $CFCl_3$ proceeds through an intermediate with a significantly longer lifetime. This result suggests the possibility that the lifetime of $CBrCl_3^{-*}$ against dissociation could be longer than a molecular vibration. It is conceivable therefore that the excess internal energy resulting from the initial electron capture step in reaction 31 could be at least partially removed in collisions with the buffer gas molecules prior to dissociation by either reaction 31a or 31b. Because reaction 31a is energetically favored over reaction 31b by nearly 14 kcal mol^{-1} (50), the production of bromide ion would be expected to be increased by removal of internal energy from the vibrationally excited intermediate molecular negative ion. In argon/10 % methane, an ion will collide with buffer gas molecules at a frequency of approximately 5×10^{10} collisions per second. Therefore, if the lifetime of $CBrCl_3^{-*}$ is as long as 2×10^{-11} sec (approximately 100 bond vibrations), an increase in

bromide ion production at atmospheric pressure could be explained. Under the condition of helium at 1 Torr, used in the FALP study, ions will collide with the buffer gas molecules at a frequency of 10^7 collisions per second. Consequently removal of internal energy in collisions with the buffer gas molecules is far less probable. Additionally, helium is known to be relatively inefficient at removing energy from vibrationally excited ions (43).

Pressure dependence of EC Branching Reactions of Dibrominated Compounds

As mentioned earlier, the attachment of thermalized electrons to halocarbons typically proceeds by the dissociative electron capture in which monoatomic negative ions, (chloride, bromide, or iodide) are produced. Typically only one monoatomic negative ion will be generated as shown above in reaction 27. However, occasionally more than one dissociative electron capture channel be available, leading to two or more possible monoatomic negative ions, as discussed above for bromotrichloromethane.

Recently there have appeared reports on production of homonuclear diatomic negative ions as a product in a two channel dissociative electron capture reaction. In particular dibromide ions, in addition to bromide ions, have been observed from dibromodifluoromethane (59), and also from four other dibrominated molecules (60). The general branching reaction is represented below by reactions 32a and 32b,

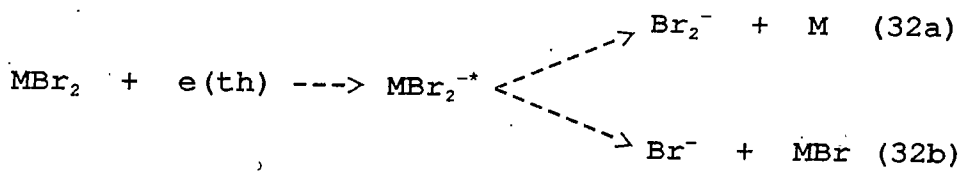

where MBr_2 is a molecule that contains two bromine atoms that are substituted on adjacent sp^3 carbon atoms and may capture a thermalized electron, e(th), dissociatively, by either of the two possible reaction channels shown.

APIMS Measurements Compared to Low Pressure Ionization.

In Figure 32 the importance of pressure on the branching ratio of reaction 32a/ 32b is demonstrated by comparisons between five separate ionization methods:

A) Mass discrimination corrected APIMS at 640 Torr nitrogen

B) flowing afterglow/ Langmier probe (FALP) at 1 Torr helium. (Smith and coworkers, reference 60)

C) pulsed high pressure mass spectrometry (PHPMS) at 2 Torr hydrogen (Knighton and coworkers, reference 61)

D) high pressure electron capture mass spectrometry at 0.5 Torr methane (L.J. Sears, MSU Mass Spectrometry Center)

E) krypton photoionization at << 1 Torr krypton. (Alajajian and Chutjian, reference 59)

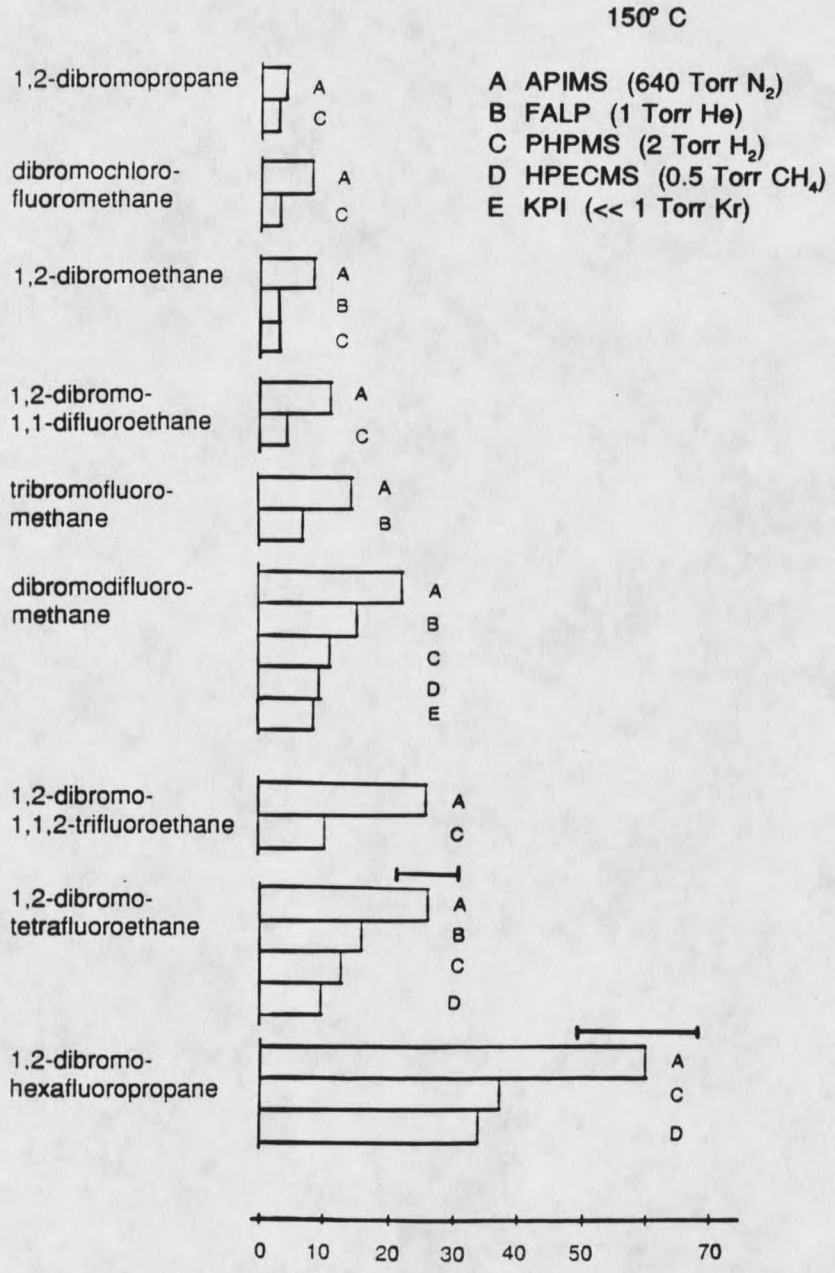

Figure 32.

Dissociative electron capture relative branching ratios leading to bromide or dibromide (expressed as % Br_2^-, 100 - %Br_2^- = %Br^-) from ten different dibrominated compounds determined by APIMS (640 Torr nitrogen),[a]FALP (1 Torr helium),[b]PHPMS (2 Torr hydrogen) , [c]HPECMS (0.5 Torr methane), and [d]KPI (<< 1 Torr krpton).

[a] Smith et al (60), [b]Knighton et al (61), [c] L.J. Sears, MSU, [d] Alajajian et al (59). See text for experiment acronyms.

The results of this comparison between ionization at varying total pressures spanning over three orders of magnitude will be interpreted in terms of the importance of collision frequency for influencing the outcome of reaction 32. Figure 32 presents the results for the dissociative electron capture branching reactions 32a/ 32b, obtained from these five separate ionization methods, for several MBr_2. It is seen that the observed branching reaction 32a/ 32b is strongly dependent upon the experimental conditions. The results shown in Figure 32 for a particular compound are ordered according to ion source pressure. In all cases production of dibromide (reaction 32) increases with pressure. Thus production of dibromide ion is consistently most favored in the API ionization conditions, and least favored in the sub-Torr KPI experiment.

Thermochemical Considerations. The heats of reaction for reactions 32a and 32b have been calculated and are shown in Table 1 for those five compounds for which thermochemical data are available (62,63). These heats of reation are important for the understanding of the variations observed between compounds for relative dibromide to bromide production.

The heat of reaction for channel 32a given by equation 33,

$$\Delta H_{32a} = H_f(M) + H_f(Br_2) - H_f(MBr_2) - EA(Br_2) \qquad (33)$$

is found to be endothermic for dibromomethane, but exothermic for the other four compounds shown in Table 1. These calculations are consistent with experiment, in that only dibromomethane does not produce dibromide ion. Due to the unavailability of thermochemical data, calculations of ΔH_{32b} are all necessarily based on the assumption that the C-Br bond enthalpy (BE) is nearly 70 kcal mol^{-1}, an estimate expected to be correct to within a few kcal mol^{-1}. The electron affinity (EA) of Br is 78 kcal mol^{-1}. The heat of reaction for reaction 32b is accordingly shown from equation 34,

$$\Delta H_{32b} = BE(C\text{-}Br) - EA(Br) \qquad (34)$$

to be negative. The feasibility of reaction 35, shown below,

$$Br_2^- \text{ ---> } Br^- + Br \qquad (35)$$

in obscuring the results for reaction 32a and 32b, will now be considered. From the respective EA's of Br and Br_2, 78 kcal mol^{-1} and 58 kcal mol^{-1}, and the BE of Br_2, 46 kcal mol^{-1}, the heat of reaction for rupture of the dibromide ion sigma bond, is estimated by equation 36,

$$\Delta H_{35} = BE(Br_2) + EA(Br_2) - EA(Br) \qquad (36)$$

to be +26 kcal mol^{-1}.

Table 1.

Thermochemical calculations for reactions 32a and 32b, all in units of kcal mol^{-1}

Compound	^1H_f (MBr_2)	^1H_f (M)	$^2\Delta H_{32a}$	$^3\Delta H_{32b}$
dibromomethane	-3.5	+93	+46	-8
dibromodifluoro-methane	-91	-49	-8	-8
1,2-dibromoethane	-9	+12.5	-28	-8
1,2-dibromotetra-fluoroethane	-189	-158	-19	-8
1,2-dibromopropane	-17	+4.8	-28	-8

[1] From references 62 and 63.

[2] Calculated from equation 33.

[3] Calculated from equation 34.

Table 1 shows that the exothermicity of reaction 32a, where favorable, is unlikely to be sufficient for driving reaction 35. Despite the fact that the heat of reaction 32a exceeds 26 kcal mol^{-1} for two of the compounds considered, it seems improbable that the energy released could be so unequally distributed between M and Br_2^- as to allow reaction 35. From this analysis it is assumed that dissociation of dibromide does not occur and therefore does not complicate the observation of the relative branching ratios of reactions 32a and 32b.

Effects of Temperature. Figure 33 shows the mass discrimination corrected APIMS observations for reactions 32a and 32b as a function of ion source temperature for many of the study dibrominated compounds. Since mass discrimination effects are temperature dependent, as shown in an earlier section of Results and Discussion, it was necessary to apply correction factors obtained at each temperature to the APIMS data presented. It can be seen that within this group of molecules, there exists either a modestly negative, or generally neutral dependence on temperature toward production of dibromide relative to bromide ion. Similarly modest negative, or neutral temperature dependencies for dibromide relative to bromide ion generation were observed in FALP (60) and PHPMS (61) temperature studies. It seems possible that for compounds which exhibit a negative temperature dependence, a link between temperature and the internal energy of the electron capture intermediate, MBr_2^{-*}, may be evident. A negative dependence on temperature suggests that the electron capture channel leading to bromide ion is favored at higher MBr_2^{-*} internal energies. For example, 1,2-dibromotetrafluoro-ethane consistently generates less dibromide relative to bromide ion as the temperature is increased in APIMS, PHPMS, and FALP. One potential explanation for this effect may concern entropic factors that are particularly significant

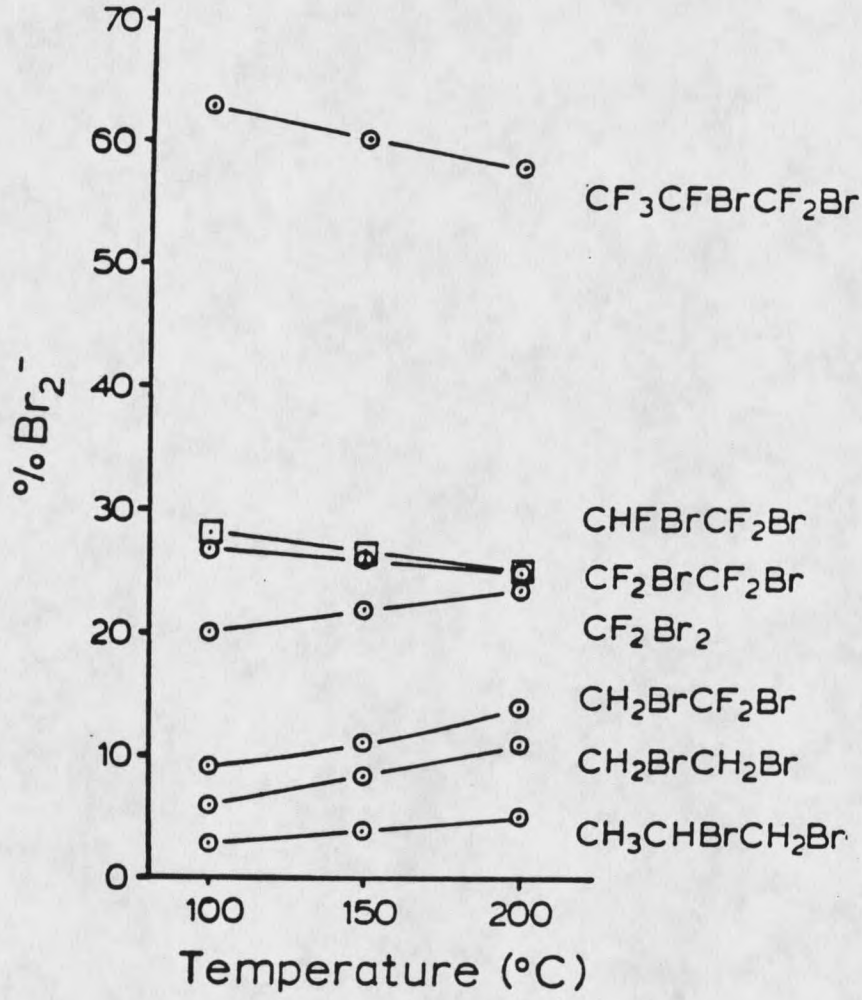

Figure 33.

APIMS temperature dependence of reaction 32a and 32b for several dibrominated compounds. Note a relative error of ± 15 % for indicated value.

for production of dibromide. It is reasonable to assume that reaction 32a leading to dibromide may be relatively sensitive to the degree of molecular order, by requiring alignment of the adjacent bromine atoms prior to formation of formation of the departing dibromide ion. Perhaps increased intramolecular disorder at higher ion source temperatures disfavors dibromide ion production from some MBr_2, thereby resulting in the observed negative temperature dependence seen for 1,2-dibromoethane.

Effect of Pressure and Identity of Buffer Gas. The systematic effect of pressure on the observed relative electron capture branching of dibromodifluoromethane is shown in Figure 34. The data points shown for pressures in the 0 to 4 Torr range have been provided by other workers utilizing three of the aforementioned low pressure ionization methods including PHPMS (symbols), FALP (point S), and krypton photoionzation (point C). The point corresponding to 640 Torr is the mass discrimination corrected APIMS observation, with error bar indicating the maximum associated uncertainty after propagation of errors for three successive measurements and three mass bias correction factors.

The effects of both pressure and buffer gas identity are best demonstrated by the pressure variable PHPMS measurements. It is seen from Figure 34 that a strong dependence in the relative production of dibromide ion

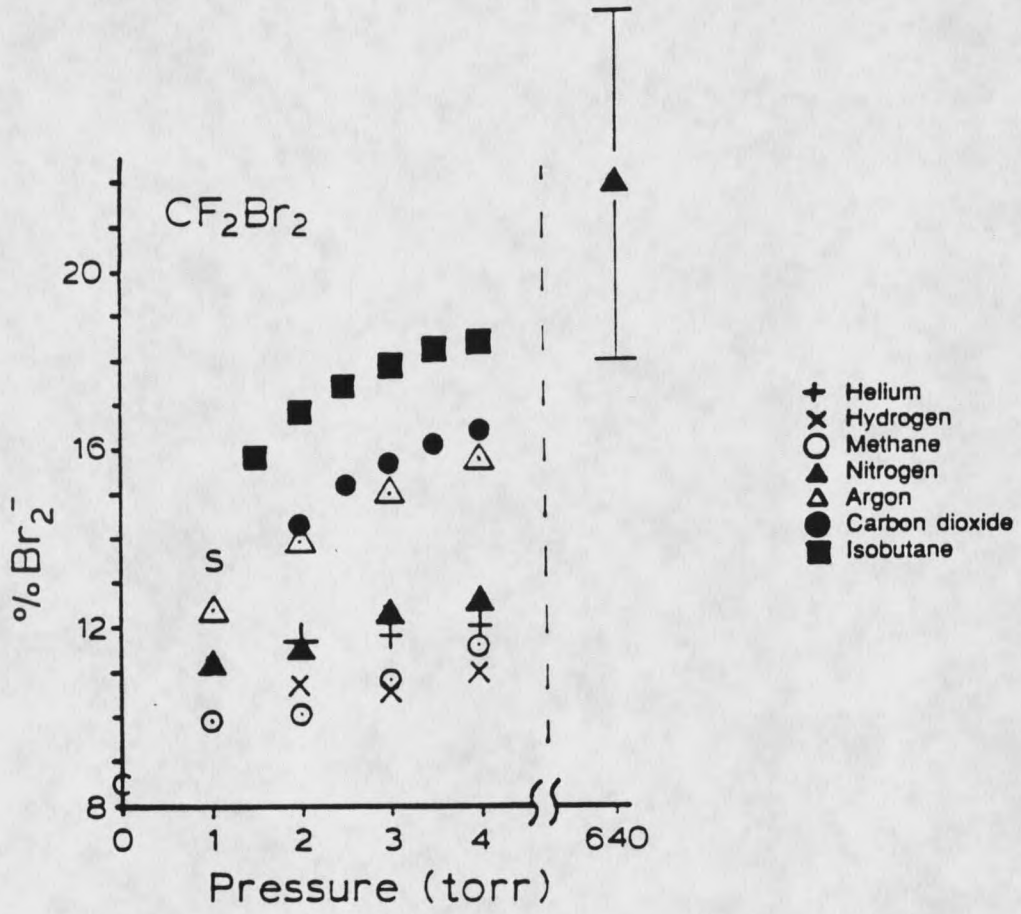

Figure 34.

PHPMS measurements showing that the dissociative electron capture branching reaction of dibromodifluoromethane exhibits a definite collisional quenching efficiency dependence. The APIMS result is also shown at 640 Torr. The PHPMS measurements were obtained from Knighton and coworkers, reference (61). Point S is from Smith et al (60) and point C from Chutjian et al (59).

rests on the identity of the buffer gas, and also that a positive pressure dependence exists for each buffer gas. The FALP (1 Torr helium, point S), and KPI (<<1 Torr krypton, point C), results are seen to be consistent with the PHPMS data. The APIMS result coincides with the upper limit for dibromide ion production among the represented experimental conditions.

Two fundamentally different explanations may be considered for rationalizing the importance of buffer gas identity and ionization pressure. The first explanation concerns the degree of electron thermalization achieved within a given buffer gas. Variations in electron energy would be expected to be important for the electron capture branching ratio. The second potential explanation concerns variations in the efficiency for collisional quenching of the vibrationally excited intermediate ion, MBr_2^{-*}, which is initially formed upon electron capture. These fundamentally different possibilities will be separately considered below.

The majority of electrons present within the PHPMS ion source are secondary electrons produced by interaction of a primary electron beam with buffer gas molecules. These secondary electrons initially have elevated energies but are rapidly thermalized upon collisions with buffer gas molecules. Electron capture cross-sections are strongly dependent upon electron energy. Due to the variability in electron capture cross section with electron energy, these

reactions occur only after the electron kinetic energy has been significantly lowered. Ideally the electrons would be completely thermalized prior to electron attachment, so that the electron energy at the time of capture could be known with certainty. Electron thermalization rates are dependent upon the identity of the buffer gas, and Warmer and Sauer have determined the second order rate constants for electron thermalization for six of the seven gases employed in the PHPMS study (64). A comparison between the thermal rate constants and the branching ratios from PHPMS show that no correlation exists. For example, Warmen and Sauer found that argon is a far less efficient electron thermalizer than methane; argon requires 1.3×10^{-3} sec Torr, whereas methane requires only 2×10^{-7} sec Torr in order to thermalize an electron. If differences in electron thermalization rates at a given pressure were important to the PHPMS study, then the methane experiments would have been expected to result in enhanced dibromide production relative to argon. However, as seen in Figure 34, the experimental result is exactly opposite. Further, it is seen that the % Br_2^- values in hydrogen are similar to those obtained in helium, but the electron thermalization rate coefficients of Warmen and Sauer indicate that hydrogen thermalizes electrons two orders of magnitude faster than helium. It is concluded therefore that electron thermalization is not an important factor toward explaining the results shown in Figure 34.

Efficiency of Collisional Relaxation. The second potential explanation for the variations in dibromide production among the buffer gases concerns the efficiency by which the vibrationally excited electron capture intermediate, MBr_2^{-*}, is stabilized prior to dissociation by reactions 32a or 32b. This possibility, as discussed in the previous section regarding bromotrichloromethane, is feasible only if some fraction of the total MBr_2^{-*} population have lifetimes against dissociation by either reaction 32a or 32b greater than the time required for collisions with buffer gas molecules. The mass discrimination corrected APIMS relative branching ratio for 1,2-dibromohexafluoropropane observed with four different buffer gases/expansion gases under three temperature conditions is shown in Figure 35. The relative uncertainty of ± 15 % associated with each measurement is indicated for the nitrogen data. It is apparent that no clear dependence exists on these tested buffer gases for APIMS conditions.

A recent report by Ahmed and Dunbar demonstrated that the efficiency for collisional relaxation of a vibrationally excited polyatomic ion is very dependent upon the identity of the collision gas (43). The study surrounded the collisional quenching of vibrationally excited bromobenzene positive ion by a range of neutral atomic and polyatomic collision partners. Since efficiencies for vibrational quenching have been shown to depend on the molecular

1,2-Dibromohexafluoropropane

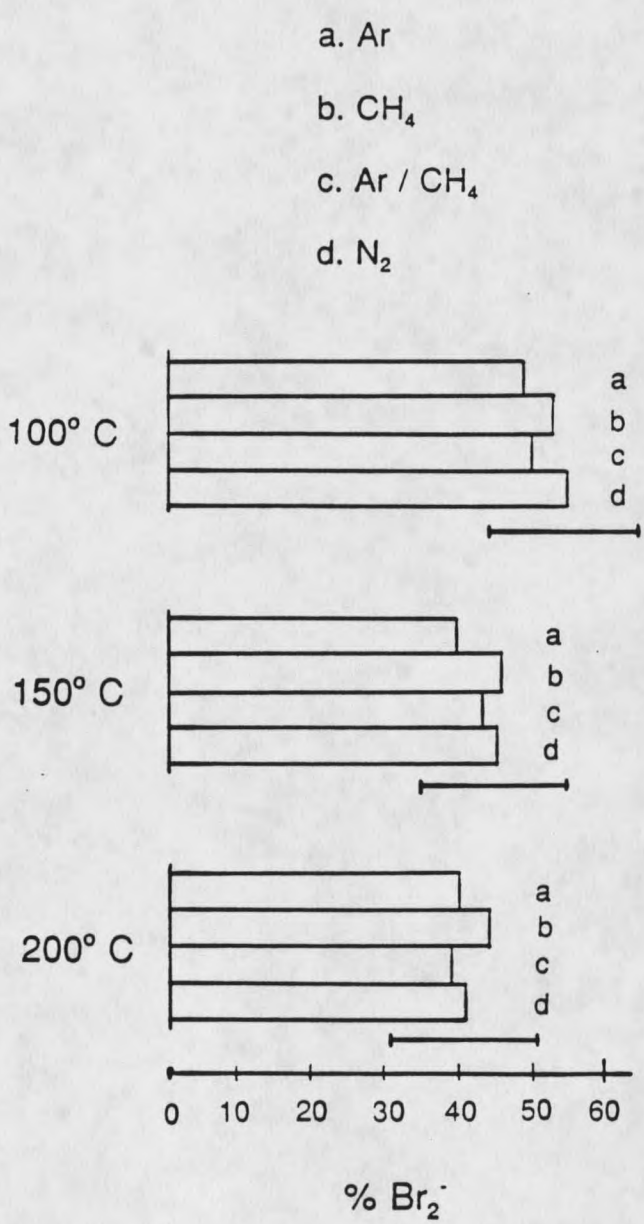

Figure 35.

Demonstration that carrier gas identity is of no discernable significance for influencing reaction 32a or 32b at atmospheric pressure. Note a relative error of ± 15 % for indicated value, as shown for nitrogen results.

complexity and mass of the collision partner, comparisons between various gases require consideration of the quenching efficiency and total pressure of a given buffer gas. The relative collisional quenching rate (RCQR) is an index for relative effective pressure to allow for comparisons between collision gases at specific pressures (61). RCQR for a given buffer gas is directly related to ion source pressure, P, the second order collision rate coefficient, k_c, and the collisional quenching efficiency, Φ_c , as shown in equation 37

$$RCQR = P \times k_c \times \Phi_c \qquad (37)$$

Ahmed and Dunbar have determined Φ_c and k_c values for the collisional relaxation of bromobenzene positive ion for a number of buffer gases. Despite the fact that the Φ_c and k_c values have not been determined for vibrational relaxation of MBr_2^{-*} of interest here, it is considered to be analytically useful to apply these relative values to the PHPMS and APIMS results.

Figure 36 shows the relative branching ratios expressed as percent dibromide obtained from Figure 34, but plotted as a function of RCQR, rather than pressure. The RCQR values calculated from equation 37 have all been normalized to the RCQR found for helium at 1 Torr. It is seen from this plot that a systematic relationship emerges that was not apparent

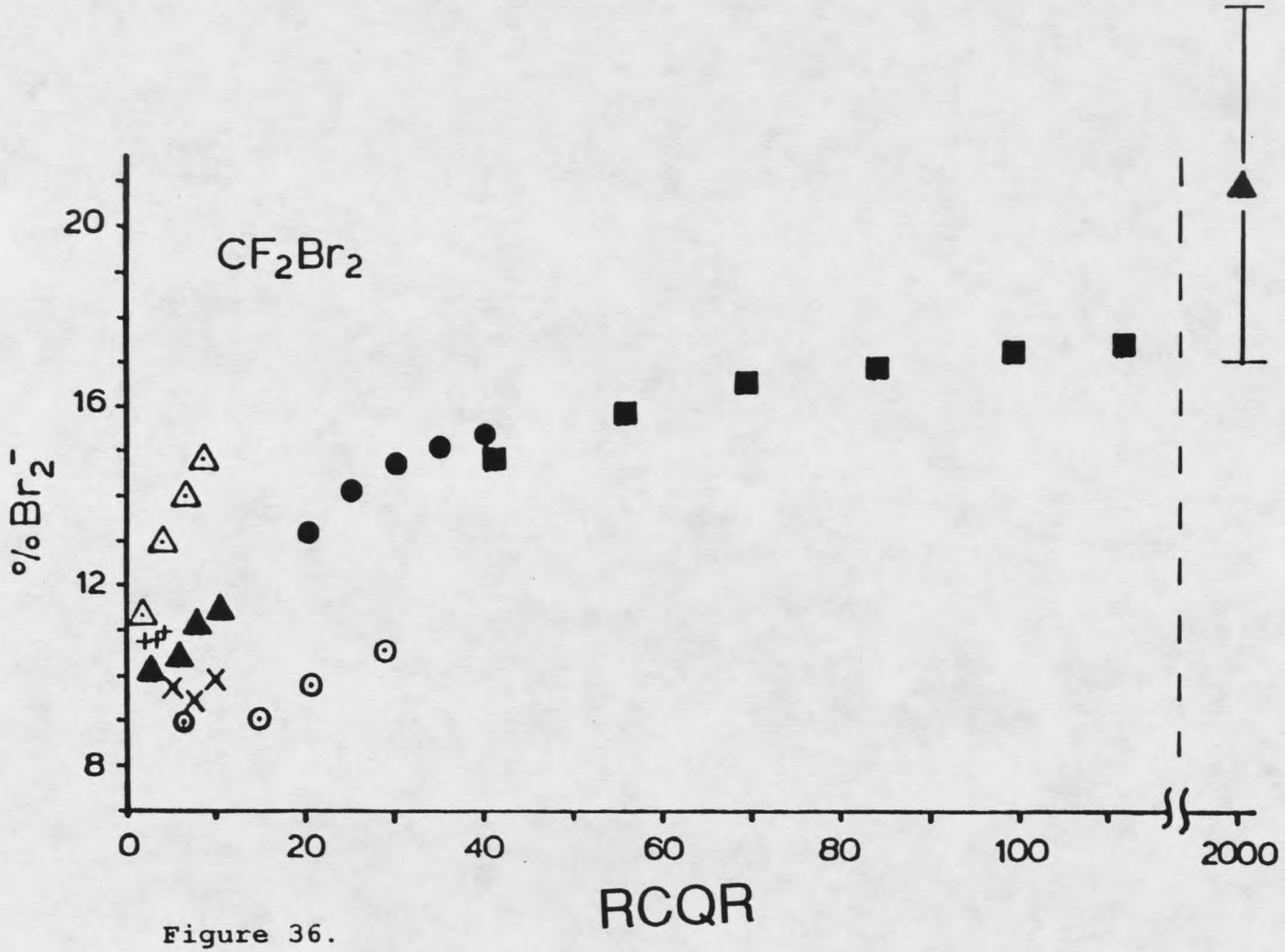

Figure 36.

Relative Collisional Quenching Rate (RCQR) treatment of the data shown in Figure 34. RCQR (equation 37) is the relative quenching rate coefficient for collisional relaxation of excited electron capture intermediates, MBr_2^{-*}, for a given buffer gas and pressure. All RCQR are normalized to RCQR of helium at 1 Torr.

from the data shown in Figure 34. The nonconformity seen for argon and methane relative branching ratios is noted, and may originate from ion dependent factors between excited bromobenzene ions and excited MBr_2^{-*} which are not important for quenching by the other study gases. The same RCQR treatment was applied to two other dibrominated fluorocarbons with results comparable or better than those shown for dibromodifluoromethane, thereby providing support for the RCQR model.

From the RCQR model, it is apparent that dissociative electron capture reactions 32a and 32b may be competitively influenced by the degree of collisional relaxation of excited MBr_2^{-*} intermediate species. Table 2 lists the relative branching ratio as percent Br_2^- observed for all of the study compounds. A comparison is made between the PHPMS low pressure limit results obtained with hydrogen buffer gas, and the mass discrimination APIMS results. It is seen in Table 2, that regardless of the compound identity, the propensity to produce dibromide ion from the APIMS ionization conditions is essentially double that from PHPMS conditions employing hydrogen buffer gas. This section will conclude with a proposed model for dissociative electron capture by dibrominated compounds able to generate either bromide ion or dibromide ion upon capture of a thermalized electron.

Table 2.

Comparison between PHPMS "low pressure limit" to APIMS for % Br_2^- production at 150° C

Compound	[1]PHPMS (2 torr H_2)	APIMS (640 Torr N_2)
dibromomethane	0	0
dibromodifluoro-methane	11	22
1,2-dibromoethane	3.2	8
1,2-dibromo-1,1-difluoroethane	4.4	11
1,2-dibromo-1,1,2-trifluoroethane	10	26
1,2-dibromotetra-fluoroethane	13	26
2,2-dibromoethane	0	0
1,2-dibromopropane	1.7	4
1,3-dibromopropane	0	0
1,2-dibromohexa-fluoropropane	37	60

[1] Data from Knighton and coworkers, reference 61.

Model for MBr_2 EC Branching Reaction. The capture of thermalized electrons by a given MBr_2 may result in a distribution of vibrationally excited intermediates, MBr_2^{-*} (v), which have characteristic lifetimes against

unimolecular dissociation leading to bromide that are dependent upon the degree of internal energy.

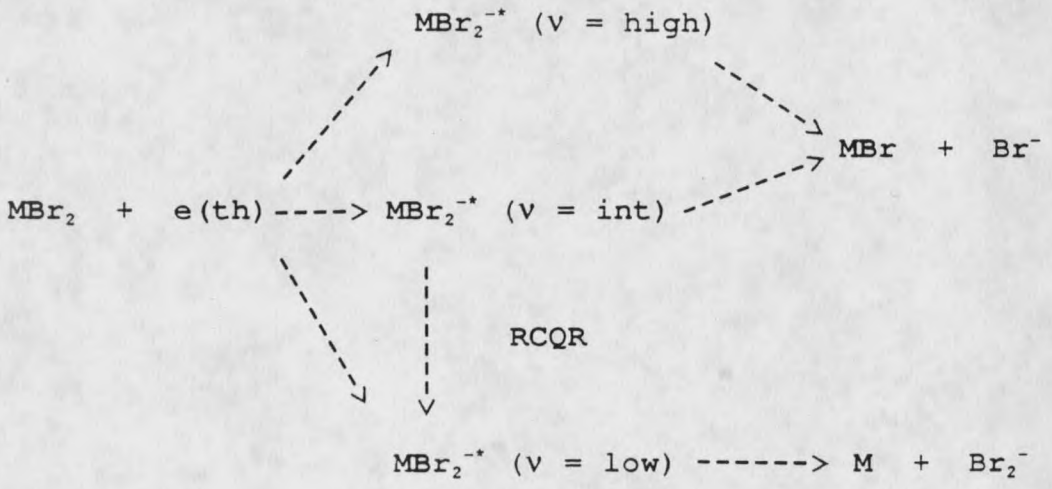

MBr_2^{-*} of very high energy are envisioned to dissociate to bromide on a timescale much shorter than the collision frequency of the buffer gas, thereby precluding the possibility for internal energy moderation of MBr_2^{-*}. The RCQR model indicates that some fraction of the excited intermediates of intermediate vibrational energy are sufficiently long-lived to allow for collisional relaxation by pressures in the Torr range and above. It suggested that these longer-lived MBr_2^{-*}(v = int) will tend to dissociate by bromide ion formation, but may be channeled toward dibromide ion as energy is increasingly transferred to neutral collision partners with increases in RCQR which depopulates

MBr_2^{-*} of intermediate energy to low, near ground state thermal energy, which always dissociate by the thermodynamically favored dibromide channel. If ground state MBr_2^{-*} are produced it is assumed that they spontaneously decompose to dibromide ion, because no molecular anions have been detected under any study condition.

Precedence for the RCQR model for the dissociative electron capture branching reactions described above may be found in a report concerning the electron capture chemistry of sulfurhexafluoride. Fehsenfeld has proposed that the lifetime for autodetachment from SF_6^- may depend upon the degree of vibrational excitation (65).

Ion-Molecule Clustering Fundamentals from APIMS

In the final three sections of Results and Discussion, the mass spectral signals observed from the API ion source will be examined for fundamental information, but without attention directed toward minimization or correction of ion sampling perturbations. Each of the following sections will involve ion-molecule clustering reactions. The first will demonstrate the availability of qualitative information concerning the electron affinity of a range of nitroaromatic compounds from APIMS, by means of clustering reactions with dimethylsulfoxide. The following section will describe the use cooling and aggregation effects associated with the

APIMS free jet expansion to obtain structural insight into halide and dihalide hydrate cluster ions that have not previously been observed. The final section will involve the effects of solvation on the stability of classically stable molecular anions, and reveal that the API conditions, which are conducive to high solvent partial pressures, may potentially provide insight into the intrinsic structural characteristics of some widely studied negative ions, as well as explain the occurrence of unexpected ions observed during perfluorocarbon analysis by thermospray mass spectrometry.

Nitroaromatic Molecular Anion Clustering to DMSO

The following set of measurements pertains to the clustering of a molecule of dimethylsulfoxide (DMSO) to a range of substituted nitroaromatic molecular anions, and is a follow up to an earlier report by Kreiger and Grimsrud (66). Ionization of the nitroaromatic of interest, M, is effected by resonance electron capture, as shown below in reaction 38. M with an electron affinity in excess of 0.5 eV may a attach a thermal electron,

$$M + e(th) \rightleftharpoons M^- \qquad (38)$$

to generate a stable molecular anion, M^-, upon dissipation of the energy released throughout the available internal

degrees of motion. The electron affinity for a neutral molecule is intimately associated with the characteristics of the resultant anion formed. Compounds which have high electron affinities typically possess one or more electron withdrawing substituents, such as a halogen or nitro group. The ability to delocalize the negative charge in the resultant molecular anion will reduce the electrostatic interactions that may occur with a given solvating molecule. Conversely, minimal charge delocalization provides a region of high charge density which enhances the coulombic attraction between the anion and the dipole of a solvating species, providing that steric factors do not interfere. The molecular anion generated by reaction 38 may cluster with a molecule of DMSO, as shown by reaction 39,

$$M^- + DMSO \rightleftharpoons M^- \cdot DMSO \qquad (39)$$

resulting in some characteristic equilibrium distribution of unclustered to clustered molecular anions within the API ion source, dependent upon DMSO partial pressure and temperature.

The nitroaromatic molecules, M, investigated for clustering of their molecular anion to DMSO include nitrobenzene (NB), the isomers of fluoronitrobenzene (o-FNB, m-FNB, and p-FNB), chloronitrobenzene (o-ClNB, m-ClNB, p-ClNB), cyanonitrobenzene (o-CNB, m-CNB, p-CNB), and

dinitrobenzene (o-DNB, m-DNB, p-DNB).

The relative propensities of the molecular anion of the above compounds for clustering to a molecule of DMSO is shown in Figure 37. The degree of clustering is represented by the observed ratio of clustered ion to unclustered molecular anion current, M^-DMSO. It is seen that, despite sampling perturbations associated with APIMS sampling, a clear correlation can be observed between electron affinity and propensity for clustering by reaction 39. The data used to construct the plot shown in Figure 37 are presented again in Table 3 in order to illustrate that the observed clustering propensities available from APIMS generally reflect the relative clustering propensities derived by PHPMS thermodynamic equilibrium conditions of Chowdhurry and coworkers (67). It is to be noted that the magnitude of the APIMS derived relative clustering propensities are not expected to match those obtained by PHPMS due to APIMS sampling collisionally induced dissociation effects which have been previously observed for the FNB^- DMSO clusters by Krieger and Grimsrud. An exception to observation of qualitative clustering propensities consistent with the relative thermodynamic propensities is seen for the isomers of fluoronitrobenzene. The reported FNB thermodynamic clustering order is p > o > m, verses the APIMS relative order of o > p > m.

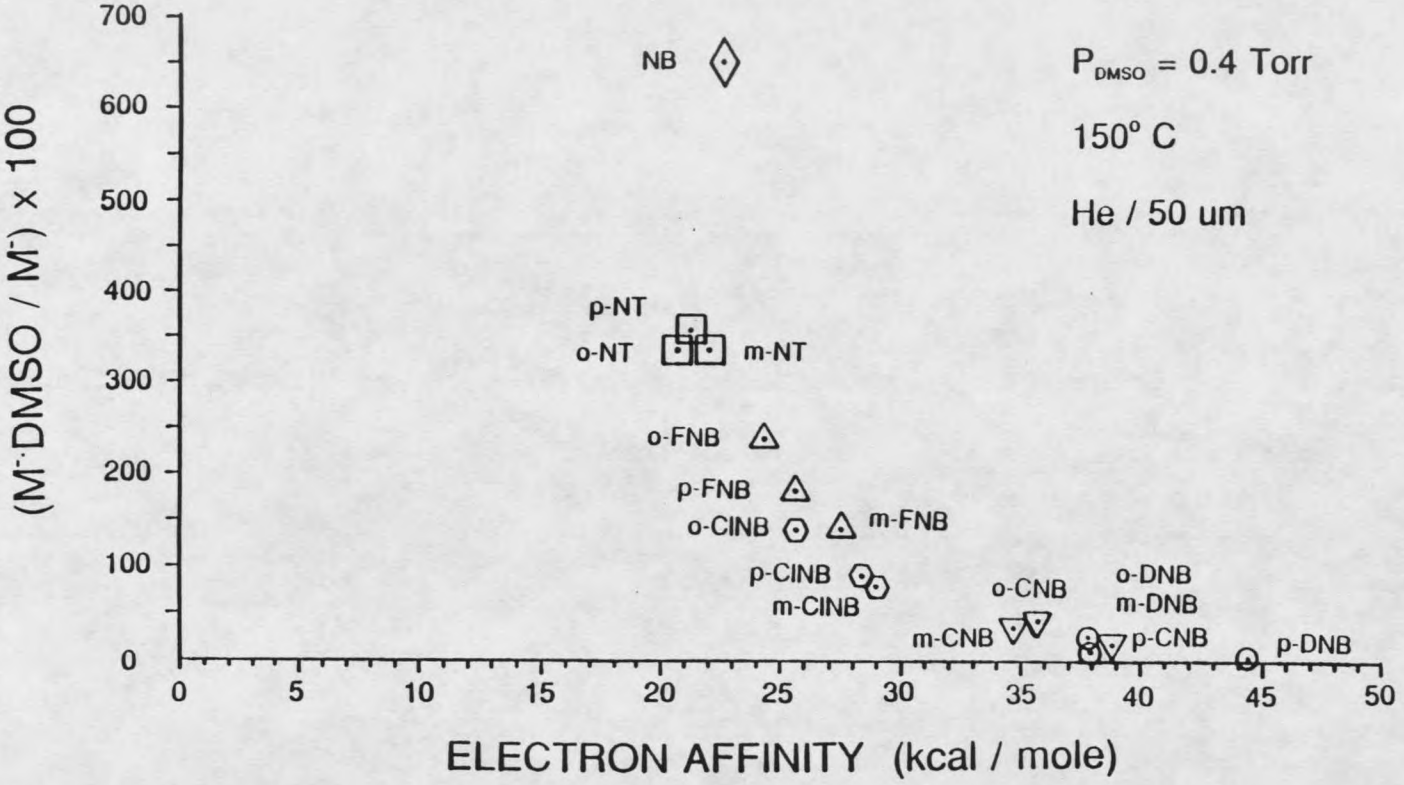

Figure 37.

APIMS M^-DMSO clustering ratios (= M^-DMSO / M^-) for a range of substituted nitroaromatic compounds plotted as a function of compound electron affinity. Compounds shown include Nitrobenzene (NB); the isomers of nitrotoluene (o-, m-, p-NT), of fluoro-nitrobenzene (o-, m-, p-FNB), of chloronitrobenzene (o-, m-, p- ClNB), of cyanonitrobenzene (o-, m-, p-CNB), and dinitrobenzene (o-, m-, p-DNB). DMSO partial pressure is 0.4 Torr with ion source at 150° C. Helium expansion/buffer gas sampled with a 50 μm aperture.

Table 3.

Clustering Ratios (= M^-·DMSO / M^-)
150° C and 0.4 Torr DMSO. Helium buffer/ expansion gas sampled with a 50 μm aperture.

Compound	[1]Electron Affinity (kcal / mole)	Clustering Ratio (x 100)	[2]R T C Order reflected ? (Yes / No)
o-dinitrobenzene	36.9	16.0	Y
m-dinitrobenzene	36.9	9.5	Y
p-dinitrobenzene	44.3	1.7	Y
o-cyanonitrobenzene	35.8	45.8	Y
m-cyanonitrobenzene	34.8	34.8	Y
p-cyanonitrobenzene	38.7	17.1	Y
o-chloronitrobenzene	25.7	143	Y
m-chloronitrobenzene	28.8	80	Y
p-chloronitrobenzene	28.2	87	Y
nitrobenzene	22.8	650	-
o-fluoronitrobenzene	24.2	240	[3] N
m-fluoronitrobenzene	27.7	143	[3] Y
p-fluoronitrobenzene	25.0	185	[3] N
o-nitrotoluene	20.7	333	[4] -
m-nitrotoluene	22.1	339	[4] -
p-nitrotoluene	21.2	352	[4] -

[1] Electron affinities from reference 67.

[2] R T C = Relative Thermodynamic Clustering order. Y indicates that qualitative consistency is observed by the APIMS DMSO Clustering and equilibrium.

[3] Isomer identities confirmed by retention time.

[4] No data for comparison.

This discrepancy was examined more closely by varying the ion source temperature, DMSO partial pressure, and identity of the buffer/expansion gas. Table 4 summarizes the results obtained from every experiment designed to test the FNB$^-$DMSO FNB isomeric clustering disparity.

Table 4.

APIMS DMSO Clustering Ratios (= M^-DMSO / M^-) for o-,m-, and p-Fluoronitrobenzene[1] at 125 and 225° C.
P_{DMSO} is 0.25 Torr. Helium buffer/ expansion gas sampled with a 50 μm aperture.

[1]Isomer	Temperature (° C)	Clustering Ratio	Normalized Ratio	[2]Order (1,2,or 3)
ortho	125	5.05	1.00	1
	[3]150	2.40	1.00	1
	[4]150	0.80	1.00	1
	225	0.16	1.00	1
meta	125	3.63	0.72	3
	[3]150	1.43	0.60	3
	[4]150	0.67	0.84	3
	225	0.11	0.72	3
para	125	4.24	0.84	2
	[3]150	1.85	0.77	2
	[4]150	0.71	0.88	2
	225	0.14	0.91	2

[1] Isomer identities have been confirmed by retention times. HP-methyl silicone wide bore capillary, 90° C, 9 mL min^{-1}, R_t(ortho) = 2:20, R_t(meta) = 1:45, R_t(para) = 1:55.

[2]Order refers to isomer with the greatest propensity to cluster with DMSO for the indicated experimental condition. 1 indicates the highest clustering propensity.

[3] same conditions, but 0.4 Torr DMSO.

[4] Argon buffer gas, and 0.4 Torr DMSO.

Regardless of the APIMS condition studied, the same relative clustering propensities (o > p > m) were observed for the FNB's . The identity of the FNB isomers have been verified by comparison of relative retention times to those for the ClNB's, and therefore sample mix-up is not suspected. It is

interesting to note that the PHPMS derived thermodynamic clustering order for the ClNB's (o > p > m) matches the observed by the APIMS derived relative order (o > p > m) which would also be consistent with the APIMS FNB results. No explanation can be presently found to account for the alteration in the relative clustering propensities observed for the FNB's in the APIMS and PHPMS experiments.

From the above discussion, it appears that APIMS allows a means by which qualitative isomeric information may be obtained for anions which can be made to cluster to a solvating agent. It is conceivable that the relative clustering propensities, as demonstrated here for a wider range of substituted nitroaromatics than previously reported, may find practical application for analytical APIMS wherever such additional analyte information would be deemed valuable for structural isomer identification.

Preferred Cluster Ion Stabilities from APIMS

In this section the cooling and condensation dynamics of the APIMS free jet expansion will be advantageously employed for generation of previously unreported halide hydrate and dihalide hydrate cluster ions. As for the previous study involving isomer dependent clustering of substituted nitroaromatic molecular anions to a molecule of

dimethylsulfoxide, only qualitative information will be sought in the comparison of relative mass spectral ion currents.

Gas phase cluster ions are important systems of study as probes into the intrinsic chemical and physical properties of matter found at the gas to condensed phase interface. A recent review article by Keesee and Castleman provides an appreciation for the fundamental interest which propels research investigating the reactivities, energetics, spectroscopic behavior, and structures of ion-molecule cluster complexes (18). The degree of aggregation within a cluster can significantly influence its properties and behavior, and such aggregate dependent properties and behavior are important factors in studies of nucleation phenomena. An earlier review by Derrick (37) also highlights progress and motivation for the study of cluster ions. The chemical significance of solvation of halide ions is surveyed by Sharp (68).

A large body of measurements regarding the energetics of gas phase ion-molecule clustering equilibria has provided insight into the structural properties of specific ion-solvent clustering systems. Thermodynamic parameters are primarily obtained from Pulsed High Pressure Mass Spectrometry techniques. An important question pertains to how large a cluster must be before it will display bulk solution properties. Results from measuring successive

clustering steps tend to indicate a general convergence in the energetics of solvation as the number of solvating species increase. The successive attachment of ligands is expected to become progressively less dependent on the nature of the central ion, and eventually the energy of further ligand addition must asymptotically approach the heat of condensation onto a microdroplet having some central charge (69,70). However, well defined inner coordination shells are possible for certain cluster ions on the gas phase. Abrupt changes in the enthalpy of solvation between any two successive clustering reactions are indicative of geometrical preferences and/or steric constraints. There are a number of examples of preferred geometries (69-72) involving fewer than ten solvating molecules, for example $Li^+(NH_3)_2$, $Li^+(NH_3)_4$, $Na^+(NH_3)_4$, $Sr^+(NH_3)_8$, but no such preferential solvation shells have been observed for K^+ or Rb^+ ammonia solvates. For the halide hydrate cluster ions, there appears to be little noticeable selectivity in the successive solvation steps beyond a first coordination sphere of 4 to 6 waters. The data is however limited for the halide hydrates as the largest clusters, which have been investigated by Hiraoka and co-workers by means of PHPMS (73), do not exceed ten water molecules. This is because experimental pressure limitations of the PHPMS technique rarely allow for clustering of more than ten solvent molecules about the ion of interest.

Novel Halide Hydrate Cluster Ions Generated by APIMS.

The halide ions of interest are formed by electron capture within the an Atmospheric Pressure Ionization (API) source. Fluoride ion is generated from C_7F_{14} upon solvation of the parent molecular anion by water corresponding clustering induced decomposition mechanism to be discussed in the following section (74). Chloride, bromide, and iodide ions are generated by direct electron capture from CCl_4 , CBr_2H_2, and CH_3I, respectively. Argon gas is humidified upon passage through a water filled bubbler device, and this wet Ar stream is mixed with the GC eluent for a buffer gas water partial pressure of 10 Torr. The API ion source is maintained at 38° C. Ionized gas is ventilated through a 50 μm aperture into the expansion chamber held at 10^{-4} Torr, which comprise the conditions for a free jet expansion as described in Theory. Extensive cooling and net clustering occurs in the expansion on the vacuum side of the ion sampling aperture. Figure 38 shows the resultant cold cluster ions formed in the very low (est. 20° K) temperatures in the jet.

The extent of the condensation occurring within the free jet expansion can be appreciated in Figure 39 which shows the initial halide hydrate cluster ions present in the thermally equilibrated static API ion source (38° C, 10 Torr water) prior to cooling and condensation in the expansion. The pre-expansion equilibrium distributions may be

calculated from the thermodynamic parameters of Hiroaka and coworkers (73). The calculated equilibrium relative halide hydrate cluster ion abundances seen in Figure 39a indicate that hydration is most favored about the fluoride ion, with n in $F^-(H_2O)_n$, ranging from 4 to 8 water molecules, with the n = 6 cluster most abundant. The observed cold fluoride hydrate cluster ion distribution generated from the argon APIMS free jet expansion shown in Figure 38a ranges from 2 to beyond 24 water molecules, with the distribution centered about the n = 16 cluster. Similar effects are observed from inspection of Figures 38 and 39 for the other halide hydrate cluster ions.

The mass spectra presented in Figure 38 reproducibly showed several clear discontinuities in the abundances for specific cluster ions beyond ten waters for F^- and Cl^- hydrates. Specifically there are especially stable cluster ions (so-called "magic numbers") for the fluoride hydrates comprising 10, 12, 14, 16, 19 water molecules, and for the chloride hydrates comprising 10, 12, 14, 16 water molecules. These free jet expansion results, consistent with the literature, also show that the propensity to exhibit preferred coordination shells indeed decreases as the core anion radius is increased, that is progressing from F^- to I^-, since the enthalpy change for any particular clustering reaction varies inversely with ionic radius. This observation is in line with the current general

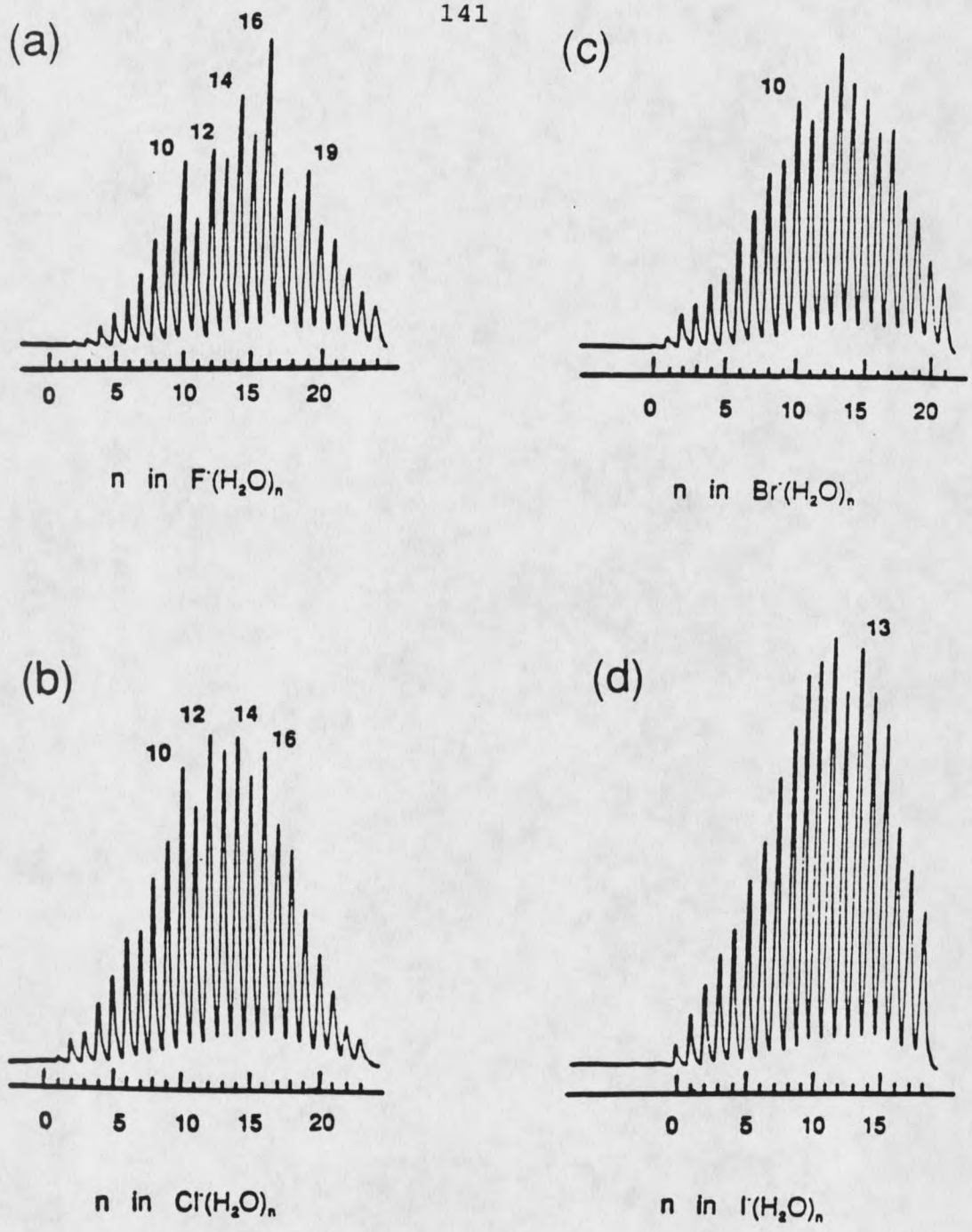

Figure 38.

Cold halide hydrate cluster ions formed by condensation events occurring within the APIMS free jet expansion. Ion source temperature 38° C, 10 Torr partial pressure of water in argon buffer/expansion gas sampled through a 50 μm aperture. (a) fluoride hydrates, (b) chloride hydrates, (c) bromide hydrates, and (d) iodide hydrates.

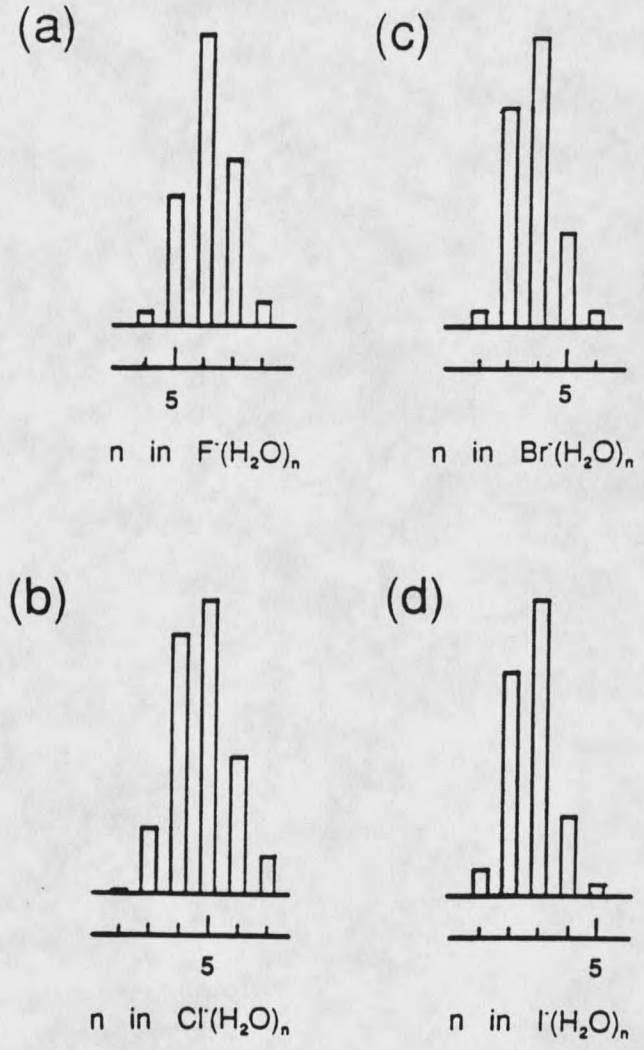

Figure 39.

Halide hydrate clusters ions present within the thermally equilibrated conditions of the API ion source prior to aggregation in the free jet expansion. Temperature 38° C, 10 Torr water. Calculated from thermodynamic parameters of Hiraoka (73). (a) fluoride hydrates, (b) chloride hydrates, (c) bromide hydrates, (d) iodide hydrates.

description of fluoride as a so-called "structure-maker" in aqueous solution (75). A structure-maker is an ion that reinforces the structure of the bulk solvent. This classification has contrasted fluoride to the other halide ions as solution "structure-breakers" because of much weaker hydrogen bonding, and a concomitant surrounding region of increased disorder. These free jet expansion results would perhaps illuminate chloride as potentially a weak structure maker based upon closer exhibited similarities to fluoride than to bromide and iodide. Clearly enhanced cluster ions appear in the population of moderately sized fluoride hydrates, whereas only subtle preferred cluster geometries may be inferred within a similar series of the iodide hydrates.

The highly symmetric smaller core negative ions fluoride and chloride therefore appear to have a longer range influence on the solvation shell, at least for cold clusters formed in the free jet expansion, than may earlier have been expected. These enhanced stability observations are certainly explained by particularly ordered networks of hydrogen bonding that are possible with a highly symmetric solvating agent such as water. This view is supported by other well known enhanced stability cluster ions formed in a free jet expansion involving a similar number of water molecules. One very well known example in the proton hydrates series is $H^+(H_2O)_{21}$, which has been observed with

our experimental apparatus and earlier by others, and is proposed to assume a pentagonal dodecahedron clathrate structure (37). Yang and Castleman have recently reported other special stabilities for 6, 15, 17, 24, 25, 26 waters solvating the proton (76).

An additional feature of interest in Figure 38 are the clearly alternating even/odd hydrate pattern of stability for the smaller core negative ions F^- and Cl^-. Such repeating oscillation in even/odd stabilities has been reported in charged atomic clusters, for example $[Na_x]^+$, for which it is known that there is a corresponding oscillation in ionization potentials for the neutral precursors (37).

The enhanced stabilities observed lead directly to questions regarding specific cluster ion structures. Various coordination shell geometries may be proposed based upon logical placement of water molecules, arranged in hydrogen bonded networks, about a core anion with nobel gas electronic configuration of reasonable radius. One such proposed structure for $F^-(H_2O)_{10}$ is provided in Figure 40. Such models require validation either by empirical or theoretical means. Energy minimization calculations are often the only test when no other direct experimental evidence is available. There have been theoretical efforts aimed at the energetics and structure of the halide hydrates up to six waters (77).

Lybrand and Kollman have investigated potential

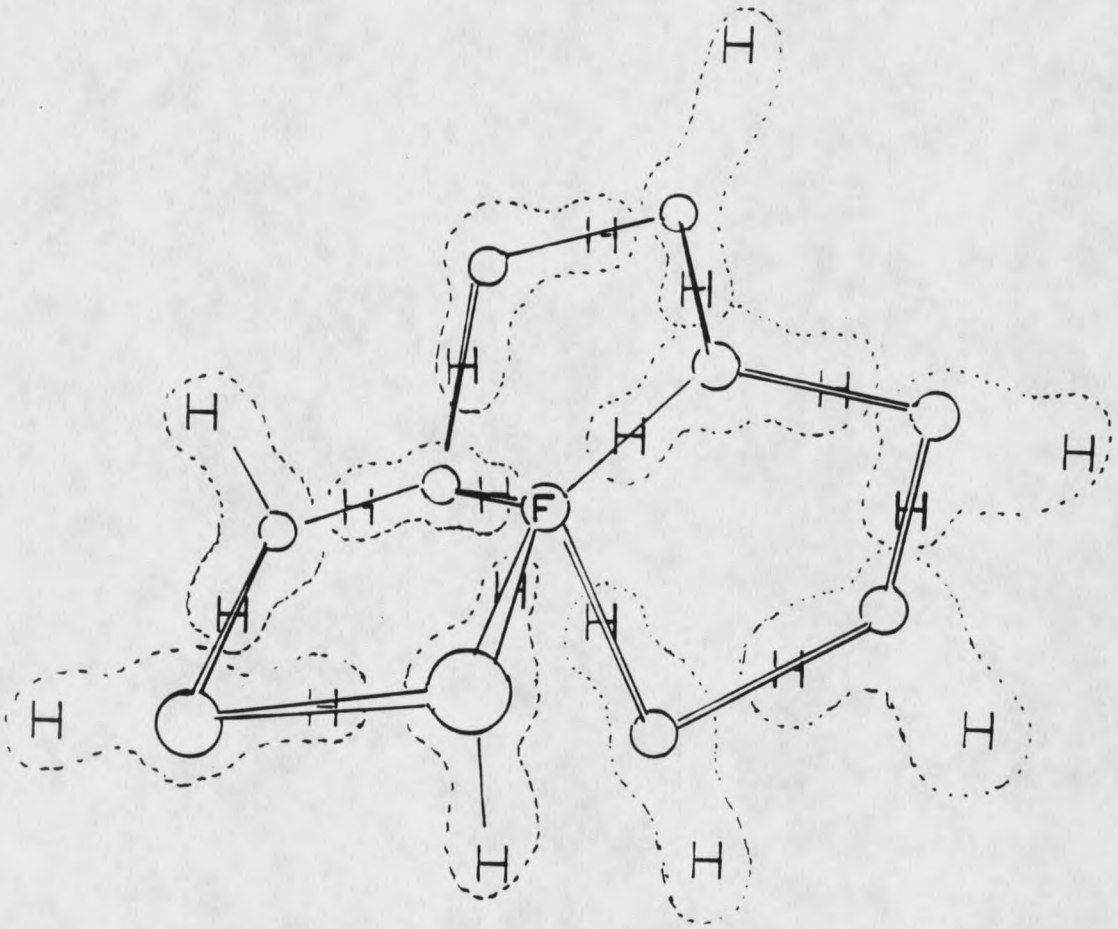

Figure 40.

Proposed structure for $F^-(H_2O)_{10}$ based on logical placement for hydrogen bonded water molecules.

functions to carefully model the interactions of importance within various simple cationic and anionic hydrates (78). The studies involved refinement of energy calculations, which are ultimately used to obtain cluster ion structural insight. The approach involved inclusion of non-additive or many body potential function terms chosen in preference to using standard pair potentials to account for polarizability effects within gas phase ion hydrates. The energy minimization calculations indicated distinct differences in the character of the solvation shells of cations verses anions. In particular the waters solvating anions were in general predicted to be oriented in a manner much more conducive to ordered hydrogen bonding than for cases of cation hydration. The developed force fields provided excellent agreement with experimental successive hydration energies that where measured in Kebarles laboratory (26,79). These encouraging results by Kollman and coworkers perhaps justify application of such calculations for obtaining potentially useful insight to address the structural issues raised by the observations of unexpected special stabilities for the moderately sized halide hydrate cluster ions.

It is proposed that additional halide solvates may be formed and studied by means of the condensation events of the free jet expansion, with the objective of probing for other potentially interesting special cluster ion

stabilities. The next such system suggested are the $X^-(CO_2)_n$, which are known to cluster favorably, and have recently been reported by Hiraoka, with up to about 8 carbon dioxide molecules within the conditions of the PHPMS experiment (80).

Novel Dibromide Hydrate Cluster Ion Generated by APIMS.

Figure 41a shows the hydrates of Br_2^- also formed in the free jet expansion. The second envelope of ions present corresponds to the bromide hydrates already shown in Figure 38. The dibromide ion is formed in a dissociative electron capture reaction which accompanies production of bromide ion. These ions can not be separated prior to expansion in the jet, hence the two cluster ion envelopes. A pen trace over the dibromide ion hydrate profile is shown in Figure 41b in effort to visualize these clusters from the bromide hydrates. Inspection of the dibromide hydrate clusters shows an enhanced stability for the 9, 11, 13 water clusters.

Relevance to Other Studies. This observation may have some related precedent noted in reference 16 from work by Lineberger and coworkers (81) concerning $Br_2^-(CO_2)_n$ special stabilities and solvent caging effects in the gas phase. It was found that photo-dissociation of cold $Br_2^-(CO_2)_n$ formed in a free jet expansion is progressively attenuated by successive addition of carbon dioxide molecules finally with total inhibition of the photodissociation channel upon

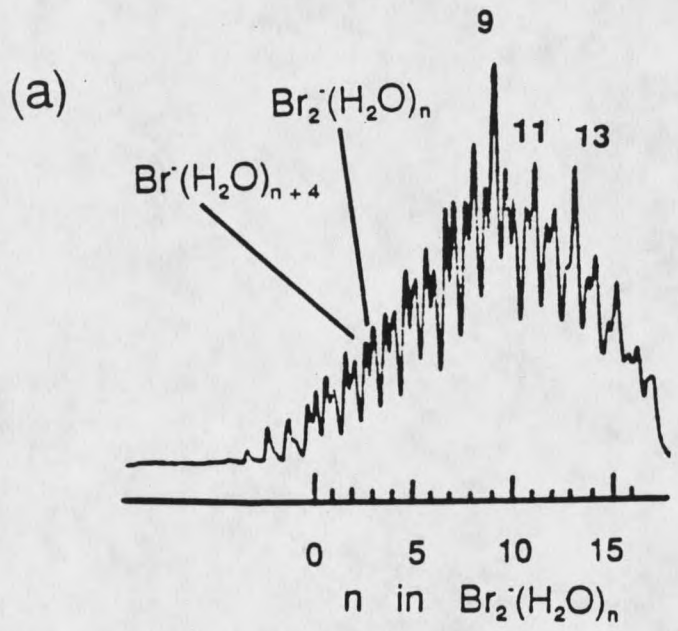

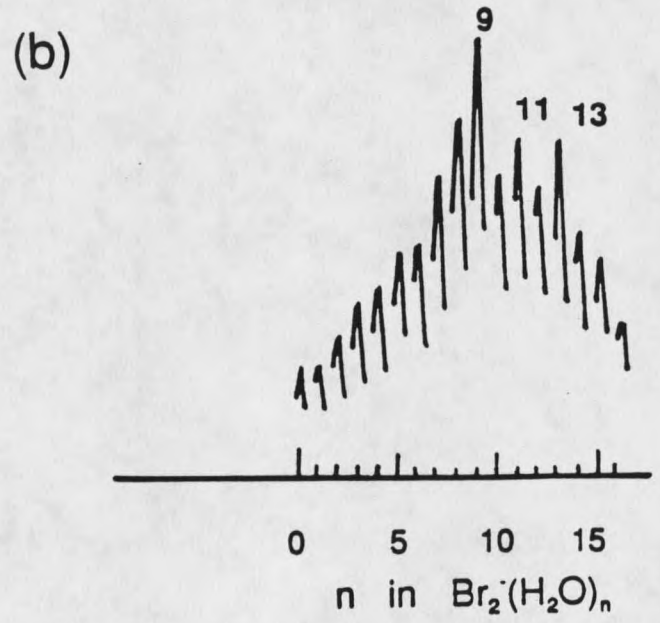

Figure 41.

(a) Cold dibromide hydrate cluster ions formed in free jet expansion, interspersed with bromide hydrate cluster ions. Dibromide and bromide simultaneously generated by electron capture branching reaction of 1,2-dibromohexafluoropropane. (b) Pen trace of dibromide hydrates in (a) to illuminate the dibromide hydrate cluster ions of interest.

reaching the 13 cluster. Weak special stabilities were observed in the time of flight mass spectra for 8, 10, 12 carbon dioxide molecules about dibromide (82). Molecular dynamics work has met with some success for modeling the caging effects, whereby doubly capped minimum energy structures are implicated in the structural control of caging. Perhaps these photo-dissociation cage effects involving $Br_2^-(CO_2)_n$ and the appearance of enhanced stability $Br_2^-(H_2O)_n$ clusters merits attention towards determining the structural features which influence the spectroscopic and structural properties of this ion.

Cluster Assisted Decomposition

This section concludes efforts toward utilization of APIMS for fundamental information, and concerns the unexpected decomposition of the well-studied perfluorinated molecular anions, SF_6^- and $C_7F_{14}^-$, upon association with appropriate solvating agents. The APIMS observations which follow may provide additional evidence to a pool of existing observations regarding the unusual structural nature of these perfluorinated molecular anions, generated by resonance electron capture. Additionally, the existence of these unusual clustering assisted decomposition reactions will be related to the thermospray analysis of perfluorocarbons (PFC's), and shown to be of potential significance toward an explanation of unusual $(M-F)^-$

ionization products.

Previous Measurements by PHPMS. Both SF_6^- and $C_7F_{14}^-$ are among the most widely studied negative ions. Their neutral precursors are known to resonantly attach thermal electrons exceedingly fast to form a molecular anion which is very stable against electron transfer, exhibiting a strong kinetic barrier even when thermodynamically favored. While conducting ion-molecule clustering equilibria measurements involving $C_7F_{14}^-$ and SF_6^- solvation by methanol using PHPMS, Knighton observed, in addition to the expected cluster ion, various unexpected product ions (74). Depending upon the experimental conditions of ion source temperature and methanol partial pressure, $(M-F)^-$, $(M-2F)^-$, and $F^-(HF)_n$ ions were observed which were shown to be generated by the decomposition of the core molecular anion clustered to methanol. The clustering energetics and clustering assisted fragmentation dynamics were subsequently examined. Knighton showed that two decomposition mechanisms were operative for the conditions of the PHPMS. Fragment ions are competitively produced by unimolecular and bimolecular processes. The first order reaction involves the decomposition of the molecular anion clustered to one molecule of methanol. The second order reaction involves association of the singly clustered anion with a second molecule of methanol. The dominant mechanism for methanol-assisted decomposition of $C_7F_{14}^-$ and SF_6^- was found to be

determined by ion source temperature, with the unimolecular decomposition reaction becoming progressively dominant at high temperature. Further details regarding these PHPMS experiments are found in reference 74.

APIMS Methanol Solvation. Figure 42 shows the observed cluster assisted decomposition effects for $C_7F_{14}^-$ in the presence of methanol under the conditions of API ion source. For reference, the electron capture-API (EC-API) mass spectrum of C_7F_{14} at 150° C without the presence of a solvating agent is shown by Figure 42a . It is seen that the molecular anion predominates, with only negligible ion current for the $(M-F)^-$ ion. At low ion source temperatures the relative intensity of $(M-F)^-$ is reduced below that shown in Figure 42a. The EC-APIMS spectrum of C_7F_{14} with 13 Torr methanol partial pressure of methanol at 150° is shown in Figure 42b. This spectrum is dominated by the $(M-F)^-$ fragment ion, and the molecular anion, M^-, is no longer observable. As shown in Figure 42c, the EC-API mass spectrum is further altered by the combined effects of 13 Torr methanol and low (40° C) ion source temperature. It is seen from this spectrum that the intensity of $(M-F)^-$ is very low, and the ion current is comprised primarily of fluoride ion-methanol clusters, $F^-(MeOH)_n$, where n = 2 to 9 methanol molecules. Figure 43 shows the EC-API mass spectra for C_7F_{14} at 150° C over a range of methanol partial pressures, with each observed ion presented graphically as percentage of the

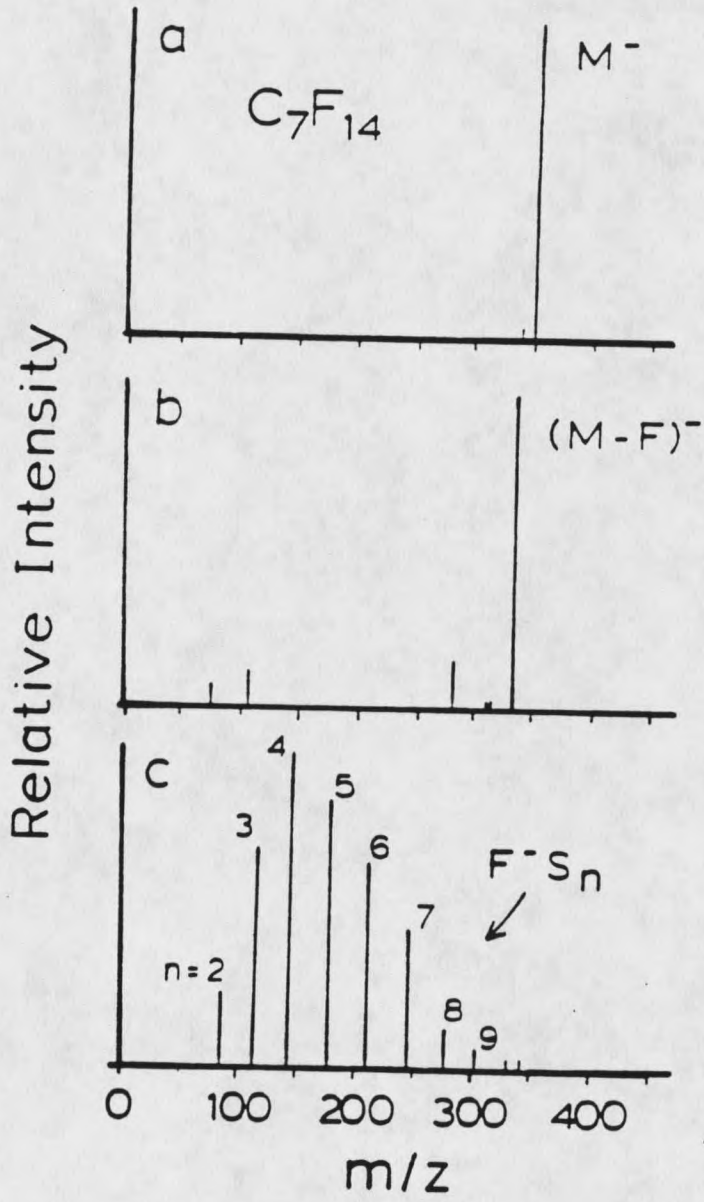

Figure 42.

Electron capture-API (EC-API) mass spectra of perfluoromethylcyclohexane with methanol vapor added to nitrogen buffer gas.

(a) 150° C ion source, (control).
(b) 150° C ion source, 13 Torr methanol.
(c) 40° C ion source, 13 Torr methanol.

total negative ion current. It is clear that conditions which favor clustering progressively transfer the ionization to fluoride ion solvated by varying numbers of methanol molecules. This trend shown in Figure 43 is consistent with the following proposed reaction sequence in which the final location of negative charge is influenced by the degree of solvation of the reaction intermediate shown in reaction 40

$$MS^- \longrightarrow [\, M\cdots F(S)_n \,]^- \begin{cases} \longrightarrow (M\text{-}F)^- + F + nS & (40a) \\ \longrightarrow F^-(S)_n + (M\text{-}F) & (40b) \end{cases}$$

As the partial pressure of methanol, S, is increased, clustering becomes more favorable and a larger number, n, of methanol molecules will be available for clustering to the intermediate species as the bond to a departing fluorine atom is lengthened. As n is made larger, the magnitude of this stabilizing force will be much greater if the negative charge is retained on the fluorine atom rather than the larger portion of the intermediate species. Therefore, as the partial pressure of methanol is increased, the preferred location of negative charge moves from the (M-F) moiety to the fluorine atom, with formation of fluoride solvates.

In Figure 44 the EC-API mass spectra of SF_6 are shown for conditions identical to those described for C_7F_{14} above. Again, in the absence of added methanol vapor (Figure 44a),

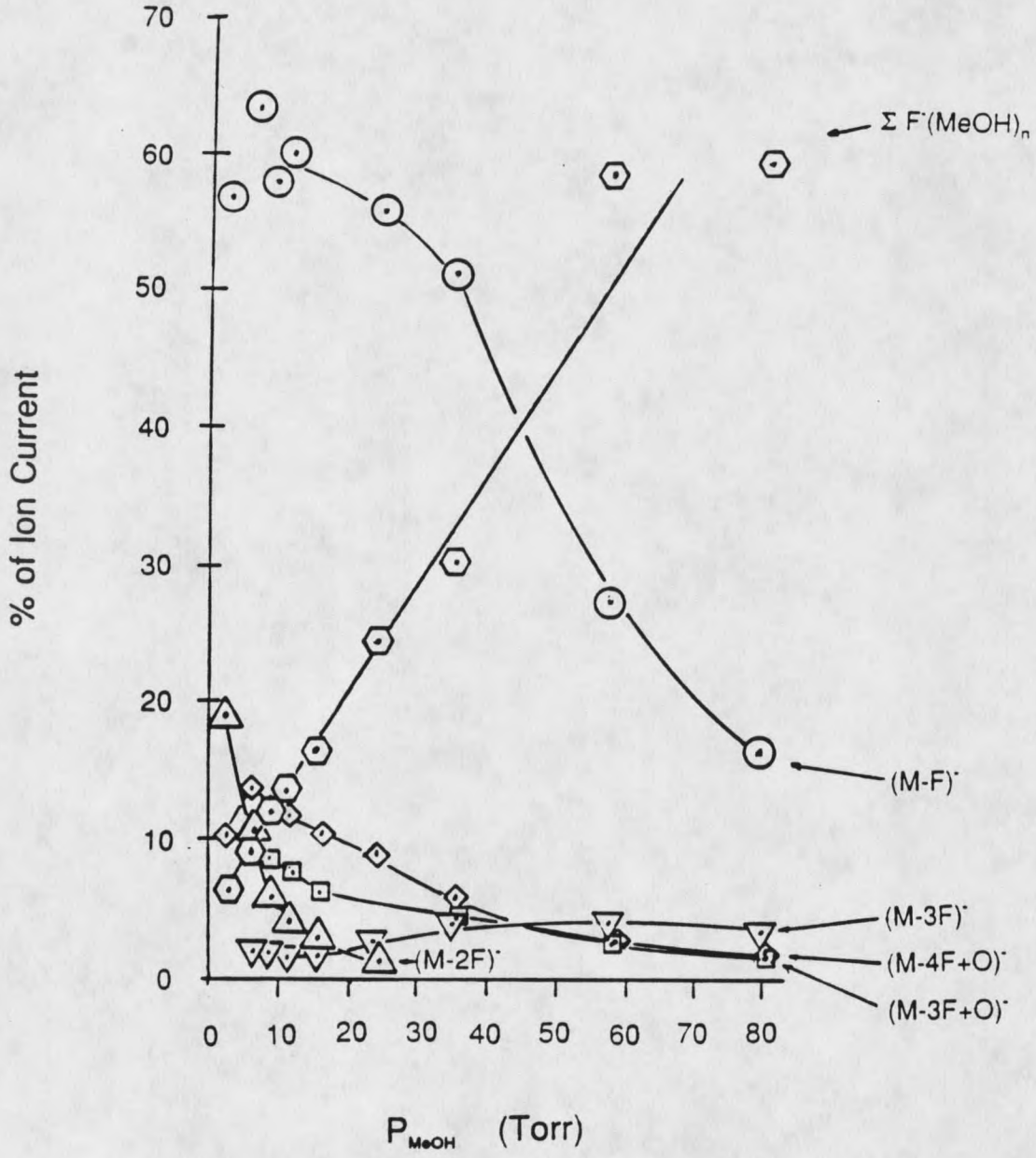

Figure 43.

Electron capture-API (EC-API) mass spectra of perfluoro-methylcyclohexane at varying methanol partial pressures from 0 to 80 Torr with ion source temperature of 150° C. It is seen that more favorable clustering conditions are accompanied by enhancement in fluoride hydrate cluster ions production.

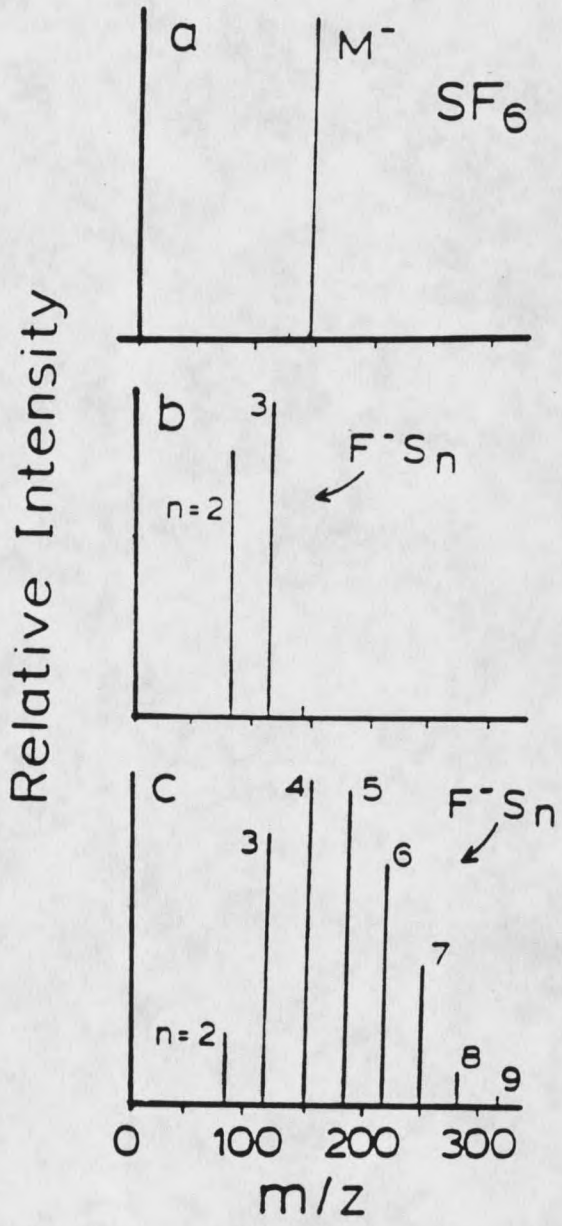

Figure 44.

Electron capture-API (EC-API) mass spectra of sulfur-hexafluoride with methanol vapor added to nitrogen buffer gas.

(a) 150° C ion source, (control).
(b) 150° C ion source, 13 Torr methanol.
(c) 40° C ion source, 13 Torr methanol.

the predominant product ion is the molecular anion, with only a minor $(M-F)^-$ contribution to the total negative ion current. However, when 13 Torr partial pressure of methanol is present in the ion source, only fluoride ion- methanol clusters are observed, with no evidence for $(M-F)^-$ fragment ions at either high (150° C, Figure 44b) or low (40° C, Figure 44c) temperature. The $(M-F)^-$ fragment ion was dominant from C_7F_{14} at 150° C and 13 Torr methanol, hence formation of fluoride solvates is seen to be more labile in the case of SF_6 relative to C_7F_{14}. Referring to the proposed decomposition scheme shown in reaction 40, it is apparent that SF_5 is perhaps less able to compete with a highly solvated fluorine atom for retention of the negative charge than is C_7F_{13}. The explanation for this difference may follow from a consideration of size and electron affinity factors. It is reasonable to assume that the smaller relative size of SF_5 provides less of a blocking force to solvation by methanol molecules, thereby allowing for more access to the fluorine atom with the lengthened bond. Also it is known that SF_5 has a lower electron affinity than C_7F_{13}, thereby being less competitive for retention of charge (74).

APIMS Water Solvation. The effects of water as the cluster assisted decomposition solvating agent will be considered next. The EC-API mass spectrum of C_7F_{14} at 150° C with 15 Torr water partial pressure in shown in Figure 45a. This spectrum is seen to be very similar to that shown

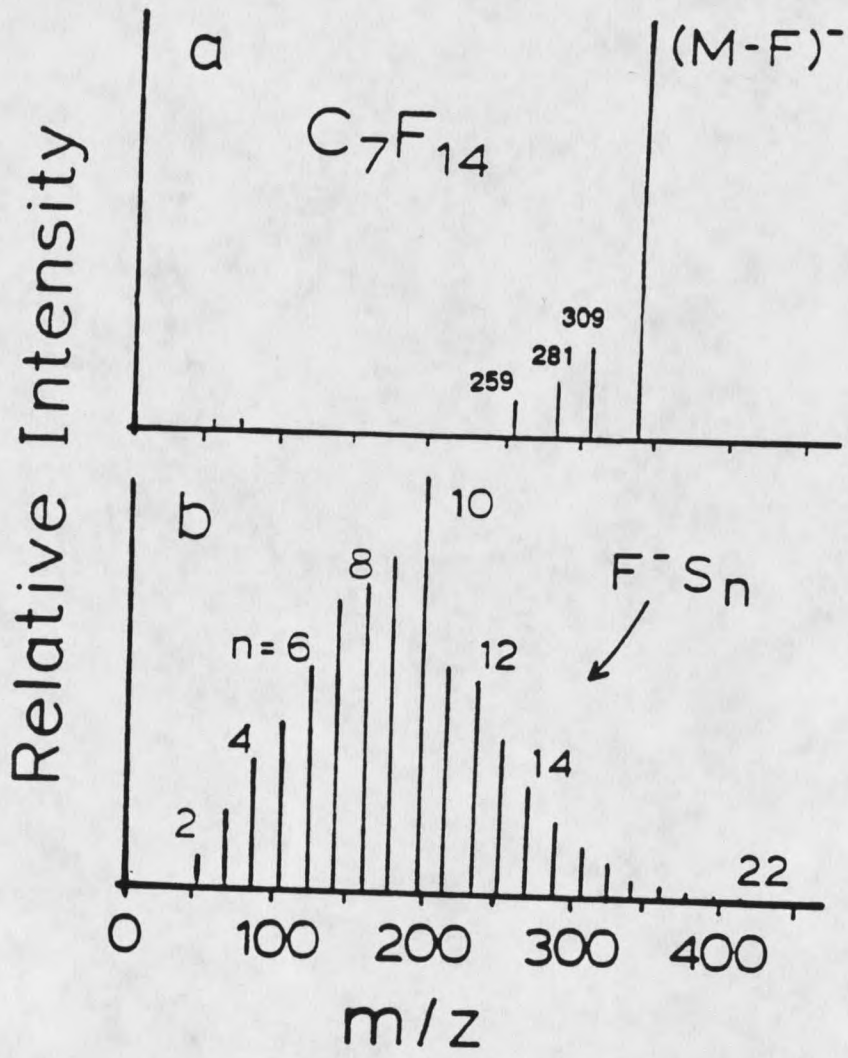

Figure 45.

Electron capture-API (EC-API) mass spectra of perfluoromethylcyclohexane with water vapor added to nitrogen buffer gas. See Figure 42a for the control spectrum.

(a) 150° C ion source, 15 Torr water.
(b) 40° C ion source, 15 Torr water.

in the analogous experiment in which 13 Torr methanol was present in the buffer gas (Figure 42b) rather than water. As in the methanol experiment, the $(M-F)^-$ fragment ion comprises the majority of the ion current. Also in parallel to the methanol experiment (Figure 42c), use of water as solvating agent in the low mole percent range at low temperature results in fluoride ion-solvates, as seen by the envelope of $F^-(H_2O)_n$, where n= 2 to 22. The particularly stable $F^-(H_2O)_{10}$ cluster ion described above can be seen in this spectrum. This distribution of fluoride hydrates does not represent the actual cluster ion relative abundances present within the ion source under these conditions of water partial pressure and temperature, but results from the condensation effects of the APIMS free jet expansion. Calculations based upon the thermodynamic parameters of Hiroaka (73) indicate that the free jet expansion associated with sampling this low temperature ion source with a 50 μm aperture with nitrogen buffer/expansion gas have sufficient cooling effects to result in promotion of aggregation forces. The calculated equilibrium distribution of $F^-(H_2O)_n$ present within the ion source consists of n= 5 to 8, with n = 6 being the most abundant fluoride hydrate.

APIMS DMSO Solvation. The effects of solvation by dimethylsulfoxide (DMSO) on the EC-API mass spectra of SF_6 and C_7F_{14} are shown in Figure 46. It can be seen that DMSO is much less efficient at inducing fragmentation of the core

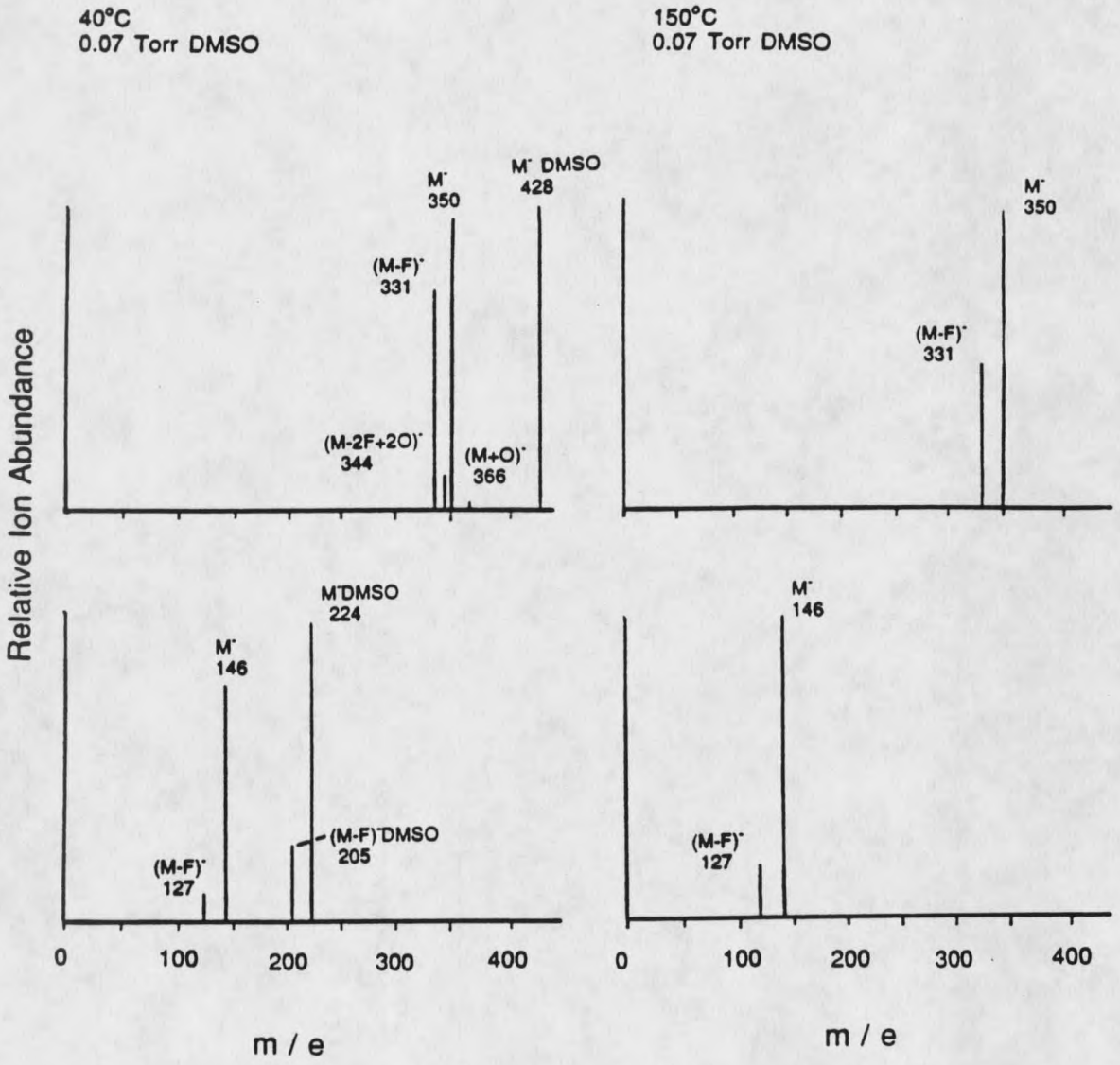

Figure 46.

Electron capture-API (EC-API) mass spectra of sulfer-hexafluoride and perfluormethylcyclohexane with DMSO vapor (0.07 Torr) added to nitrogen buffer gas.

C_7F_{14} at (a) 40° C, and at (b) 150° C.

SF_6 at (c) 40° C, and at (d) 150° C.

molecular anions, even when the conditions allow for appreciable clustering as evidenced by very substantial M^-DMSO ion currents. For example, in Figure 46a, DMSO is shown to cluster strongly with the C_7F_{14} parent molecular anion, and yet in contrast to low temperature experiments involving either water or methanol, M^- and $(M-F)^-$ comprise a large fraction of the total negative ion current. At the higher ion source temperature in the presence of DMSO (Figure 46b), $(M-F)^-$ is less favored, in accordance with clustering, which is less favored. The EC-API mass spectra of SF_6 in the presence of DMSO are shown in Figures 46c and 46d. Again, at the low temperature (Figure 46c) where clustering to DMSO is seen to be very favorable by the substantial M^-DMSO signal, the clustering assisted decomposition of SF_6 is much less efficient by DMSO relative to methanol, as evidenced by minor fragmentation leading to $(M-F)^-$. At the high temperature with DMSO vapor present in the ion source, the EC-API mass spectrum of SF_6 is only slightly enhanced in $(M-F)^-$ relative to the control conditions in which no solvating agents are present (Figure 44a). It is concluded that relative to methanol or water, DMSO is a much less effective solvating agent for initiation of clustering assisted decomposition despite the greater propensity it has to cluster with the molecular anions of SF_6 and C_7F_{14}.

Relevance to PFC Analysis. The APIMS measurements described above indicate that the molecular negative ions of perfluorocarbons (PFC's) may not be generally observable under electron capture or negative chemical ionization conditions when polar protic compounds such as methanol or water are present at partial pressures of several Torr. Since ambient air typically contains this much water, for example, only cluster assisted decomposition generated fragment ions might be expected in the analysis of PFC's in whole air samples directly introduced into the APIMS ion source.

A recent report by Huang and coworkers (83) relates the predominant occurrence of $(M-F)^-$ fragment ions during the analysis of PFC's , C_7F_{14} included, by liquid chromatography/ mass spectrometry (LC/MS). It was observed that the detection of PFC's eluting into a thermospray apparatus required use of an accessory electron emitting filament with water added to the LC mobile phase. Huang proposed that a charge exchange mechanism may be implicated, in which $OH^-_n(H_2O)_m$ ions transfer an electron to the parent PFC molecule with concomitant fluorine-carbon bond rupture. The APIMS results shown in Figure 46a indicating formation of $(M-F)^-$ from C_7F_{14} under electron capture conditions in the presence of water, suggest the possibility that cluster assisted decomposition may account for the observations by Huang and coworkers. Other PFC's investigated by APIMS

include C_6F_{12} and $C_{10}F_{18}$, and it appears that cluster assisted decomposition is very general, leading to $(M-F)^-$ fragment ions at high temperatures, and fluoride solvates at lower temperatures in which clustering is favored.

$(MF_{n-1})F^-$ Molecular Anion Structure. Experiments involving SF_6^- by Drzaic and Braumen (84), and $C_7F_{14}^-$ by Grimsrud and coworkers (74), demonstrate that the photon energy required to photodetach the electron from either of these molecular anions is in large excess of the neutral parent electron affinity. SF_6^- is also known to exhibit a high kinetic barrier to thermodynamically allowed electron transfer reactions, either as the electron donor or recipient. Additionally, SF_6^- has been shown to undergo fluoride transfer to stronger Lewis acids (85). Braumen has proposed, based upon this large body of evidence and theoretical energy minimization calculations, that the geometry of SF_6^- may be significantly distorted from the octahedral structure of neutral SF_6. Specifically, it has been suggested that SF_6^- may best be described as an ion-molecule association complex of the form $F^-(MF_{n-1})$.

It is interesting to consider the possibility that the APIMS cluster assisted decomposition reactions discussed above may offer additional evidence supporting the ion-molecule complex concept for SF_6^- and $C_7F_{14}^-$. Despite the fact that the preferred geometries for these molecular anions may be distorted through clustering with a solvating

agent, the appearance of $F^-(H_2O)_n$ under favorable solvating conditions seems consistent with the notion of a distorted structure which lengthens the bond to one or more fluorine atoms. With regard to the reaction 40, this seems entirely reasonable, as solvation would always be initiated at the most accessible fluorine in the proposed distorted anion, $F^-(MF_{n-1})$.

SUMMARY

Despite the impressive analytical utility of APIMS, this form of mass spectrometry has been infrequently applied to fundamental investigations of gas phase ion chemistry. This is attributable to sampling errors which preclude the accurate observation of relative ion abundances representative of chemistry occurring within the API ion source. The objective of this study has been the characterization of various APIMS sampling errors in order to permit application of this mass spectrometric technique to fundamental study. Two of the three sampling errors that have been examined originate from dynamics occurring within an adiabatic free jet expansion which accompanies the non-effusive flow of the API ion source contents into a mass spectrometer vacuum chamber. The chemical systems of study fall into two broad categories : electron capture processes and ion-molecule clustering reactions.

The first category of sampling error takes the form of perturbations in observed equilibrium cluster ion abundances, and is due to collisional cooling and aggregation, as well as collisionally induced dissociation dynamics, occurring within the APIMS free jet expansion. Ion-molecule clustering equilibrium sampling errors were studied with the proton hydrate water clusters. Sampling

errors due to the cooling and aggregation forces in the APIMS free jet expansion were shown to be generally problematic under all experimental conditions of varying buffer/ expansion gas or sampling aperture diameter at low ion source temperatures. However, the appearance of accurate cluster ion sampling occurred at higher ion source temperatures (≥150° C) with use of a 22 μm aperture and helium or hydrogen buffer/ expansion gas. The fortuitous cancellation of free jet expansion aggregation and collisionally induced dissociation obvious for other gases, is not thought to explain cluster ion sampling results obtained with helium and the 22 μm aperture. This is attributed to several properties unique to helium including a low collision cross-section, low efficiency for energy transfer, and high self-diffusion coefficient, all factors which minimize clustering and declustering forces.

It has been demonstrated that valuable qualitative fundamental information may be obtained from APIMS generated relative ion currents, regardless of the sampling errors on equilibrium cluster ion distributions. This was demonstrated in two different studies. The first involved the clustering of substituted nitroaromatic molecular anions that can be made to cluster to a molecule of dimethylsulfoxide. It was shown that isomeric dependent propensities for clustering, which are intimately related to the electron affinity of the neutral nitroaromatic, are

retained. This permits use of APIMS for deriving qualitative information regarding ion-molecule clustering systems. The second study involved advantageous application of the extensive cooling and aggregation dynamics of the free jet expansion for generation of moderately sized halide hydrate and dihalide hydrate cluster ions. Preferred cluster ion stabilities were noted to occur frequently within the fluoride hydrate series, $F^-(H_2O)_n$, for n = 10, 12, and 16. This tendency for preferred cluster ion stabilities was found to be less pronounced as the core halide ion radius increased, and is consistent with the concept from solution phase chemistry that the smaller radius fluoride ion is a structure-maker. The dibromide hydrate cluster ion series, $Br_2^-(H_2O)_n$, also generated by the free jet expansion, showed preferred stabilities for n = 9, 11, and 13. These observations regarding dibromide ion water cluster preferred stabilities take precedence from reports of dibromide ion carbon dioxide clusters, $Br_2^-(CO_2)_n$, which exhibit similar preferences for n = 8, 10, and 12, and become resistant to photodissociation when n = 10.

A second sampling error resulting in significant mass and ion type discrimination of particular importance for ions of widely differing mass, has been characterized. It has been demonstrated that lower mass ions are always less efficiently sampled from the APIMS free jet expansion, and the degree of bias is dependent upon the experimental

sampling conditions. The important parameters include choice of expansion gas, ion source temperature, sampling orifice diameter, and ion extraction potential. By quantitative determination of relative ion sampling efficiency for a given set of experimental conditions, the observed ion currents may be corrected to derive the relative ion source abundances of interest.

This protocol for mass discrimination correction has been applied to study numerous two-channel dissociative electron capture branching reactions. By comparison to results obtained from several low ionization pressure experiments, collision frequency is revealed to be an important variable in determining the relative product ratios. In the case of bromotrichloromethane, which may capture an electron to form either bromide or chloride, it was confirmed that the relative product ratio for the initial electron capture reaction leading to bromide and chloride is 4 to 1, respectively, as earlier established by APIMS, and the Photodetachment-modulated Electron Capture Detector which also operates at atmospheric pressure. In contrast, results from the Flowing afterglow/Langmier probe low ionization pressure technique indicated an initial electron capture branching ratio for bromotrichloromethane for bromide to chloride of 1 to 1. A second study examined the importance of pressure for the two-channel dissociative electron capture reactions of numerous dibrominated

fluorocarbons and hydrocarbons which lead to either bromide or dibromide ion. Comparison between mass bias corrected APIMS (640 Torr) and several low ionization pressure experiments including Pulsed High Pressure Mass Spectrometry (1 to 4 Torr), Flowing afterglow/Langmier probe (1 Torr), and High Pressure Electron Capture Mass Spectrometry (0.5 Torr) was possible. Differences in the observed relative product ratios indicated the importance of both pressure and identity of the buffer gas in determining the efficiency of collisional stabilization of the excited electron capture intermediates, MBr_2^{-*}. Both two-channel dissociative electron capture systems of study above demonstrate the importance of collisions in modifying the internal energy of the excited intermediates, thereby influencing the favored channel of dissociation, tending toward the thermodynamically favored product at higher pressures For the above to hold, the excited intermediates must have lifetimes against dissociation by either available channel on the timescale of the collisions in a low Torr gas, or approximately 100 picoseconds.

A third sampling error ascribed to aperture contact potentials was examined. It was shown that charging events, which occur when moderate electrostatic fields are present, can dynamically alter absolute mass spectral ion currents and lead to total inhibition of ion sampling.

Cluster assisted decomposition reactions recently

observed by Pulsed High Pressure Mass Spectrometry have been investigated by APIMS. It has been shown that the perfluorinated molecular anions, SF_6^- and $C_7F_{14}^-$, which have been widely studied and are known to possess unusually high stability against either electron photodetachment or charge transfer reactions can be made to decompose to varying degrees upon solvation with appropriate solvating agents. As conditions which favor ion-molecule association are enhanced the molecular anion is decomposed to the $(M-F)^-$ fragment ion. Further enhancement of solvation conditions progressively eliminates the parent molecular anion, as well as the $(M-F)^-$ fragment, transferring the total ion current to solvates of fluoride, $F^-(S)_n$, where S is either methanol or water. It is speculatively noted that generation of such fluoride solvates may support proposals that these perfluorinated molecular anions differ geometrically from their neutral precursors, and that a distortion associated with the lengthening of a bond to fluorine is the site at which cluster assisted decomposition is initiated. The polar aprotic solvent dimethylsulfoxide is much less effective at initiating cluster assisted decomposition of either SF_6^- or $C_7F_{14}^-$. These cluster assisted decomposition reactions, as observed by APIMS, may explain the occurrence of unexpected $(M-F)^-$ fragment ions observed during thermospray analysis of numerous perfluorocarbons when electron capture is made to occur in the presence of water vapor.

LITERATURE CITED

1. Knewstubb, P.F.; Sugden, T.M. Proc. Roy. Soc. **A255**, 520 (1966).

2. Shahin, M.M. J. Chem. Phys. **45**, 2600, (1966).

3. Horning E.C.; Horning M.G.; Carroll, D.I.;Dzidic, I.; Stillwell, R.N. Anal.Chem. **45**(6), 936, (1973).

4. Carroll, D.I.; Dzidic, I.; Stillwell, R.N.; Horning, M.C.; Horning, E.C. Anal. Chem. **46**, 706, (1974).

5. French, J.B.; Thomson, B.A.; Davidson, W.R.; Reid, N.M.; Buckley, J.A. in Mass Spectrometry in Environmental Science Karasek, F.W.; Hutzinger, O.; Safe, S.,(Eds), Plenum, 1984, p. 101-121.

6. Sciex, Inc., 55 Glen Cameron Rd, Thornhill, Ontario, Canada, L3T IP2.

7. Extrel Corp., 240 Alpha Dr, Pittsburgh, PA, USA, 15238.

8. Dzidic, I; Carroll, D.I.; Stillwell, R.N.; Horning, E.C. Anal. Chem. **47**, 8, (1975).

9. Benoit, F.M.; Davidson, W.R.; Lovett, A.M.; Nacson, S.; Ngo, A. Anal. Chem. **55**, 805, (1983).

10. Kefkau, S.N.; Dulak, J.G.; Fite, W.L.; Buchner, J.D.; Dheandanoo, S. Anal. Chem. **61**, 260, (1989).

11. Huang, E.C.; Wach, S.T.; Conboy, J.J.; Henion, J.D. Anal. Chem. **62**(13), 713A, (1990).

12. Bruins, A.P. Mass Spectrom. Rev. (submitted 1990)

13. Carroll, D.I.; Dzidic, I.; Horning, E.C., Stillwell, R.N. Appl.Spectros. Rev. **17**(3), 337, (1981).

14. Proctor, C.J.; Todd, J.F.J.; Org. Mass Spectrom. **18**(12), 509, (1983).

15. Siegel, M.W. in Plasma Chromatography, Timothy Carr (Ed), Plenum Press, New York, (1984).

16. Castleman. A.W.; Keesee, R.G. Chem. Rev. **86**, 589, (1986).

17. Comita, P.B.; Braumen, J.I. Science **227**, 863, (1985).

18. Castleman, A.W.; Keesee, R.G. Science, **241**, 36, (1988).

19. Kebarle, P. Ann. Rev. Phys. Chem. **28**, 445, (1977).

20. Dushman, S. Scientific Foundations of Vacuum Technique, John Wiley and Sons, New York, 1962, p. 81.

21. Levy, D.H. Science **214**(4518), 263, (1981).

22. Hagena, O.F. Surface Science **106**, 101, (1981).

23. Johnston, M.V. Trends in Anal. Chem. **3**(2), 58, (1984).

24. Campargue, R. J. Phys. Chem. **88**, 4466, (1984).

25. Amirav, A.; Even, U.; Jortner, J. Chemical Physics **51**, 31, (1980).

26. Arshadi, M.; Yamdagni, R.; Kebarle, P. J. Phys. Chem. **74** (7), 1475, (1970).

27. McDaniel , E.W. Collision Phenomena in Ionized Gases, John Wiley and Sons, New York, (1964), p. 503-506.

28. Sears, L.J.; Campbell, J.A.; Grimsrud, E.P. Biomed. Environ. Mass Spec. **14**, 401, (1987).

29. Smith, D.; Adams, N.G. in Physics of Ion-Ion and Electron-Ion Collisions, F. Brouillard and J.W. McGowan (Eds), Plenum Press, New York, p. 501.

30. Warden, S.W.; Crawford, R.J.; Knighton, W.B.; Grimsrud, E.P. Anal. Chem. **57**, 659, (1985).

31. Cunningham, A.J.; Payzant, J.D.; Kebarle, P. J. Am. Chem. Soc. **94** (22), 7627, (1972).

32. Kebarle, P.; Searles, S.K.; Zolla, A.; Scarborough, J.; Arshadi, M. J. Am. Chem. Soc. **89**, 6393, (1967).

33. Knighton, W.B.; Grimsrud, E.P. Anal. Chem. **54**, 1892, (1982).

34. CRC Handbook of Chemistry and Physics, 46th Edition, CRC Press, Boca Raton, Florida, 1965, p. D-93.

35. Guthrie, A.; Wakerling, R.K. Vacuum Equipment and Techniques, McGraw-Hill Book Company, Inc., New York, 1949, p. 246.

36. Dahl, D.A.; Delmore, J.E. Simion PC/PS2 USERS MANUAL, Version 3.1, EG and G/ Idaho Engineering Natl Labs, Nov. 1987.

37. Derrick, PJ in Advances in Mass Spectrometry J.F.J. Todd (Ed), John Wiley and Sons, New York, 1985, p. 85.

38. Kebarle, P.; Hogg, A.M. J. Chem. Phys., **42**, 798, (1965).

39. Dzidic, I.; Carroll, D.I.; Stillwell, R.N.; Horning, E.C. Anal. Chem. **48**, 1763, (1976).

40. Searcy, J.Q.; Fenn, J.B. J. Chem. Phys. **61**(12), 5282, (1974).

41. Searcy, J.Q. J. Chem. Phys. **63**(10), 4114, (1975).

42. Lau, Y.K.; Ikuta, S.; Kebarle, P. J.Am. Chem. Soc. **104**, 1462, (1981).

43. Ahmed, M.S.; Dunbar, R.C. J. Am. Chem. Soc. **109**, 3215, (1987).

44. Morris, R.A.; Viggiano, A.A.; Dale, F.; Paulson, J.F. J. Chem. Phys. **88**(8), 4772, (1988).

45. Siegel, M.W.; McKeown, M.C. J. Chromatogr. **122**, 397, (1976).

46. Siegel, M.W.; Fite, W.L. J. Phys. Chem. **80**, 2871, (1976).

47. Sigmond, R.S. in Gaseous Dielectrics III Proc. Third Int. Symp. on Gaseous Dielectrics, Knoxville, Tennessee, 1982, L.G. Christophorou (Ed), Pergamon Press, New York, 1982, p. 92.

48. Grimsrud, E.P.; Kim, S.H.; Gobby, P.L. Anal. Chem. **51**, 223, (1979).

49. McDaniel, E.W. Collision Phenomena in Ionized Gases, John Wiley and Sons, New York, 1964, p. 696.

50. Grimsrud, E.P.; Kim, S.H. Anal. Chem. **51**, 537, (1979).

51. Reis, V.H.; Fenn, J.B. J. Phys. Chem. **88**, 4451, (1984).

52. Smith, D.; Adams, N.G.; Alge, E. J. Phys. B: At. Mol. Phys. **17**, 461, (1984).

53. Alge, E.; Adams, N.G.; Smith, D. J. Phys. B.: At. Mol. Phys. **17**, 3827, (1984).

54. Randeniya, L.K.; Smith, M.A., U. of Arizona, Dept. of Chemistry, USA, preprint 1990.

55. Adams, N.G.; Smith, D.; Herd, C.R. Int. J. Mass Spectrom.Ion Proc. **84**, 243, (1988).

56. Mock, R.S.; Zook, D.R., Grimsrud, E.P. Int. J. Mass Spectrom. Ion Proc. **91**, 327, (1989).

57. Walter, C.W.; Lindsay, B.G.; Smith, K.A.; Dunning, F.B. Chem. Phys. Lett. **154**, 409, (1989).

58. Walter, C.W.; Smith, K.A.; Dunning, F.B. J. Chem. Phys. **90**, 1652, (1989).

59. Alajajian, S.H.; Bernius, M.T.; Chutjian, A. J. Phys. B: At. Mol. Opt. Phys. **21**, 4021, (1988).

60. Smith, D.; Herd, C.R.; Adams, N.G.; Paulson, J.F. Int. J. Mass Spectrom. Ion Proc. preprint 1990.

61. Zook. D.R.; Knighton, W.B.; Grimsrud, E.P. Int. J. Mass Spectrom. Ion. Proc (submitted 1990).

62. CRC handbook of Chemistry and Physics, 69th Edition, CRC Press, Boca Raton, Florida, 1989, p. F-183.

63. Lias, S.G.; Bartmess, J.E.; Liebman, J.F.; Holmes, J.L.; Levin, R.D., Mallard, W.G. J. Phys. Chem. Ref. Data **17**, 1, (1988).

64. Warmen, J.M.; Sauer, K.S. J. Chem. Phys. **62**, 1971, (1975).

65. Fehsenfeld, F.C. J.Chem. Phys. **53**, 2000, (1970).

66. Krieger, L.; Grimsrud, E.P. Int. J. Mass Spectrom. Ion Proc. **83**, 189, (1988).

67. Chowdhurry, S.; Grimsrud, E.P.; Kebarle, P. J. Phys. Chem. **91**, 2551, (1987).

68. Sharpe, A.G.; J. Chem. Ed. **67**(4), 309, (1990).

69. Castleman, A.W.; Tang, I.N. J. Chem. Phys **57**(9), 3629, (1972).

70. Castleman, A.W.; Holland, P.M.; Lindsay, D.M.; Peterson, K.I. J. Am. Chem. Soc. **100**(19), 6039, (1978).

71. Holland,P.M.; Castleman, A.W. J. Chem. Phys. **76**, 742, (1982).

72. Tang, I.N.; Lian, M.L.; Castleman, A.W. Chem. Phys. Lett. **53**, 560, (1978).

73. Hiraoka, K.; Mizuse, S.; Yamabe, S. J. Phys. Chem. **92**, 3943, (1988).

74. Knighton, W.B.; Zook, D.R.; Grimsrud, E.P. J. Am. Soc. Mass Spectrom. (accepted 1990).

75. Emsley, J.; Arif, M.; Bates, P.A.; Hursthouse, M.B. J. Molec. Struct. **220**, 1, (1990).

76. Yang, X.; Castleman, A.W. J. Am. Chem. Soc. **111**, 6845, (1989).

77. Gowda, B.T.; Benson, S.W. J. Comp. Chem. **4**(3), 283, (1983).

78. Lybrand, T.P.; Kollman, P.A. J. Chem. Phys. **6**(15), 2923 (1985).

79. Dzidic, I.; Kebarle, P. J. Phys. Chem. **74**, 1466, (1970).

80. Hiroaka, K.; Mizuse, S.; Yamobe, S. J. Phys. Chem. **87**(6), 3647, (1987).

81. Lineberger, W.C; Alexander, M.L.; Levinger, M.A.; Johnson, M.A. paper Phys. 0016 presented at the 191st Annual Meeting of the American Chemical Society, New York, 13 to 18 April 1986.

82. Alexander, M.L.; Levinger, N.E.; Johnson, M.A.; Ray, D.; Lineberger, W.C. J. Chem. Phys. **88**(10), 6200, (1988).

83. Huang, S.K.; Klein, D.H.; McLoughlin, M. Biomed. and Environ. Mass Spec. **18**, 106, (1989).

84. Drzaic, P.S.; Braumen, J.I. J. Am. Chem. Soc. **104**, 13, 1982.

85. Haartz, J.C.; McDaniel, D.H. J.Am. Chem. Soc. **95**(26), 8562, (1973).